Study on the degradation of carbon materials
for electrocatalytic applications

vorgelegt von
M. Sc.
Youngmi Yi
aus Busan, Südkorea

Von der Fakultät II - Mathematik und Naturwissenschaften
der Technischen Universität Berlin
zur Erlangung des akademischen Grades
Doktor der Naturwissenschaften
Dr.rer.nat.

genehmigte Dissertation

Promotionsausschuss:

Vorsitzender: Prof. Dr. Arne Thomas

Berichter/Gutachter: Prof. Dr. Robert Schlögl

Berichter/Gutachter: Prof. Dr. Peter Strasser

Berichter/Gutachter: Prof. Dr. Jaeyoung Lee

Tag der wissenschaftlichen Aussprache: 1. Juli 2014

Berlin 2014

D 83

Abstract

Carbon materials are essential in chemical energy storage and conversion systems because of their high electrical and thermal conductivity, a large diversity in structure, and relatively low cost. Although its versatility has led to an advanced performance of electrochemical applications, carbon still does not provide its full capacity due to corrosion under operating conditions. Thermodynamically, the electrochemical oxidation of carbon is possible at a potential above 0.2 V (*vs*. reversible hydrogen electrode (RHE)) in an aqueous environment. Thus, carbon degradation is likely to happen when carbon is used as an electrode material for oxygen evolution that occurs above 1.23 V in water electrolysis.

The work described in this thesis focuses on the study of the electrochemical and thermal oxidative degradation of carbon nanotubes (CNTs). It is known that the sidewalls of CNTs are essentially inert, whereas open end and defect sites of CNTs provide the active species for electrochemical reactions. This unique structure of CNTs could influence high activity and stability in electrochemical applications.

In this thesis, the electrochemical oxidation of CNTs was performed at high anodic potentials where both oxygen evolution and carbon oxidation occur simultaneously. For thermal oxidation, CNTs were treated at a temperature at which the combustion of carbon takes place. The morphological and structural changes during the oxidative degradation of CNTs were measured by electron microscopy, Raman and infrared spectroscopy. The effect of the degradation on the electrochemical behavior of carbon was analyzed by cyclic voltammetry, linear sweep voltammetry and electrochemical impedance spectroscopy.

The results indicate that the degradation of carbon initially purifies the CNTs via oxidizing amorphous carbon, subsequently attacks the graphitic walls and create defects. The oxidation of CNTs produces various oxygen-containing surface functional groups and the growth of surface oxides reaches a limiting value for the formation of a passive oxide. This research can pave the way for the utilization of carbon-based catalysts in electrocatalytic applications involving oxygen, such as water splitting, regenerative fuel cells, and metal-air batteries.

Zusammenfassung

Kohlenstoffmaterialien sind unentbehrlich in Energiespeicher- und Energieumwandlungs-systemen, da sie eine hohe elektrische und thermische Leitfähigkeit aufweisen, in einer großen strukturellen Vielfalt existieren und relativ niedrige Kosten verursachen. Obwohl die Anwendung von Kohlenstoffmaterialien aufgrund ihrer Vielseitigkeit zu einer gesteigerten Effektivität in elektrochemischen Anwendungen geführt hat, liefert sie bei den gewünschten Betriebsbedingungen durch die auftretende Kohlenstoffkorrosion noch nicht ihre maximale Effizienz. Thermodynamisch kann Kohlenstoff in wässrigem Milieu oberhalb von einem elektrochemischen Potential von 0.2 V - relativ zur reversiblen Wasserstoffelektrode (RHE) - elektrochemisch oxidiert werden. Daher ist die Zersetzung von Kohlenstoff sehr wahrscheinlich, wenn es als Elektrodenmaterial für die Sauerstoffentwicklung in der Wasserelektrolyse oberhalb von 1.23 V verwendet wird.

Diese Doktorarbeit konzentriert sich auf die Untersuchung der elektrochemischen und thermisch oxidativen Degradation von Kohlenstoffnanoröhren (CNTs). Es ist bekannt, dass die Seitenwände von CNTs besonders inert sind, wohingegen die offenen Enden und Defektstellen die aktiven Zentren für elektrochemische Reaktionen darstellen. Diese einzigartige Struktur der CNTs könnte die hohe Aktivität und Stabilität in elektrochemischen Anwendungen beeinflussen.

In dieser Arbeit wurde die elektrochemische Oxidation von CNTs bei hohem anodischen Potential durchgeführt, bei dem sowohl Sauerstoffentwicklung als auch Kohlenstoffoxidierung gleichzeitig stattfinden. Für die thermische Oxidation wurden die CNTs bei einer hohen Temperatur behandelt, bei der die Verbrennung des Kohlenstoffs einsetzt. Die morphologischen und strukturellen Veränderungen während der oxidativen Zersetzung der CNTs wurden mittels Elektronenmikroskopie, Raman- und Infrarotspektroskopie verfolgt. Die Wirkung der Kohlenstoffzersetzung auf das elektrochemische Verhalten wurde mittels zyklischer Voltammetrie, linearer Voltammetrie und elektrochemischer Impedanz-Spektroskopie untersucht.

Die Ergebnisse deuten darauf hin, dass die Degradation von CNTs über die oxidative Entfernung von amorphem Kohlenstoff verläuft. Anschließend werden die graphitischen Wände angegriffen und in der Folge Defekte erzeugt. Bei der Oxidation von CNTs entsteht eine Vielzahl an sauerstoffhaltigen funktionellen Oberflächenspezies, deren Bildung einen Grenzwert erreicht, was zu einer Passivierung führt. Die Ergebnisse können den Weg für die Verwendung von kohlenstoffbasierten Katalysatoren in elektrochemischen Anwendungen, wie Wasserspaltung, regenerative Brennstoffzellen und Metall-Luft Batterien ebnen.

Table of Contents

1 Introduction

This chapter presents general information about carbon materials for electrochemical applications relevant to the scope of this thesis. The first part of this chapter describes why carbon is interesting for electrochemical applications. Furthermore, carbon degradation/oxidation is discussed. In the second and third part, promising electrocatalytic applications are introduced in which carbon materials are employed as electrocatalysts. General principles and technical challenges of water electrolysis and fuel cell are elucidated. The focus of the second part is the recent research trend of using carbon-based materials for water electrolysis. While carbon materials are widespread as electrode materials on the cathode, the application of these materials for the anode in water oxidation is a great challenge because of the accelerated carbon corrosion at the high oxidative potentials. In the third part, the principle of the limited performance for fuel cells is elaborated. During the start-up and shut-down of fuel cells, the cathode potential increases and accelerates the kinetics of electrochemical carbon corrosion. The fourth part demonstrates other electrochemical applications in which carbon materials are mostly used; batteries, supercapacitors, and electrochemical sensors.

1.1 Carbon in electrochemistry

Carbon nanostructures feature numerous outstanding intrinsic properties that are attractive for many electrochemical applications; high electrical and thermal conductivity, a large diversity in crystallinity, morphology and porosity, a reasonable corrosion-resistance and low thermal expansion. Moreover, carbon materials are readily available at a relatively low cost [1, 2].

Carbon exists in various allotropic forms, including diamond, graphite, amorphous carbon, graphene, fullerenes and carbon nanotubes (Figure 1.1). The properties of the allotropes strongly depend on the bonding nature of the carbon atoms within the structure. Diamond, which is built up by sp^3 hybridized carbon atoms, possesses excellent

1

mechanical properties and thermal conductivity. In contrast, graphite is an aromatic planar system constituted by sp^2 hybridized carbon atoms with delocalized π electrons that confer a high electrical conductivity along the planes. Graphene, carbon nanotubes and fullerenes are all closely related to graphite and exhibit unique physical and chemical properties. In addition to the wealth of allotropes, the structural unit of carbon materials, which is a stack of layers of carbon hexagons, tends to agglomerate. This results in diverse textures that govern the degree of graphitization, more or less ordered, which can be adjusted according to the particular application needs. Furthermore, carbon materials can be produced in a wide variety of forms, such as powders, fibers, foams, fabrics and composites, thin solid films, and porous sheets. Therefore, the characteristics of carbon materials are very attractive for electrochemical applications [1, 3, 4].
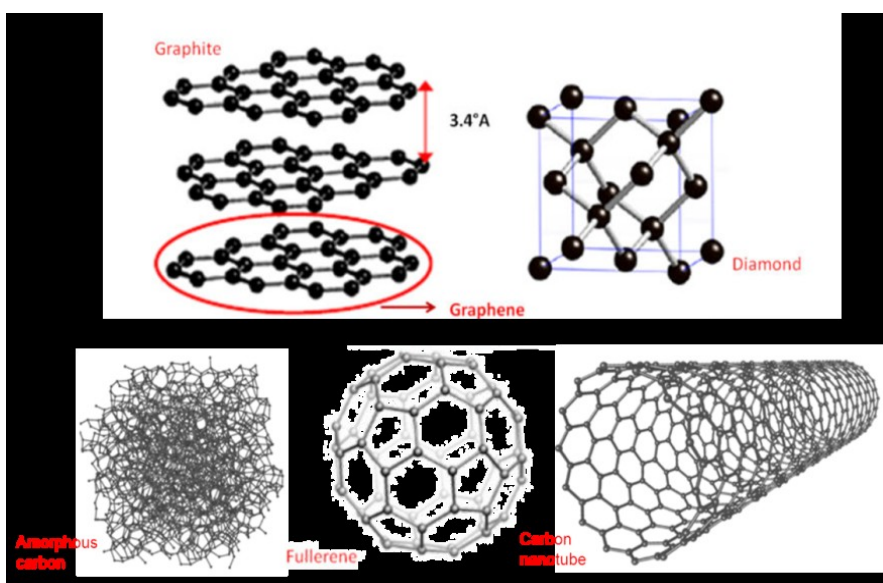
Figure 1.1. Different allotropes of carbon; modified from [5].

Carbon is mainly used as an electrode, either directly as an electrocatalyst itself or as a conductive support for electrochemically active materials [1]. Its textural properties such as porosity and specific surface area affect the accessibility of the electrolyte. A carbon electrode is well polarizable, however, its electrical conductivity depends on the thermal treatment, microtexture, hybridization, and content of heteroatoms [6]. With this respect,

2

the synthesis and post-activation treatment of carbon materials has to be optimized in order to obtain carbon electrodes tailored for particular electrochemical uses [7].

In electrochemical applications, carbon is exposed to a wide range of potentials, to aqueous/nonaqueous electrolytes, to reactive gases, and to ambient temperature. Carbon materials are relatively chemically stable in strongly acidic and alkaline media within a wide temperature range. The practical potential limits for the carbon electrode is usually dictated by hydrogen and oxygen evolution in aqueous solution. The anodic and cathodic potential limits for the carbon electrode depend on different electrolyte and temperature, since carbon corrosion may limit the practical anodic potential. Nevertheless, carbon has a wide potential window compared to other electrode materials. For instance, a graphite electrode can be used at more positive and more negative potentials than platinum in the same electrolyte [1].

Carbon is thermodynamically oxidized to carbon dioxide and monoxide in aqueous solution.

$$C + 2H_2O \rightarrow CO_2 + 4H^+ + 4e^- \qquad E^0 = 0.207 \text{ V} \qquad \text{(Eq. 1.1)}$$

$$C + H_2O \rightarrow CO + 2H^+ + 2e^- \qquad E^0 = 0.518 \text{ V} \qquad \text{(Eq. 1.2)}$$
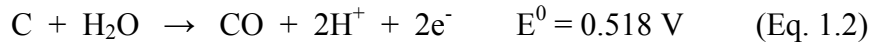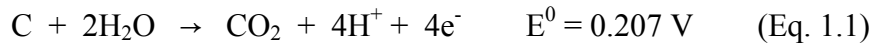
In addition, CO is thermodynamically unstable with respect to CO_2.

$$CO + H_2O \rightarrow CO_2 + 2H^+ + 2e^- \qquad E^0 = -0.103 \text{ V} \qquad \text{(Eq. 1.3)}$$

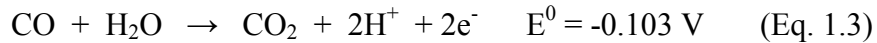The rate of carbon oxidation depends on potential, temperature and time. Since these oxidation reactions are kinetically very slow, they are almost negligible at the potential relevant for the oxygen reduction reaction (below 1.2 V) under normal operation conditions for fuel cells [8]. However, when the anodic potential is high enough for oxygen evolution, carbon corrosion can occur with fast kinetics.

A possible pathway for carbon oxidation begins with the adsorption of oxygen atoms on the surface. Subsequently, oxide species form as reaction intermediates. Finally, the surface oxide is further oxidized and CO_2 evolves (Eq. 1.4), alternatively, also a direct electrochemical oxidation of carbon can take place (Eq. 1.5) [1].

$$\text{Carbon} \rightarrow \text{surface oxide} \rightarrow CO_2 \qquad \text{(Eq. 1.4)}$$
$$\text{Carbon} \rightarrow CO_2 \qquad\qquad\qquad \text{(Eq. 1.5)}$$
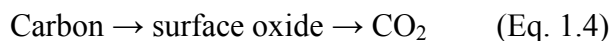
In order to specifically understand the oxidation behavior of carbon, it is necessary to identify the reactive sites at which the oxidation occurs as well as the nature of surface oxides that are produced. Carbon oxidation is initiated at defect sites, such as edges and corners of the basal planes, since these exhibit unsaturated valences and σ-electrons [9, 10]. At crystallographic defects, surface species, i.e. functional groups, are preferentially generated. The nature of surface functional groups on carbon has been investigated with a large number of experimental techniques. These techniques include X-ray photoelectron spectroscopy, temperature programmed desorption, Boehm titration, and Fourier-transform infrared spectroscopy. Due to the limitations of each technique, it is only possible to understand a qualitative analysis of the surface chemistry [1, 11]. It was found that lactones, anhydrides, carboxylic acids, quinones, and phenols are formed by the electrochemical oxidation of carbon. However, the role of surface oxide species on carbon is still unclear. Some of these surface functional groups can be reversibly oxidized and reduced, whereas others can be oxidized irreversibly via an electrochemical process to form gaseous CO_2 [11-13], as shown in Eq. 1.4.

The electrochemical oxidation of carbon, commonly referred to as carbon corrosion, can lead to a loss of structural carbon and to a significant change of the surface properties. Furthermore, it decreases the electrical conductivity, which is associated with the disruption of the aromatic character of the graphitic lattice planes. In addition, carbon oxidation induces an aggregation of isolated metal particles when carbon materials are used for a catalyst support [9, 12]. Consequently, carbon corrosion is considered to be one of the most serious problems when carbon is used as a conductive support for electro-active elements in electrochemical applications.

1.2 Electrocatalytic application of carbon in water electrolysis

One of the ways to efficiently utilize sustainable energy sources is to store hydrogen which is produced by water electrolysis. Hydrogen as an energy source has the advantages of being a low polluting fuel, high combustion heat and abundant sources. Although water electrolysis is a relatively expensive method for hydrogen production, it can produce high purity hydrogen from non-fossil fuels. Therefore, it is regarded as an environmentally friendly technique.

1.2.1 The principle of water electrolysis

Water electrolysis splits water into molecular hydrogen and oxygen using electricity.

$Anode \quad : \quad 2H_2O \ \rightarrow \ O_2 + 4H^+ + 4e^-$ E = 1.23 V vs. SHE   (Eq. 1.6)

$Cathode : \quad 4H^+ + 4e^- \ \rightarrow \ 2H_2$ E =   0 V vs. SHE   (Eq. 1.7)

$Total \quad : \quad 2H_2O \ \rightarrow \ O_2 + 2H_2$ E = 1.23 V vs. SHE   (Eq. 1.8)
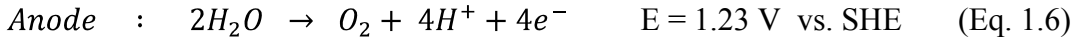
Water is oxidized to oxygen (oxygen evolution reaction, OER) and reduced to hydrogen (hydrogen evolution reaction, HER). The reversible cell potential for this reaction is 1.23 V, which is equivalent to $\Delta G^0 = -2FE = 237.2$ kJ/mol at 25 °C. With consideration of thermal energy in thermodynamics, water is isothermally electrolyzed by applying an electrical energy equivalent to $\Delta H^0 = 285.8$ kJ/mol, that is 1.48 V. This value is independent of the solution pH, but is affected by temperature and gas pressure [14]. The general electrochemical reaction is dependent on pH media of the electrolytes .

<table>
<tr><td></td><td>Acidic media</td><td>Alkaline media</td><td></td></tr>
<tr><td>Anode :</td><td>$H_2O \rightarrow \frac{1}{2}O_2 + 2H^+ + 2e^-$</td><td>$2OH^- \rightarrow \frac{1}{2}O_2 + 2H_2O + 2e^-$</td><td>(Eq. 1.9)</td></tr>
<tr><td>Cathode :</td><td>$2H^+ + 2e^- \rightarrow H_2$</td><td>$2H_2O + 2e^- \rightarrow H_2 + 2OH^-$</td><td>(Eq. 1.10)</td></tr>
</table>
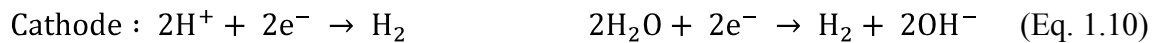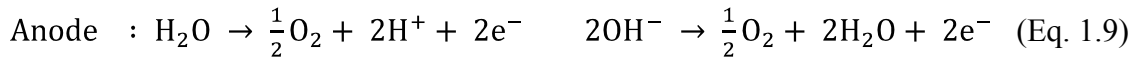
The detailed reaction mechanism for water electrolysis possesses various pathways, which are to a wide extend not known in so far. The cathodic reaction shows relatively ideal kinetics on noble metal electrodes, whereas the anodic reaction has slow kinetics due to the complexity of managing four electrons and protons to evolve one oxygen molecule. For this reason, the anode requires a significantly higher overpotential to carry out oxygen evolution at reasonable rates (Figure 1.2). Herein, OER dominates the overall cell performance for electrocatalytic water splitting [15].
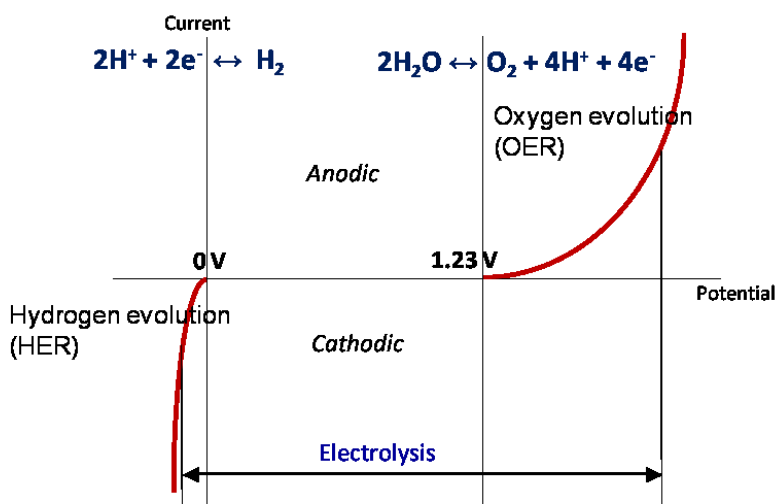
Figure 1.2. A schematic diagram for electrocatalytic water splitting.

1.2.2 Technical challenge - oxygen evolution reaction (OER)

The oxygen evolution involves four electrons and is more complex compared to hydrogen evolution where only two electrons are transferred. OER is a multiple-step process involving the formation of both oxygenated intermediates and surface oxides. A variety of reaction pathways has been proposed for the OER that depends on the electrocatalyst and experimental conditions.

Trasatti has suggested a volcano curve for OER catalysts using the relationship between the OER overpotential and the strength of the metal-oxygen bonds in the surface oxide (Figure 1.3) [16]. RuO_2 and IrO_2 have the lowest overpotentials and the optimized bond strengths which mean that oxygen atoms are easily adsorbed and released on the surface. Materials to the left of the volcano plot maximum represent a relatively weak metal-

oxygen bond, whereas materials to the right like Co_3O_4 and Fe_3O_4 are easily oxidized and strongly bound with oxygen so that the desorption of gaseous oxygen is kinetically limited. In addition, Trasatti emphasizes that oxygen evolution can only proceed when the electrode potential is higher than the potential of the metal/metal oxide couple [14, 16, 17].
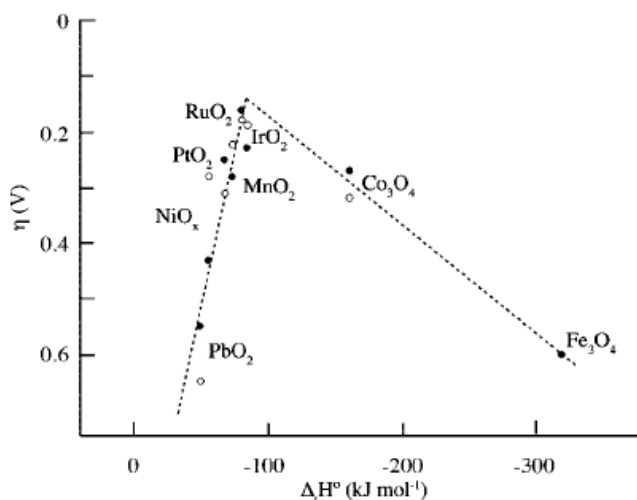
Figure 1.3. Electrocatalytic activity in O_2 evolution at various oxide electrodes as a function of the enthalpy of the lower → higher oxide transition. (○) alkaline and (●) acid solutions [16, 18].

1.2.3 Oxygen evolution electrocatalysts

Electrocatalysts for oxygen evolution are usually noble metal (e.g., Pt, Au, Ir, Rh, Ru, Ag), but their metal oxides are more active than the corresponding metals [19, 20]. Pt is a relatively poor electrocatalyst for oxygen evolution, in contrast to its high electrocatalytic activity for oxygen reduction. This probably originates from a poorly conductive platinum monooxide layer, which forms during the OER. Ru and Ir form conductive metallic oxides and thus have been used as OER electrocatalysts. Ru oxide is the best catalyst for oxygen evolution, but thermodynamically unstable due to a possible formation of higher valent Ru oxides, so it forms corrosion products at high anodic potentials. Ir oxide exhibits a strong resistance to corrosion during oxygen evolution, but possesses lower activity than Ru [16, 18]. Dimensionally stable anodes (DSAs), which

7

typically consist usually of RuO_2 and/or IrO_2 on a Ti substrate, have been developed and established as the anode material in industrial electrochemical processes such as water electrolysis and the chlor-alkali process [21]. For the electrode stability, other metal oxides e.g. TiO_2, SnO_2, Ta_2O_5, ZrO_2 are added to DSAs [22, 23].

The oxides of first row transition metals, in particular Ni and Co, possess the desirable electrocatalytic activity for oxygen evolution. However, their use is restricted as a consequence of corrosion problems. Co, Ni, Mn and Fe based complex oxides and crystal structures have been considered to improve the OER activity and stability in alkaline media [24-26].

Recently, nanostructural catalysts have been studied for the OER. The particle size and shape of the catalyst can determine the surface area and active sites for oxygen evolution. Krtil et $al.$ have studied RuO_2, $Ru_{1-x}Co_xO_2$ and $Ru_{1-x}Ni_xO_{2-y}$ with respect to the effect of size and shape of nanoparticles in acidic media. They reported that the crystal edges on the prismatic part of RuO_2 nanocrystals are the primary sites for the recombination of surface oxygen. The OER activity is independent on the particle size, but is affected by adding Co and Ni [27-29]. Lee et $al.$ reported that rutile RuO_2 and IrO_2 nanoparticles (~ 6 nm) shows high intrinsic specific activity as well as OER mass activity in both acidic and alkaline media [30]. Tilley et al. have reported the size dependence of cubic nanoparticles of Co_3O_4 as OER active materials in alkaline media. An increase in the surface area of the catalyst due to the controlled particle size increases the OER activity [31].

Nocera et al. observed that Co-phosphate (Co-Pi) bulk catalysts electrodeposited in a cobalt nitrate/phosphate buffer solution shows a promising water oxidation activity in the neutral and mildly basic pH regime [32, 33]. This Co-Pi has a self-repair mechanism which involves the dissolution/redeposition of Co ion during oxygen evolution. Furthermore, Ni-borate catalysts deposited from nickel/borate buffer solution were reported [34]. They suggest that these catalysts deposited on semiconductor materials, such as indium tin oxide (ITO) and fluorine-doped tin oxide (FTO), can be used under mild conditions and at current densities commensurate with a non-concentrated solar photovoltaic cell.

1.2.4 Oxygen evolution catalyst supports

Bulk catalysts have a limited surface area for electrochemical activity, so catalyst supports are used to increase the active surface area of the catalysts. A catalyst support provides a physical surface for the dispersion of small particles, which is necessary for high surface area and electrical conductivity. Therefore, it could improve the catalytic efficiency due to the better catalyst utilization and the reduction of the catalyst loadings. However, supported OER catalysts are difficult to apply in water electrolysis because of the highly corrosive condition. From the point of view of the electrocatalytic efficiency, the electrochemically stable materials for catalyst supports have been studied for the OER.

Ma *et al.* prepared Ir supported on TiC for oxygen evolution in acidic media and found that supported Ir is more active and stable than unsupported Ir [35]. Weidner *et al.* reported Pt, Ru, and Ir supported on anatase and rutile TiO_2 for oxygen evolution in acidic media [36]. They insist that the high surface area of TiO_2 can be sufficiently conductive for electrocatalytic applications. Electrically conductive Ti suboxides have been applied to water electrolysis and the oxygen electrodes for utilized regenerative fuel cells (URFCs) [37]. Sb doped SnO_2 (ATO) has been used as a catalyst support for IrO_2 and RuO_2 [38, 39]. Although these materials show a high stability in an OER environment and acceptable electrical conductivity, most of them have a low surface area, resulting in poor metal dispersion and a low electrocatalytic activity. Moreover, some of the conducting metal oxides are not chemically inert, and often degrade to higher oxides.

Boron doped diamond (BDD) is a well-known support for noble metal oxide films. Diamond possesses morphological stability and corrosion-resistance under both acidic and alkaline conditions without any structural degradation. However, the anchoring of a metal on BDD surface and surface area has to be improved [40].

1.2.5 Carbon in oxygen evolution catalysts

Since dimensionally stable metal oxide anodes (DSAs) have been developed, technical interest in carbon anodes for electrolytic processes such as water/brine electrolysis and

9

chlorine-alkali industry has diminished [41]. Recently, a large effort on the efficient utilization of sustainable energy aroused interest in the use of carbon-based materials for water electrolysis, with the aim of overcoming the costs involved in the production of conventional electrodes. Furthermore, the exploitation of many interesting carbon structures; like graphene, carbon nanotubes and mesoporous carbon, has raised the possibility of carbon-based materials to be used for water electrolysis. Hence, the applications of various structures of carbon for the OER have been the subject of recent research.

In principle, carbon as an electrode material for OER is not stable enough due to the issues of carbon corrosion. However, carbon materials possess high electrical conductivity and tunable surface area, and a relatively low cost compared to other materials such as conducting metal oxides. Carbon supported catalysts provide an enhanced electrocatalytic activity for the OER compared to a bulk catalyst.

It is well-known that nitrogen-doped carbon is active for the oxygen reduction reaction (ORR) in alkaline media. Furthermore, Zhao *et al.* reported that oxygen evolution as a reverse reaction of oxygen reduction can be also activated on nitrogen-doped carbons [42]. Nitrogen doped carbon nanomaterials, which are pyrolyzed from the hybrid of a melamine/formaldehyde polymer and nickel nitrate, show high oxygen evolution activity and are comparable to iridium and cobalt oxide catalysts. This startling finding leads one to expect the possibility of efficiently using non-noble oxygen evolution electrocatalysts. However, since the authors of this finding do not distinguish oxygen evolution and carbon oxidation, their conclusions bring the reported intrinsic OER activity of nitrogen doped carbon into question.

Strasser *et al.* [43] compared the intrinsic catalytic activity and stability of carbon supported Ru, Ir, and Pt nanoparticles for the OER in acidic media. They used carbon black as the catalyst support. Ru nanoparticles on carbon show the highest OER activity, but they are not suitable as a practical OER catalyst due to a low stability. Pt/C suffers from the additional deactivation under OER conditions. Ir/C exhibits the most practical activity and stability combination for the OER compared to bulk catalyst.

Toma *et al.* [44, 45] reported that the polyoxometalate anion, which is a molecular catalyst for water oxidation, in combination with multiwall carbon nanotubes

(MWCNTs) shows good activity for the OER in neutral media. The MWCNTs improve the electrical contact between the redox-active center and the electrode surface.

Mette *et al.* [46] observed a promising OER activity on MnO_x supported on CNTs in neutral media. Owing to the CNTs support, a relatively low amount 5 wt.% of MnOx shows an enhanced OER activity. Furthermore, distinct differences in the oxidation state of the Mn centers and structures in Mn oxides on the carbon support affect the water oxidation [47].

Dai *et al.* [48] prepared Co_3O_4 nanocrystals on graphene for a bi-functional catalyst, that performs oxygen reduction and evolution in alkaline media. Although Co_3O_4 or graphene oxide alone has little catalytic activity, their hybrid exhibits unexpectedly high ORR and OER activities that arise from a synergetic chemical coupling effect. Furthermore, recently Dai *et al.* reported another catalyst, ultrathin nickel−iron layered double hydroxide (NiFe-LDH) nanoplates on mildly oxidized multiwalled carbon nanotubes (CNTs) [49]. The crystalline NiFe-LDH phase in nanoplate form exhibits higher electrocatalytic activity and stability for oxygen evolution in alkaline media than commercial precious metal Ir catalysts. With the high intrinsic activity on the crystalline structure, the underlying CNT network enhances electron transport and facilitates high OER activity of the NiFe-LDH nanoplate/CNT complex.

1.3 Electrocatalytic application of carbon in fuel cells

Fuel cells are the electrochemical systems that convert a fuel with oxygen as the oxidant gas directly into electrical energy and heat with high efficiencies. There are several types of fuel cells, classified by on the operating principles and conditions. Proton exchange membrane fuel cells (PEMFCs) are based on a proton conducting polymer electrolyte membrane.

1.3.1 The principle of PEM fuel cells

The basic principle of fuel cells is the reverse process of water electrolysis, illustrated the following equations;

$Anode$: $2H_2 \rightarrow 4H^+ + 4e^-$ $\quad\quad$ E = 0 V vs. SHE $\quad$ (Eq. 1.11)

$Cathode$: $O_2 + 4H^+ + 4e^- \rightarrow 2H_2O$ $\quad\quad$ E = 1.23 V vs. SHE $\quad$ (Eq. 1.12)

$Total$: $O_2 + 2H_2 \rightarrow 2H_2O$ $\quad\quad$ E = 1.23 V vs. SHE $\quad$ (Eq. 1.13)
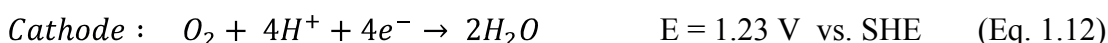
Hydrogen gives up electrons and protons (Hydrogen oxidation reaction, HOR). The protons migrate to the electrolyte, and the electrons are forced through an external circuit to produce an electrical current. Oxygen accepts the electrons and the protons to form water (Oxygen reduction reaction, ORR). Both reactions are accelerated by platinum-based catalysts [50].
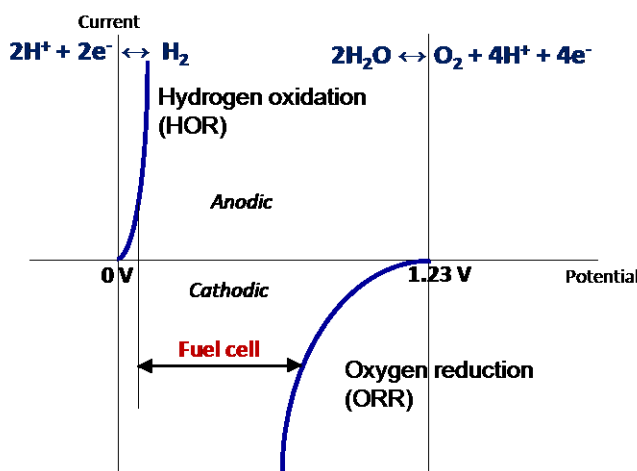

Figure 1.4. A schematic diagram for fuel cells.

The thermodynamically predicted overall potential of a fuel cell is 1.23 V at zero current (open circuit potential, OCV). As the temperature rises from room temperature (25 °C) to a operating condition (80 °C), the maximum cell voltage decreases from 1.23 V at 25 °C to 1.18 V at 80 °C [51]. However, the reversible cell voltage is not realized during the fuel cell operation. The polarization curve, which is the plot of the cell potential versus the current density, represents the performance of a fuel cell, as shown in Figure 1.5. The OCV of the cell is generally lower than its thermodynamic value as a result of mixed potential at the electrodes due to unavoidable parasitic reactions, mainly at the cathode. The cell voltage decreases with increasing current density. This irreversible phenomenon arises from electrochemical kinetic limitations at the electrode surface (activation overpotentials, η_a), mass transport or concentration losses that result from the change in concentration of the reactants at the electrode surface as a function of the reaction rate (concentration overpotentials, η_c), and ohmic losses in the ionic and electronic conductors [50]. It is believed that the activation overpotential for the ORR is much higher than that of the HOR due to the slow kinetics of oxygen reduction. Therefore, much research has been directed toward the improving the efficiency of the electrocatalyst for oxygen reduction.
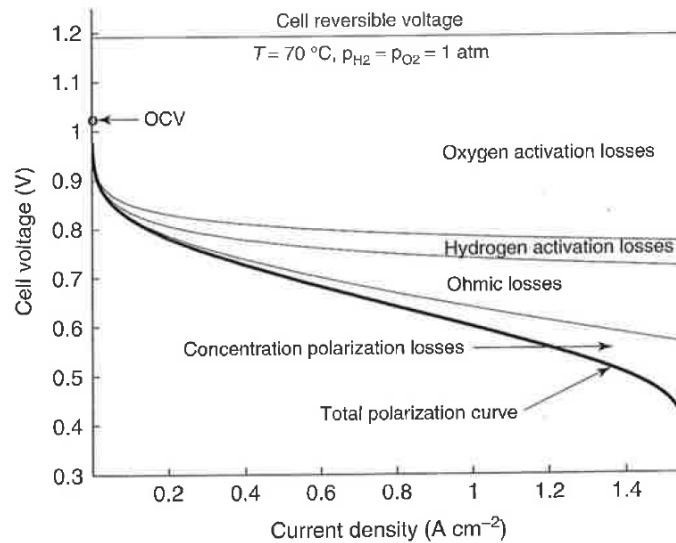

Figure 1.5. Typical polarization curve of fuel cells [50].

1.3.2 Technical challenge – cathode stability

The cathode reaction in fuel cells, i.e. the oxygen reduction reaction (ORR), is a key issue for the overall performance of fuel cells. Owing to the sluggish kinetics of the ORR, a high metal loading of a Pt catalyst is required compared to the anode.

Although Pt has a low solubility, Pt dissolves in the presence of oxygen which is the case at the cathode in fuel cells. Pt dissolution leads to particle sintering due to Oswald ripening, coalescence and particle migration [8, 52]. The agglomeration of Pt nanoparticles to bigger particles results in the loss of Pt active surface area, and consequently a performance degradation of fuel cells [53]. Since Pt is usually very stable even in acidic media, Pt dissolution has not been considered seriously in normal operating conditions (below 1 V vs. RHE). However, the degradation of catalysts can be exacerbated under abnormal operating conditions, such as start-up and shut-down in fuel cell vehicles.
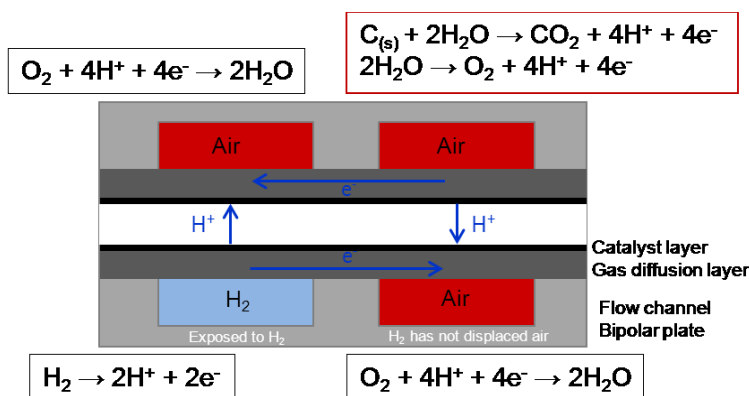
Figure 1.6. Schematic diagram of fuel flow path and electrode reactions during shut-down/start-up of Fuel cells; "reverse current" conditions.

Under prolonged shut-down, all areas of both the anode and the cathode are filled with air. In this case, when hydrogen is supplied into the anode by start-up, the inlet section is only in hydrogen whereas the outlet section is still in air. In the region where hydrogen is absent, i.e. hydrogen starvation at the outlet section, this gas distribution at the anode increases the local potential difference in excess of 1.8 V vs. RHE, resulting in carbon corrosion and oxygen evolution at the cathode (Figure 1.6) [8, 54]. As a result, the start-

14

up/shut-down cycling induces significant damage to the cell. The corrosion caused from carbon oxidation creates not only a loss of electrical contact, but also the detachment/agglomeration of Pt particles on the carbon support. Therefore, many researchers have made substantial efforts to minimize the rate of the electrochemical oxidation of carbon for the cathode in fuel cells [8, 55].

To increase the corrosion-resistance of carbon supports, graphitization of carbon is considered to improve the stability of fuel cells [56, 57]. Graphitic carbon is kinetically more resistant to oxidation than amorphous carbon. Figure 1.7 shows a mass spectrometry measurement performed during CO_2 formation using Pt supported on graphitized carbon (G-Pt/C) and Pt supported on non-graphitized carbon. G-Pt/C shows a substantial reduced CO_2 generation.
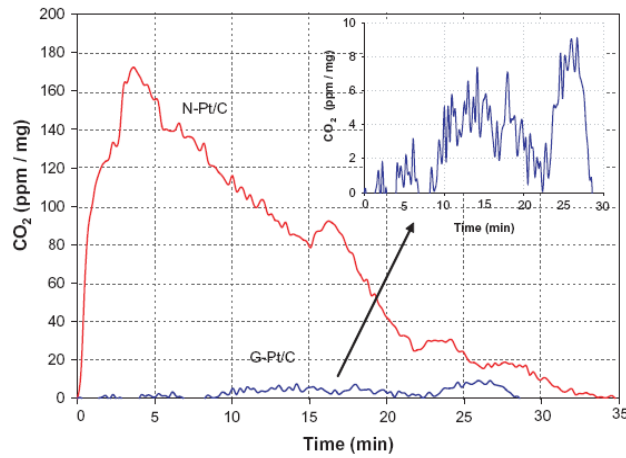
Figure 1.7. CO_2 mass spectra profile with Pt supported on non-graphitized carbon (N-Pt/C) and Pt supported on graphitized carbon (G-Pt/C) at 1.4 V in single cell for fuel cells [56].

In conclusion, the degradation of carbon materials at high potential accompanying oxygen evolution reaction should be considered in water electrolysis as well as fuel cells. However, while carbon corrosion in fuel cells has been examined vigorously, the literature on the corrosion of carbon anodes in water electrolysis has been, in comparison, almost nonexistent in the past several years.

1.4 Other electrochemical applications of carbon

Other representative applications of carbon in electrochemistry are batteries, supercapacitors and electrochemical sensors. Their performances are strongly influenced by the physicochemical properties of carbon materials. Therefore, the discovery of novel carbon structures boosts the development of their applications.

Batteries: Batteries convert chemical energy directly into electrical energy. The energy and power in batteries are dependent on the quality and characteristics of the materials used to construct the cell. Carbon is used as an electrode or as an additive to improve the electronic conductivity in batteries. For example, in Li-ion batteries, the carbon anode intercalates/deintercalates Li ions in and out of the carbon structure upon charge/discharge. Moreover, carbon materials are considered to be used as electrocatalysts and/or supports for bifunctional air electrodes in metal/air batteries to develop a low cost electrode [17]. The recent interests in batteries for environmentally-friendly electrical vehicles and efficient storage of renewable energies require higher energy and power density, safety, and cycle life. The development of carbon nanotubes and graphene is able to meet the required high energy density for advanced Li-ion batteries, thus much research has been progressed on this field [2-4, 7].

Supercapacitors: Supercapacitors are an energy storage system with high energy and power density. They are usually adapted for the applications that require energy supplies for few seconds. Supercapacitors consist of two identical electrodes immersed in an electrolyte. When the electrode is biased, the ions of opposite charge are accumulated on the electrode surface. Supercapacitors are classified by electrochemical double layer capacitors (EDLCs) and pseudocapacitors, depending on the charge storage mechanism. EDLCs are operated by adsorbing/desorbing charged ion from an electrolyte onto the surface of the electrodes, and are proportional to the electrode surface area. On the other hand, pseudocapacitors are obtained from the faradaic charge transfer reaction between the electrode and the electrolyte. A pseudocapacitive contribution is observed in conducting polymers, metallic oxides and carbon-riched with heteroatoms (nitrogen and

oxygen). In order to enhance the performance of supercapacitors, many researches have been worked on the increase of surface area, the surface functionalization of carbon and/or the coating the carbon materials with conducting polymers such as polyanilline and polypyrrole or transition metal oxides such as manganese oxides [3, 4, 6].

Electrochemical sensors: Electrochemical sensors and biosensors are analytical devices that convert the electrochemical response of the analyte into an electrical signal. The electrochemical potential window, the electron transfer rate and redox potentials are considered for the optimal performance of the sensors. The electrode requires favorable electrochemical properties such as fast electron transfer and good reproducibility [58, 59]. Carbon-based nanomaterials have been widely used in electrochemical sensors due to their excellent catalytic activity, superior conductivity, large surface area, ease of functionalization and biocompatibility [60]. Especially nanostructured carbon materials promote electron transfer in electrochemical reactions. For example, carbon nanotubes show fast electron transfer kinetics due to the activity of edge-plain-like graphite sites at the CNT ends. Furthermore, the existence of functional groups on the carbon surface facilitates electron transfer [61]. It has been reported that the modified CNT electrodes exhibit the promising sensitivity for glucose, dopamine, ascorbic acid, uric acid, norepinephrine, NADH and hydrogen peroxide [62, 63]. Of late, graphene has been also considered as a promising material for sensors. The unique electronic structure of graphene and carbon nanotubes is beneficial for fast electron transfer [59, 60].

2 Scope of the work

This chapter describes the specific background and approach of this PhD-project, derived from the background information in Chapter 1. The first part describes the main idea and the motivation for this thesis based on the recent research trend of carbon-based energy conversion and storage technologies. Experiments involving the carbon materials which are described in this thesis; carbon nanotubes are described in second part. The third part gives a general overview of the thesis.

2.1 Motivation

Renewable energy from intermittent sources such as solar and wind, needs to be stored or converted into continuously available energy. The conversion of these sources into hydrogen and oxygen by electrocatalytic water splitting will possibly be a key technology and an environmentally friendly solution for the global energy crisis. Hydrogen as an energy carrier can be supplied to fuel cells or used to reduce CO_2 to valuable organic chemical compounds [64].

One of the major challenges for water splitting is the oxygen evolution reaction (OER), which has a larger overpotential than the hydrogen evolution reaction (HER). OER also occurs at highly anodic potential and corrosive environment. For this reason, extensive efforts have been made to find effective electrocatalysts which provide high OER activity with a low overpotential. The oxides of Ru and Ir are considered as the best OER catalysts, and are usually unsupported due to an oxidizing condition. However, the use of catalyst supports can reduce the loading of noble metal catalyst and improve catalytic efficiency due to higher electrical conductivity, high surface area and better utilization via metal dispersion.

Carbon materials have been used as a catalyst support for most electrochemical reactions because of its high conductivity and suitable porous structure. Nevertheless, the electrochemical oxidation of carbon is inevitable for carbon supported catalysts under the OER conditions. The corrosion caused from carbon oxidation creates a loss of electrical

contact necessary for electron transfer. Despite these limitations, carbon is still promising as the catalyst support for water electrolysis [1]. Compared to other alternative support materials, carbon is abundant, highly conductive and available at relatively low cost. Moreover, it has a high surface area and provides better metal-support interactions than conducting metal oxides. Hence, current interest in the efficient utilization of sustainable energy arouses the potential application of carbon materials for water electrolysis to overcome higher-priced techniques [26, 43-46, 48, 49].

This project aims to explore the possible application of the carbon supported catalyst for oxygen evolution in electrocatalytic water splitting. When the electrode is operated at the potential above the equilibrium potential of water oxidation the anodic current is expected to contribute to only OER, but all other possible reactions cannot be totally ruled out. Figure 2.1 illustrates the overpotentials for the oxygen evolution reaction (η_{OER}) and the carbon oxidation reaction (η_{COR}) when the supported catalyst is at the highly anodic potential which is above the thermodynamic potential for oxygen evolution. Carbon can be thermally oxidized at 0.207 V, as described in chapter 1.1. The reaction for carbon oxidation has very slow kinetics, thus it is not serious under the typical potential for oxygen reduction below 1.2 V. However, under OER conditions the driving force applies to carbon electrochemical corrosion. When the potential above 1.23 V is supplied to get a certain current (i_p) for oxygen evolution on the carbon supported catalyst, the overall faradaic current is likely to have a significant contribution to the carbon oxidation reaction (COR) besides OER. The reactions of both water and carbon are competitive on the carbon supported catalyst under the condition for water splitting.
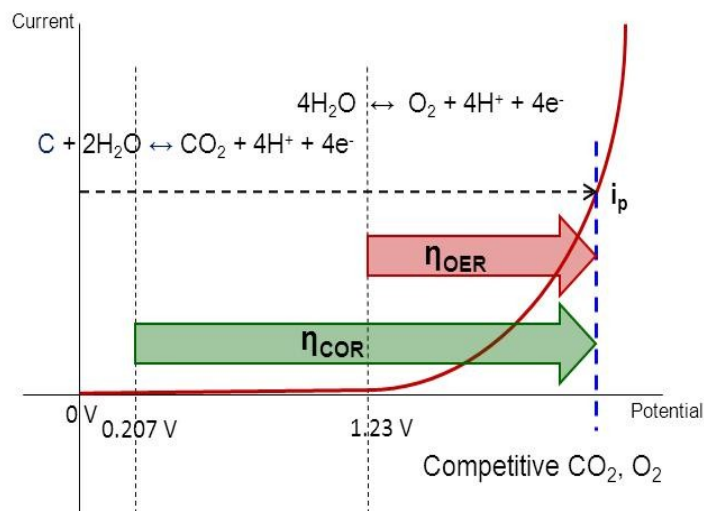
Figure 2.1. The overpotential for oxygen evolution and carbon oxidation at an anodic potential for water electrolysis.

Furthermore, when carbon materials are used as the catalyst support for the anode in water electrolysis, several possible reactions occur at the surface of the electrode. Figure 2.2 describes some of representative reactions which can be simply assumed. Owing to the electrochemical oxidation of carbon, the carbon support forms oxygen-containing surface functional groups which either stay on the surface or are further oxidized to gaseous products. Moreover, the carbon oxidation produces gaseous CO and CO_2. CO is thermodynamically unstable, so it is directly further oxidized to CO_2. Water is oxidized to gaseous O_2 on a (oxidized) metal as well as the carbon support. It can additionally lead to the dissolution of the supported metal or metal oxide species [20]. Depending on the kind of the supported metal and metal oxide, the carbon oxidation can be accelerated by Pt [65], and be inhibited by Ru and Ir [55].

Figure 2.2. Some of representative reactions occurring on carbon supported catalyst at high anodic potentials for water splitting.

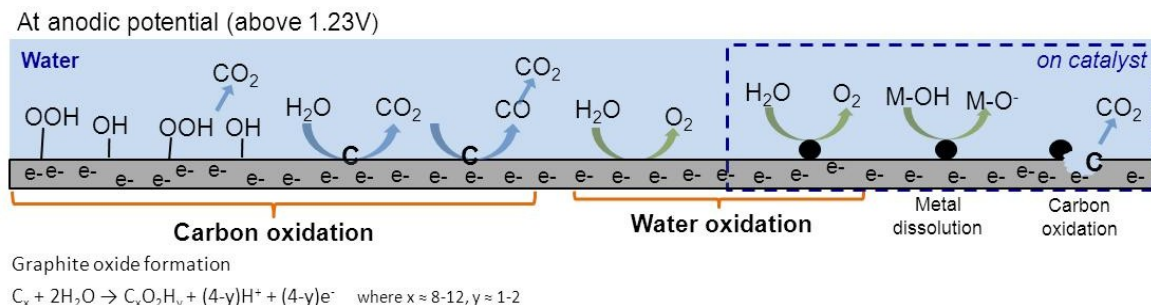The intention of this thesis is to understand the degradation of carbon materials under the oxidizing conditions. First of all, the electrochemical degradation of carbon at a high anodic potential for OER was examined. The behavior of carbon materials in the OER environments can be a background phenomenon for carbon supported catalysts for OER. The change in the physicochemical properties of carbon during the degradation could provide the possibility of carbon materials for the electrochemical application involving oxygen. Secondly, thermal oxidative degradation of carbon was explored to compare with the electrochemical degradation. The thermal oxidation of carbon also limits a catalytic reaction at a high temperature in an oxidative atmosphere. Furthermore, the effect of thermal oxidative treatment for the electrochemical activity and stability under OER conditions was investigated. It could turn out the major factors for the electrochemical degradation. Through the understanding of the progress of both degradations, the limitation of carbon oxidation for the applications would be effectively controlled and further possible utilization of carbon materials comes out for the electrocatalytic applications.

2.2 Materials – carbon nanotubes

In this thesis, carbon nanotubes (CNTs) have been selected as a specimen to examine the degradation under highly oxidizing conditions. CNTs are one-dimensional (1D) tube structures formed by rolling up one graphene sheet or wrapping concentric cylinders. Since they are a well-defined graphitic structure, the structural changes of carbon during the degradation can be clearly monitored.

CNTs are the most promising of all nanomaterials and demonstrate excellent properties relevant to electrochemical applications [2, 3, 62, 66]. Particularly, the electrochemical behavior of CNTs has been likened to that of highly oriented pyrolytic graphite (HOPG). The side walls of a CNT are equivalent to the basal plane of graphite; and the open ends of CNTs are like the edge-plane-steps on the HOPG surface. The electrochemical response of CNTs suggests that the sidewalls of multiwall carbon nanotubes (MWCNTs) are essentially inert, and open ends and defect sites are responsible for the electrochemical activity observed [66]. This unique structure of CNTs could influence high activity and stability in electrochemical systems.

CNTs exhibit many interesting features for electrocatalysts, owing to the high electronic conductivity in individual graphene sheets and fast electron transfer on the sidewall. Therefore, CNTs can improve the catalytic activity for electrochemical reaction as providing superior corrosion-resistant as compared to other carbon structures, such as carbon black. The rolled graphene sheets with fewer defects prevent the attack of oxidative species on the closed structure, resulting in significantly improved resistance to carbon corrosion [53, 67].

In practice, Pt supported on CNTs improves the activity and stability for fuel cells compared to Pt supported on carbon black. As a result of high corrosion resistance, CNTs as the catalyst support shows less loss of Pt active surface area and the improved oxygen reduction reaction (ORR) activity [68-70]. Furthermore, recent research reported that the varying degrees of functionalization on single wall carbon nanotubes (SWCNTs) could reduce the Pt loading on the support [71].

Commercial MWCNTs (Baytube, Bayer Material Science AG, Germany) used in this work were synthesized using a chemical vapor deposition (CVD). As-received MWCNTs

contain carbonaceous impurities and metal catalyst particles. Since these impurities affect the properties of the CNTs, it is important to remove them from the MWCNTs. Purification with nitric acid is a common method to remove metal and carbon impurities from the MWCNTs. However, this method creates the density and type of surface functional groups and damages carbon structures. In this work, multi-step purification processes of the MWCNT samples were used under mild conditions to minimize structural damages. A nitric acid treatment was carried out using dilute nitric acid to eliminate metal catalysts from the MWCNTs. An ultrasonic treatment allows the weakly attached amorphous carbon to detach and further decompose into organic fragments via pyrolytic and/or oxidative pathways. An alkaline solution washing step improved the dissolution of oxidized amorphous carbon and oxidation debris [72, 73].

2.3 Overview of this thesis

The present work contributes to the understanding of the degradation of MWCNTs in oxidative environments. In order to explore the variation of morphology and physicochemical properties of MWCNTs during the degradation process, the MWCNT samples were further characterized.

The electrochemical oxidative degradation of MWCNTs is dealt with in Chapter 3. The electrochemical oxidation of MWCNTs was carried out at the high anodic potential accompanying carbon oxidation and oxygen evolution. During the electrochemical oxidation of MWCNTs, the variation of electrochemical properties, such as the electrochemical response of electron transfer, specific capacitance, oxidation activity and complex resistance, was monitored using electrochemical measurements.

The thermal oxidative degradation of MWCNTs is discussed in Chapter 4. MWCNTs were thermally oxidized at the temperature at which combustion starts in an oxidative atmosphere. Thermal behavior of the MWCNT samples was characterized using temperature programmed desorption and oxidation. Depending on the thermal oxidative treatment, the effect on electrochemical properties is also demonstrated by electrochemical characterization.

The summary and outlook part in Chapter 5 provide a comparison of the electrochemical and the thermal oxidative degradation of MWCNTs. Moreover, future work based on this research is presented.

3 Electrochemical degradation of multiwall carbon nanotubes (MWCNTs) at high anodic potential in acidic media

Youngmi Yi, Chinmoy Ranjan, Elena Willinger, Marc Willinger, Julian Tornow, Robert Schlögl

Abstract

A great interest in the efficient utilization of sustainable energy makes the potential application of carbon-based materials for water splitting attractive to overcome higher-priced techniques. However, carbon is limited as a catalyst support for the oxygen evolution reaction (OER) due to the electrochemical oxidation of carbon. In this study, we investigated the electrochemical degradation of multiwall carbon nanotubes (MWCNTs) under OER conditions in acidic media. Electrochemical oxidation of MWCNTs induces structural changes and the formation of oxygen-containing functional groups on the carbon surface. Hence, the electrochemical and physicochemical properties of the MWCNTs are changed during the electrochemical oxidation. Through a combination of electrochemical, microstructural and spectroscopic methods, we explore how MWCNTs electrochemically degrade. Through a better understanding of this degradation process, we find that it is possible to tune the electrochemical properties of MWCNTs and use them more effectively in electrochemical applications.

3.1 Introduction

Storage strategies for energy derived from renewable energy sources, such as solar, wind and geothermal, have received much attention. One such strategy involves the generation of hydrogen by electrocatalytic water splitting. The chemical energy stored in the hydrogen can be converted directly to electricity by means of fuel cells. As an alternate strategy, hydrogen can be used to reduce CO_2 into organic compounds that serve as energy carriers.

Oxygen evolution reaction (OER) is a core challenge for electrocatalytic water splitting, since it has a large overpotential and occurs in a highly oxidizing environment. Hence, an efficient electrocatalyst with suitable activity and stability is required. Preferably, such a catalyst would possess a lower noble metal content, as a stable support would allow for better dispersion and stabilization of the active phase. However, the development of an inexpensive non-noble metal catalyst would present an ideal solution [15, 46, 64].

Carbon materials are commonly used as electrocatalyst supports because of their high electrical conductivity and surface area, as well as their wide variety of structural and chemical properties. However, using carbon in electrochemistry as an electrode is limited because of the electrochemical oxidation of carbon. Carbon can be thermodynamically oxidized to carbon dioxide (Eq. 1) and monoxide (Eq. 2) [1].

$$C + 2H_2O \rightarrow CO_2 + 4H^+ + 4e^-, \ E^0 = 0.207 \text{ V vs. SHE} \quad \text{(Eq. 1)}$$
$$C + H_2O \rightarrow CO + 2H^+ + 2e^-, \ E^0 = 0.518 \text{ V vs. SHE} \quad \text{(Eq. 2)}$$
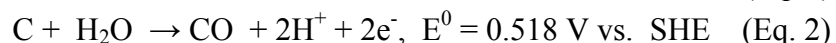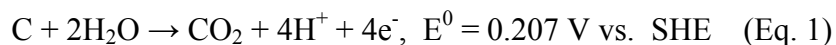
Since the kinetics of carbon oxidation is very slow, carbon can be applied without serious problems. However, when the anodic potential is high enough for oxygen evolution above 1.23 V (vs. SHE), carbon oxidation can occur with fast kinetics. This problem is exacerbated with high surface area carbon, which is more susceptible to corrosion. Thus, the studies on the electrochemical oxidation/corrosion of carbon in an aqueous solution have been focused on fuel cells and metal-air batteries [9, 10, 74, 75]. In fuel cells operation, carbon corrosion is facilitated on the cathode under abnormal conditions for start-up and shut-down [70]. Therefore, many researchers have made substantial efforts to minimize the rate of the electrochemical oxidation of carbon [8, 55]. While carbon

corrosion in fuel cells has been examined vigorously, the literature on the corrosion of carbon anodes during oxygen evolution has been, in comparison, almost nonexistent in the past several years. The loss of interest in this field likely resulted from the replacement of graphite by dimensionally stable anode (DSA) electrode in the chlor-alkali industry. Although the use of carbon is limited under the OER conditions, it is an economically competitive material for an electrocatalyst support compared to metal oxides to achieve effective performance in a water electrolyzer. Very recently, carbon-based catalysts for water electrolysis have received attention in the research [26, 43-46, 48, 49].

In the last several decades many different types of carbon structures such as carbon nanotubes/fibers, graphene, etc were discovered [7, 76]. Their electrochemical activity has been reported in several articles, whereas the electrochemical stability is rarely mentioned. Understanding the electrochemical degradation of these carbon materials is useful to enhance and influence the application of carbon electrodes in electrochemical systems. MWCNTs were chosen in this work for electrochemical oxidation. It is well known that MWCNTs exhibit excellent electrochemical activity and stability in electrochemical applications because of their unique structure and intrinsically superior properties. For example, Pt supported CNTs displays higher performance for fuel cells than carbon black. Moreover, CNTs are likely to be more corrosion-resistant than carbon black [77-79]

The intention of the present work is to study the electrochemical degradation of MWCNTs under the higher anodic potential conditions of OER in an acidic environment. We focus on the change in electrochemical and physicochemical properties of MWCNTs by electrochemical oxidation rather than the mechanism of carbon oxidation. The structural change of rolled graphene sheets of the MWCNTs can be clearly examined by electrochemical oxidation/corrosion. The electrochemically oxidized MWCNTs were investigated by electron microscopy, Raman spectroscopy, and infrared spectroscopy to analyze the morphological and structural changes. Furthermore, electrochemical characterization, including cyclic voltammetry (CV), linear sweep voltammetry (LSV) and electrochemical impedance spectroscopy (EIS) were performed to investigate the electrochemical behavior of the MWCNTs during electrochemical oxidation.

3.2 Experimental

3.2.1 MWCNT purification

The commercial MWCNTs (Baytube) provided by Bayer Material Science were purified with the established method as in previous studies [73]. The MWCNTs were treated with 3 M HNO_3 at room temperature for 24 hours under stirring conditions, followed by filtration and washing with water to remove catalyst particles involved for the growth of MWCNT. The obtained black solid was dispersed in ethanol and sonicated with a Titanium tip sonicator (Bandolin sonopuls 10% power, 5 cycles per second) for 3 hours under stirring to remove carbonaceous impurities. Afterward the MWCNT suspension was treated with 1 M NH_4OH at 70 °C while stirring for 2 hours, was subsequently filtered, and twice subjected to 24 hour soxhlet extraction with water and another 24 hour soxhlet extract with acetone, followed by drying in an oven at 110 °C for 24 hours under air.

3.2.2 Electrochemical characterization

The electrochemical measurements were conducted in a three-electrode system, which is controlled with potentiostat/galvanostat (BioLogic VSP, France). A platinized Pt wire as a counter electrode and a reversible hydrogen electrode (RHE) as a reference electrode were used, respectively. The working electrode was prepared on a glassy carbon in the form of a thin-film. A MWCNT ink with a concentration of 1.0 mg/ml was prepared by ultrasonically dispersing 5 mg powder in 5 ml solvent composed of isopropanol, water and 20 µl Nafion solution (5 wt.%, Aldrich). Nafion plays a role of a binder that attaches the film to a substrate. A 150 µl aliquot of the MWCNT ink was pipetted onto a polished glassy carbon (dia. 8 mm) and dried at 60 °C for 1 hour in air. The resulting carbon film loaded on glassy carbon was 0.3 mg of carbon per cm^2.

The electrochemical oxidation experiment was carried out in N_2 saturated 0.5 M H_2SO_4 at room temperature. The MWCNT electrode was continuously cycled between 0.05 and 1 V versus RHE until a stable cyclic voltammogram was recorded. Subsequently, it was linearly swept to 1.8 V and then was applied at a constant potential for a certain time. To

monitor the electrochemical change of MWCNTs, cyclic voltammograms were recorded during the electrochemical oxidation. The experiments were performed using several replicas of the MWCNTs, obtaining reproducible results, to overcome the experimental error of the thin-film technique. After electrochemical oxidation, the MWCNT electrodes were washed with ultrapure water and ethanol several times to remove the electrolyte for further physical and chemical characterization.

Electrochemical impedance spectroscopy was performed in the potentiostatic mode during the electrochemical oxidation of MWCNTs. The amplitude of the AC signal was 5 mV. Impedance was measured in the frequency range from 100 kHz to 100 mHz with 10 points per decade.

3.2.3 Physicochemical characterization

Scanning electron microscopy (SEM, Hitachi S4800) coupled with EDX for element analysis was used to investigate the surface morphology of MWCNT film on glassy carbon before and after electrochemical oxidation.

The morphological change of graphitic layer on MWCNTs during electrochemical oxidation was observed through high resolution transmission electron microscopy (HR-TEM, Philips CM200 FEG). Electron energy loss spectroscopy (EELS) which is equipped with a Gatan GIF energy filter in FEI Titan was also measured to obtain information about the elemental composition and the electronic structure. For this measurement, the MWCNTs powders after electrochemical oxidation were sonicated in ethanol. An aliquot was pipetted on a Cu grid with holey carbon film and dried in air.

The mass of carbon was evaluated from CHN/O analyzer (Elementar Vario EL) through high temperature combustion. The electrochemically oxidized MWCNTs samples are converted to carbon dioxide by combustion. The combustion products were separated and conducted to a thermal conductivity detector.

Raman spectroscopy performed on a HORIBA Jobin Yvon spectrometer at an excitation line 633 nm, 100x objective. It measured (using 5 different positions) the MWCNT film on a glassy carbon, and the average ratios of intensity for interesting peaks were compared.

Detection of the functional groups formed during electrochemical oxidation of MWCNTs was carried out by Infrared spectroscopy in the attenuated total reflection (ATR) mode. For this measurement, the MWCNTs powder detached from a glassy carbon are dried overnight in an oven at 60 °C to remove water in the samples. The spectra were collected with a DTGS detector and a ZnSe crystal. A spectrum, collected on average of 1024 scans with a resolution of 4 cm^{-1}, was recorded from 4000 to 500 cm^{-1}.

3.3 Results

3.3.1 The variation of oxidation current on MWCNTs

To explore the electrochemical degradation of MWCNTs, the potentiostatic oxidation was performed on MWCNTs at the potential where oxygen evolution and carbon oxidation occur simultaneously. Figure 3.1 shows the current transient of the MWCNT electrode at a fixed potential of 1.8 V versus RHE. The oxidation current increases with a higher applied potential (Figure S3.1(a)). The rate of oxidation is commonly explained by a power law, $i = k \cdot t^{-n}$, with the specific current i, the rate parameter k, and the time decay exponent n [1, 11]. However, under conditions for oxygen evolution, the reaction rate for the electrochemical oxidation of carbon does not follow the logarithmic decay of current with time (Figure S3.1(b)).
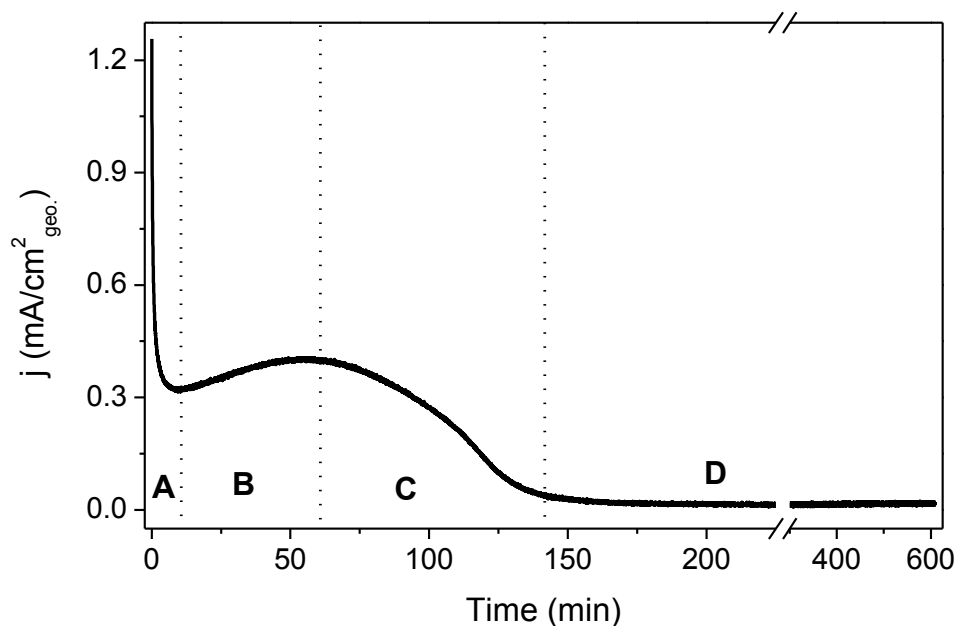

Figure 3.1. Chronoamperogram on MWCNTs at 1.8 V versus RHE in 0.5 M H_2SO_4.

From the chronoamperogram in Figure 3.1, four different regions can be identified, marked here as regions A-D. In Figure S3.2, the distinguishable regions for the electrochemical oxidation of MWCNTs were separated from the overall

31

chronoamperogram. The initial oxidation current falls abruptly, and gradually declines to a steady-state value with a time constant of circa 10 minutes (region A) [80]. This current decay generally results from the effect of double layer capacitance and diffusion-controlled behavior of porous electrode structure. The oxidation current in region A is not well fitted by a power law. The general value of the exponent for diffusion controlled decay is 0.5, but the empirical time decay exponent for region A is about 2.6 (see Figure S3.3). As a high anodic potential is applied to the MWCNT electrode, the initial current decay is presumably a superposition of the oxidation reactions of both carbon and water. This process leads to a subsequent increase of the oxidation current, which is observed in region B. A current increase in chronoamperometry could be attributed to surface oxidation and depends on an increase in the density of oxidation sites with increasing amount of surface oxide.

Figure S3.4 shows that the current increase in region B is observed for as-received and purified MWCNTs, and it is more pronounced for the purified ones. As-received MWCNTs contain much more amorphous carbon than the purified ones. The oxidation current of as-received MWCNTs in region B is higher and has a faster transition to the next region, when compared to the purified MWCNTs. Therefore, it is believed that the initial oxidation in regions A and B are associated with active sites, such as defects and edges of the carbon due to residual amorphous carbon on MWCNTs [1, 11, 81]

Initial oxides formed on the preferential sites promote the formation of gaseous products, such as CO, CO_2 and/or O_2 [1, 11]. However, as the carbon surface becomes saturated with surface oxides by electrochemical oxidation, the formation of additional oxides may be inhibited [1]. These surface oxides might slow the reaction kinetics towards the further formation of the final surface oxide and gaseous products during the electrochemical oxidation. They lead to the second current decay observed in region C. Consequently, the MWCNT electrode is fully passivated by protective surface oxides yielding the small steady-state current observed in region D [82]. Figure S3.5 shows a step potential measurement conducted in region D. Even by polarizing to reducing conditions, no change in the oxidation current for reversible reaction of surface oxides are observed, indicating the stability of the surface oxide formed in region D.

3.3.2 The morphological and structural changes

To understand the degradation of MWCNTs at a high anodic potential, morphological and structural investigations were carried out in different chronoamperometric regimes.

The SEM images in Figure 3.2 show an overview of the surface morphology on MWCNT electrodes before (pristine) and after (region C) the electrochemical oxidation. The pristine MWCNTs exhibit a flat and smooth surface with well-dispersed and densely packed agglomerates. After the electrochemical oxidation, the surface of the MWCNTs becomes rougher and clumpier. The increase of the oxygen signal in the EDX analysis confirms that surface oxides are formed on the carbon surface through electrochemical oxidation. Moreover, a small amount of sulfur is detected after the electrochemical oxidation, likely due to the effect of H_2SO_4 electrolyte. To avoid the effect of other elements in the EDX measurement, these two electrodes were prepared without a Nafion binder.
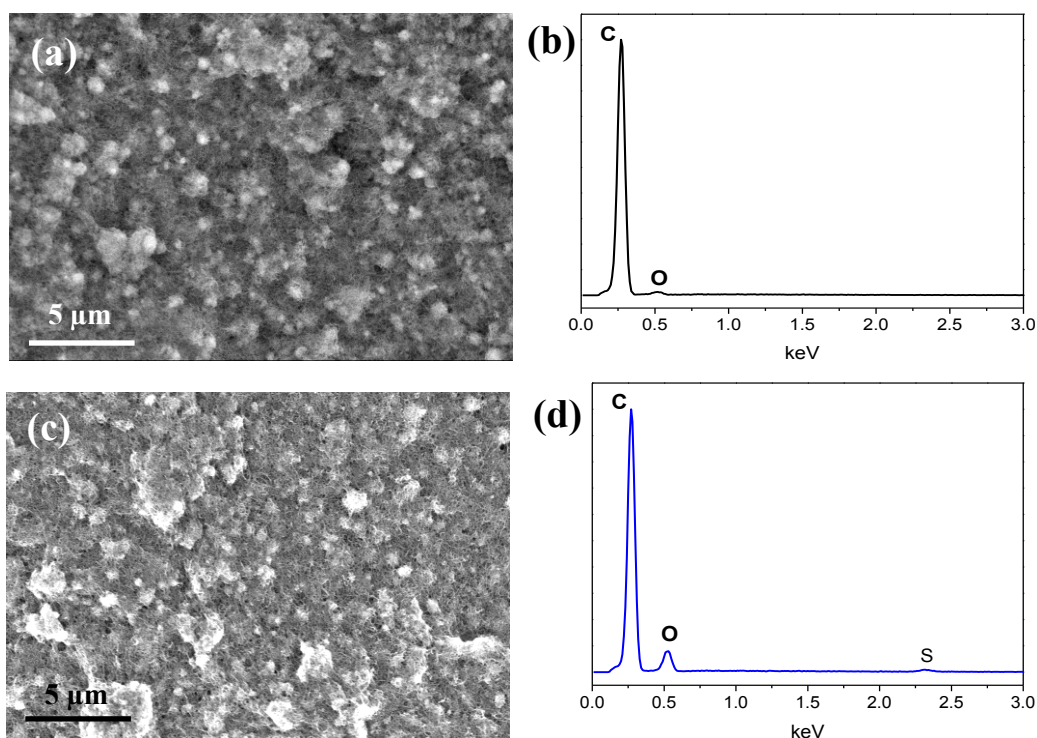

Figure 3.2. SEM images and EDX spectrum of the pristine MWCNTs (a) and (b), and the electrochemically oxidized MWCNTs (c) and (d).

The structural changes of the MWCNTs during electrochemical oxidation can clearly be observed by transmission electron microscopy (TEM). Figure 3.3(a) shows a representative TEM image of pristine MWCNTs. Despite several purification steps, some residual amorphous carbon remains on the MWCNT surface. Initial electrochemical oxidation leads to a reduction of this amorphous carbon, as shown in Figure 3.3(b). These observations suggest that a different oxidation rate exists between amorphous and graphitic carbon. With further oxidation, the surface of the MWCNTs shows a roughening and a loss in the crystalline structure in region C (Figure 3.3(c)). The TEM image of the material in region D in Figure 3.3(d) shows similar, but a little bit more pronounced features. It can be seen that a defective layer is formed on the sidewalls of the MWCNTs in region D. From the TEM investigation, we can conclude that within the electrochemical oxidation of MWCNTs, initially residual amorphous carbon is removed and afterward the revealed graphitic layers on the MWCNTs are destroyed with creating structural defects on the MWCNTs. Furthermore, the outer graphitic layers of the MWCNTs are damaged, whereas the inner graphitic layers remain mostly intact. It seems that the graphitic walls underneath the defective layers are protected from further degradation. Figure S3.6 shows more TEM images at various resolutions to support the observed trends in Figure 3.3.
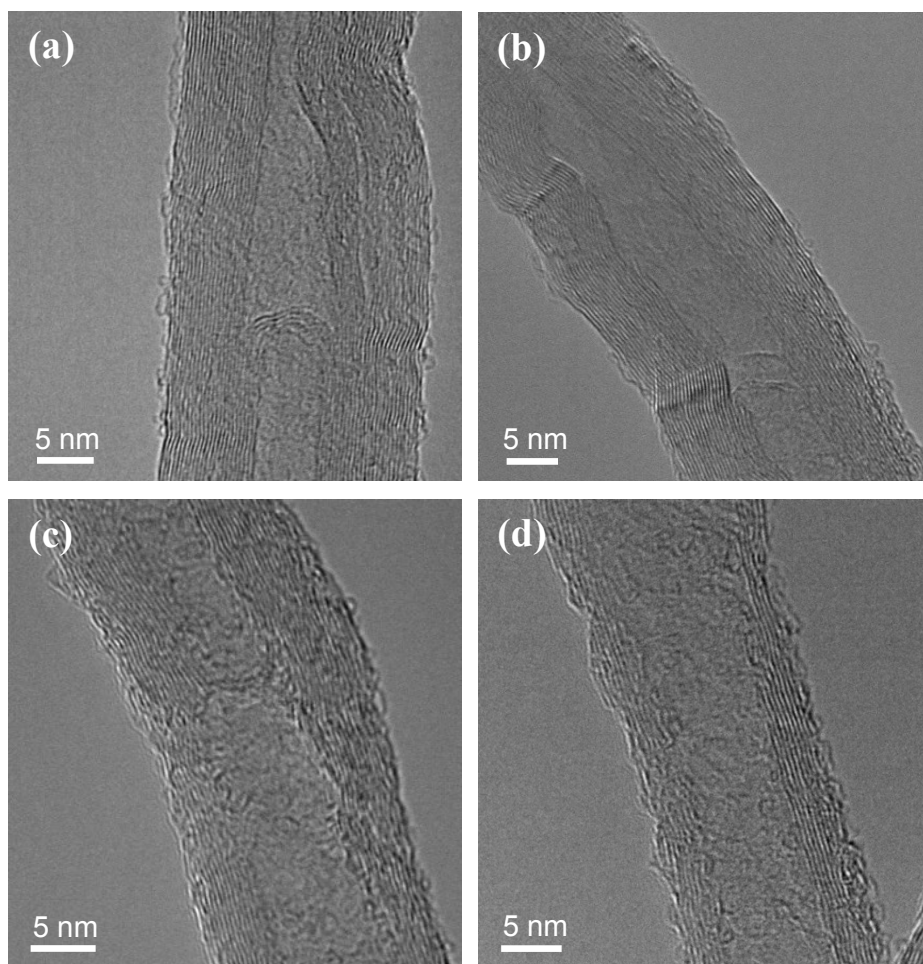
Figure 3.3. TEM images of (a) initial MWCNTs, the MWCNTs electrochemically oxidized at 1.8 V for (b) 0.5 Coulomb (region B), (c) 1 Coulomb (region C) and (d) 1.5 Coulomb (region D).

EELS provides information about the electronic structure of the tubes. The fine structure of the carbon K ionization edge, shown in Figure 3.4, reveals characteristic features due to transitions into final states with π^*- and σ^*- character. All spectra were normalized with the range which is not sensitive to structure variation, i.e. 295 eV. First peak which is assigned to π^* orbital, is a characteristic sp^2 hybridized carbon. Second peak is the main contribution of σ^* orbital. After the electrochemical oxidation, these peaks are broader and have less intensity against that of initial MWCNTs. This indicates that the electrochemical oxidation makes the structure of carbon less sp^2 ordering. The full width at half maximum of the π^* feature centered at 284 eV as well as the spectral weight of the

π^*- and σ^*- contributions can be used to estimate the sp^2 hybridization ratio and degree of graphitic order [83]. Table 1 shows the graphitic order estimated by fitting Gaussians to the π^* and σ^* features and comparing a real ratio of these characteristic features to the one obtained in the case of highly graphitic tubes. The results given in Table 3.1 show that the sp^2 ratio of the MWCNTs decreases with electrochemical oxidation, meaning the MWCNTs are less graphic. However, there is no significant change in the sp^2 ratio to justify structural differences between regions B-D.
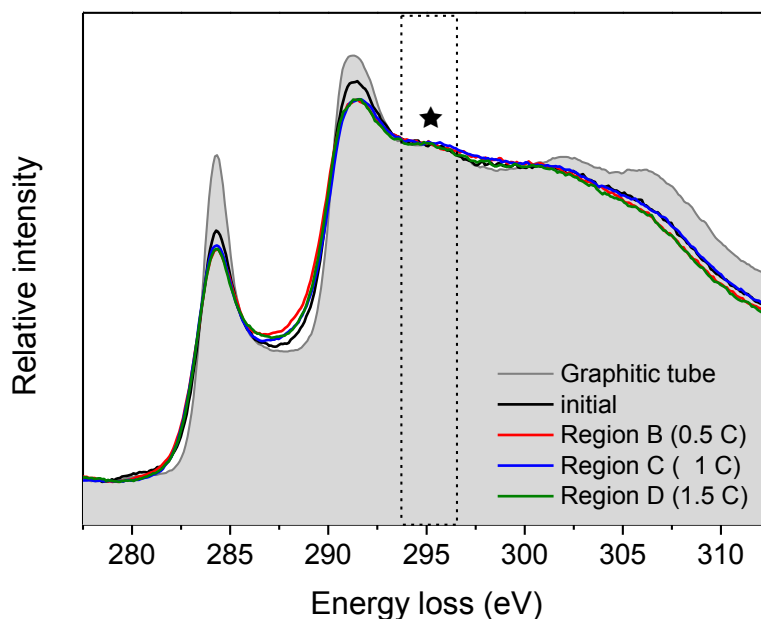
Figure 3.4. EEL spectra of MWCNTs during the electrochemical oxidation

A loss in the graphitic order due to the electrochemical oxidation is clearly observed, which can also be confirmed by the Raman spectroscopy. The intensity ratios I_D/I_G and I_{2D}/I_G shown in Table 3.1 are determined from Raman spectra of tubes from different chronoamperometric regimes. The fitting procedure is described in Figure S3.7. An increasing I_D/I_G ratio represents a loss of structural order of the MWCNTs [84, 85]. Among the different regions of electrochemical oxidation, the variations in the determined degrees of graphitization are in the range of the experimental error. However, a small difference between initial and the electrochemically oxidized MWCNTs can be explained. Compared to pristine MWCNT, I_D/I_G ratio increases after the electrochemical

36

oxidation, indicating that the electrochemical oxidation of carbon proceeds to disordered carbon.

From the evidence of the structural change of the MWCNTs during the electrochemical oxidation, as obtained from EELS and Raman spectroscopy, it can be concluded that the electrochemical oxidation of carbon induces the loss of graphitization, but no significant further change in graphitic order with higher applied charge is observed. As we have seen in HRTEM, the graphitic layers beneath the defect layer of the MWCNTs in region D are intact and protected from further oxidation. EELS and Raman spectroscopy enhance the statistical reliability in comparison to the information obtained by HRTEM. Although both are bulk methods, they demonstrate a very high sensitivity to changes in structural order that is mainly confined to the non-graphitic parts in the surface layer of the MWCNTs.

The elemental composition of the MWCNTs is also provided by EELS and shown in Table 3.1 for the different regions. With the electrochemical treatment, the relative oxygen content increases in region B and C. This can be related to the formation of the surface oxides and is in good agreement with the structural changes observed by HRTEM. According to the EELS data in Table 3.1, the oxygen content does not change significantly from region C to D. We conclude that the surface oxides are fully covered on the MWCNTs in region D, indicative of the formation of protective oxide layer. To confirm that this finding is not an artifact of the localized EELS analysis, we also conducted elemental analysis (EA) shown in Figure S3.8. It is found that carbon mass decreases with the electrochemical oxidation of MWCNTs. However, no significant change of carbon mass in region D is observed. The saturation of the oxygen concentration could be associated with a stable oxide content, which has achieved a steady state between oxide formation and dissolution towards CO or CO_2. It is therefore inferred that the existence of stable surface oxide, where the MWCNTs are protected from further corrosion, induces slow kinetics of carbon corrosion toward gaseous products. This trend can compare with the variation of oxidation current from Figure 3.1. The high oxidation current in regions A, B and C provide evidence for fast oxidation rate and a considerable loss of carbon mass. In region D, which has a low oxidation current, there is little change in carbon mass.

Table 3.1. Electrochemical and physicochemical characterization data of MWCNTs during electrochemical oxidation.

Applied charge for oxidation	Electron transfer (ΔEp) [a]	Raman [b]		EELS [c]		
		I_D/I_G	I_{2D}/I_G	Sp^2 ratio	C, %	O, %
Initial	88	2.4 ±0.04	0.25	95 %	98.3	1.7
0.5 C (region B)	75	2.56 ±0.06	0.25	85 %	97.6	2.4
1 C (region C)	85	2.48 ±0.06	0.2	89 %	96.2	3.8
1.5 C (region D)	104	2.48 ±0.05	0.2	87 %	96.7	3.3

[a] Anodic peak potential (E_a) – cathodic peak potential (E_c) from $[Fe(CN)_6]^{3-/4-}$ redox response.

[b] Intensity ratio of D/G and 2D/G from Raman spectra.

[c] Elemental composition and degree of sp2 ordering with respect to highly graphitized CNTs from EELS spectra.

3.3.3 Identification of surface functional groups – Infrared spectroscopy

Infrared spectroscopy identifies surface oxides and its structural groups on the MWCNTs. Figure 3.5 shows infrared spectra (IR) of the MWCNTs electrochemically oxidized in the different chronoamperometric regimes. Most peaks from functional groups on MWCNTs are present in the range of 900-1800 cm^{-1} [86]. Due to the effect of Nafion as a binder in electrode preparation, all spectra show the characteristic vibration of Nafion at 1220 cm^{-1} and 1156 cm^{-1} corresponding to asymmetric and symmetric C-F stretching [87]. The peaks of C-O stretching and O-H bending appear at ~1250 cm^{-1}. Even though the range overlaps with the peak for Nafion, overall bands in the range of 1000-1250 cm^{-1} decrease in intensity with electrochemical oxidation until region C.

The IR band range for C=O stretching and C=C bonds is 1500 ~ 1750 cm^{-1} [86]. In general, quinone groups formed by carbon oxidation were mostly identified with redox reaction by electrochemical measurement, discussed in section 3.3.4. In our infrared spectrum, it is likely that the absorption for quinone group downshift to the broad peak in 1635-1655 cm^{-1} region. The appearance of O-H stretching after the electrochemical oxidation supports that the coupling effects with hydroxyl groups and the extended conjugation with the weakly coupled carbonyl groups might be responsible for the downshift in the C=O stretching for surface-bound quinone groups [88].
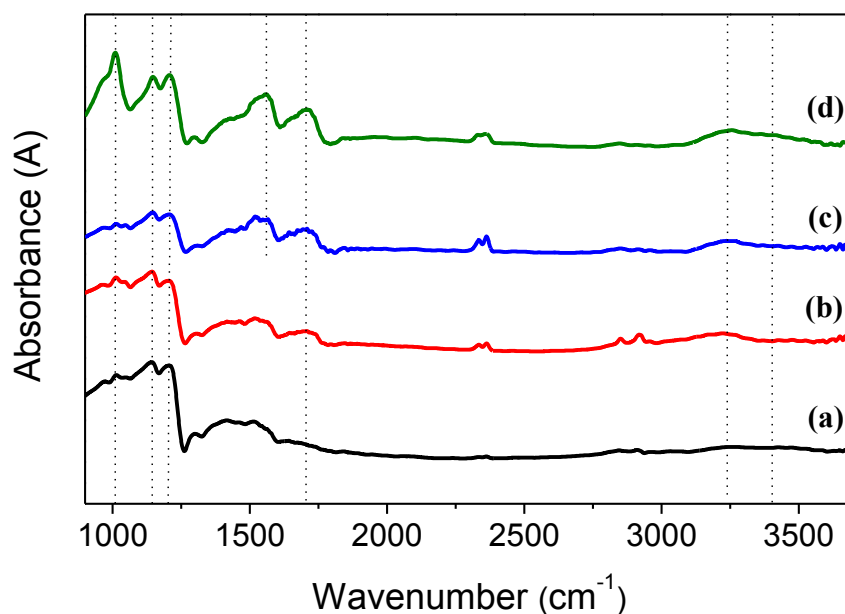
Figure 3.5. FTIR spectra of (a) pristine MWCNTs, the MWCNTs electrochemically oxidized for (b) 0.5 Coulomb (region b), (c) 1 Coulomb (region c) and (d) 1.5 Coulomb (region d).

Furthermore, the 1700 cm^{-1} band can be assigned to carbonyl (C=O) stretching in ketones, aldehydes, or carboxylic acid groups. Since the –OH stretch band from coupled carboxylic acid groups is present at 3100 cm^{-1}, the C=O band at 1710 cm^{-1} should probably be identified with carboxylic acid. According to Figure 3.5 (b)-(d), the bands at 1710 cm^{-1} and at 3100 cm^{-1} increase with electrochemical oxidation, which means carboxylic acid groups are formed on the carbon surface. In the MWCNTs oxidized in region C and D, the peak at 1520 cm^{-1} is enhanced. This indicates that the localized C=C

bond in surface defects on the MWCNTs introduces oxygen-containing groups to stabilize the structure [88]. Therefore, it can be inferred that from region C during the electrochemical oxidation of MWCNTs additional defects are created on the carbon surface by opening the graphite ring structure. As you have seen in TEM image, this fact supports the damage of crystalline structure from region C.

For the MWCNTs oxidized in region D, a strong band at 1101 cm^{-1} is exhibited and a broad band additionally appears at the high frequency of 3400 cm^{-1} (Figure 3.4(d)). The band at ~1100 cm^{-1} is located within the range expected for C-O stretching modes in ethers, esters, alcohol, or phenol compounds. The band at 3400 cm^{-1} can be attributed to OH stretching within alcoholic or phenolic groups [86]. Since ether-like oxygen and OH species are arranged in stable configuration, they may be contributed from protective surface oxides in region D.

3.3.4 The change of electrochemical behavior

Electron transfer of Fe(CN)$_6^{3-}$/Fe(CN)$_6^{4-}$ redox

The influence of the surface oxides on electrochemical behavior is analyzed by the electrochemical response of $[Fe(CN)_6]^{3-/4-}$ which is a well-known redox system, shown in Figure S3.9. A large capacitive component of the background current is observed after the electrochemical oxidation on MWCNTs. The anodic and cathodic peak separation (ΔE_p) means heterogeneous electron transfer (ET) kinetics. Table 3.1 lists the values of ΔE_p on the electrochemically oxidized MWCNTs in the different chronoamperometric regimes. The ΔE_p in region B is lower than that of pristine MWCNTs, indicative of faster ET kinetics. Hence the MWCNTs in region B are electrochemically activated, which is a well-known effect within electrochemical oxidation due to an increased number of defects, better wetting, and the formation of oxygen-containing groups [61, 89, 90]. It is interesting that the ΔE_p is getting larger for the MWCNTs oxidized in region C and the ET kinetics of the MWCNTs in region D is much slower than pristine MWCNTs. It seems that different kinds of electro-active oxides formed with prolonged oxidation

inhibit electron transfer. Therefore, the reduced electrochemical activity is in good agreement with the passivating properties of the surface oxides on the MWCNT electrode.

Cycling voltammetry in H_2SO_4

Cycling voltammetry (CV) was performed directly in H_2SO_4 electrolyte in the range of the potential applied before hydrogen and oxygen evolution. It provides information on electrochemical capacitance and the formation of surface oxides on MWCNTs. Figure 3.6(a) shows the CV on the MWCNTs dependent on the charge applied during the oxidation. The CV of pristine MWCNTs exhibits a typical double layer behavior with no faradaic current contribution. With electrochemical oxidation, the capacitive current increases significantly; in particular, the anodic and cathodic peaks around 0.6 V have become more distinguishable. In general, an increasing capacitance results from an electrochemical surface roughening and/or a modification of the capacitive contribution of surface functional groups. The surface functional groups on the MWCNTs change the isoelectrical point and thus improve the wettability of the MWCNT surfaces and thereby increase the contacted surface area. The observed faradaic current peaks around 0.6 V RHE can be addressed to oxygen-containing functional groups, generally a hydroquinone-quinone (HQ-Q) redox pair [12, 79].

The MWCNTs oxidized until region C have linear increase of the capacitive current and same redox potential for surface oxides. When the oxidation current of the MWCNTs reaches region D, the peak positions in the anodic/cathodic scans have moved to higher/lower potentials as the applied charge/oxidation time increases. This shift could indicate that different kinds of surface oxide are produced on the carbon surface in region D [77]. This would coincide with the increased number of carboxylic groups and the existence of hydroxyl groups observed in the infrared spectrum of the MWCNTs in region D (Figure 3.4).

The total capacitance and the amount of surface oxides on the MWCNTs can be quantitatively calculated from the capacitive and faradaic contributions of the CVs in Figure 3.6(a) [12, 79, 91]. The results obtained are plotted as a function of the amount of the charge applied for the electrochemical oxidation in Figure 3.6(b). The total capacitance of the electrochemically oxidized MWCNTs steadily increases until region C,

where 1 Coulomb of charge has passed. With further oxidation, entering the chronoamperometric region D, the total capacitance is saturated and no significant further increase is observed. This saturation could be one indication of a passive state on the carbon surface. However, the amount of surface oxides produced in region D increase again after applying 1.2 Coulomb on MWCNTs.
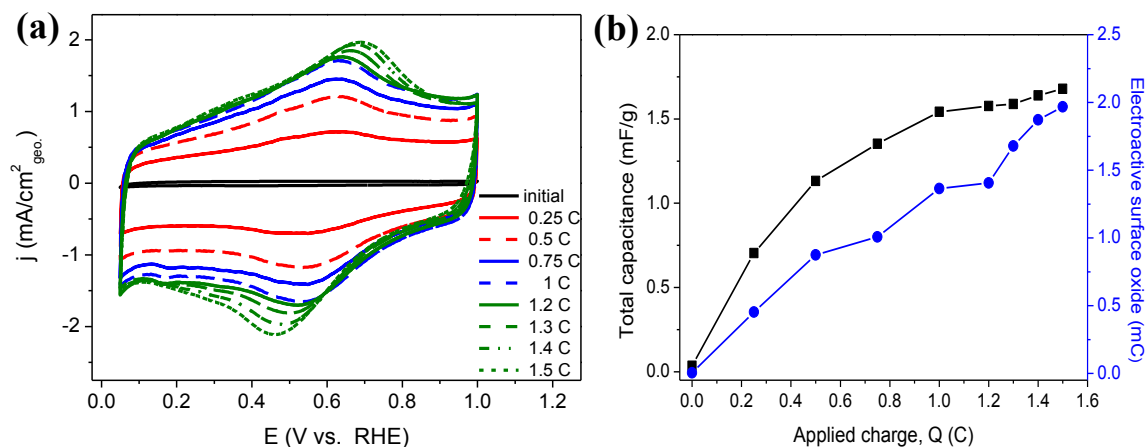

Figure 3.6. (a) Cyclic voltammetry of MWCNTs during the electrochemical oxidation with a different amount of charge applied in 0.5 M H_2SO_4, scan rate: 50 mV/s. initial MWCNTs (black), the MWCNTs oxidized in region B (red), in region C (blue) and in region D (green line). (b) The total capacitance and the amount of surface oxides as function of applied charge for MWCNTs oxidation.

Linear sweep voltammetry (LSV)

Linear sweep voltammetry (LSV) was performed on the MWCNTs oxidized with different regions to measure the change in the electrochemical activity for the oxidation (Figure 3.7). The electrochemical activity increases with the electrochemical oxidation until region C by activating the carbon structure due to the formation of surface oxides and defects. This is well matched with a trend in the kinetics for electron transfer. However, the electrochemical activity of the MWCNTs reached region D decreases and possesses a peak current. The appearance of the peak current in this potential range indicates that the oxide film formed on the electrode surface in region D results in less mass transfer. This induces the slow kinetics for the oxidation reaction, thus supports the

existence of the passive oxide on the MWCNTs with prolonged oxidation. In a corrosion study [92], if a metal forms a stable oxide by oxidation, the metal is in its passive state because the oxide film formed is likely to be a barrier between the metal and the environment.

Figure S3.10 shows the Tafel plots from the logarithm of current density. It is clear that the current density (log i) of the MWCNTs oxidized in region D starts to decrease beyond a certain potential and reaches into a primary passivation range. The Tafel slopes on the MWCNTs oxidized with different regions are listed in Table S3.2. The MWCNTs oxidized after region B show two different slopes in the potential range. It could indicate that different kinetic behavior is involved on the surface of MWCNTs for oxidation. At a high overpotential, the Tafel slope on the electrochemically oxidized MWCNTs increases as the oxidation time is longer. The high slopes result from the presence of surface functional groups which seem to be a barrier for oxidation on the carbon surface [93]. It can be conclusive that the MWCNTs oxidized in region D block on the surface through the accumulation of oxygen species on the electrode, acting as passivation.
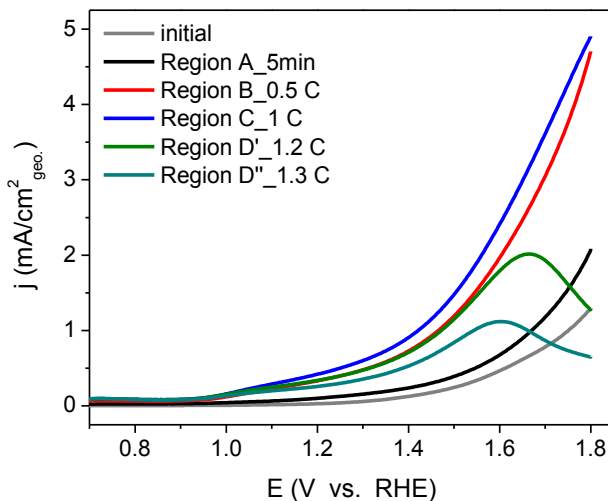

Figure 3.7. Linear sweep voltammetry of the MWCNTs during the electrochemical oxidation with a different amount of charge applied in 0.5 M H_2SO_4, scan rate 10 mV/s.

Electrochemical impedance spectroscopy (EIS)

Electrochemical impedance spectroscopy (EIS) is a powerful diagnostic tool to study the processes occurring at the electrode/electrolyte interfaces [94, 95]. This technique was used for probing the impedance change of the MWCNT electrode surface during the electrochemical oxidation.

The Nyquist plots of MWCNTs at an anodic potential of 1.8 V versus RHE are presented in Figure 3.8(a). The impedance behavior of MWCNTs is strongly dependent on the region for the oxidation. The diameter of the semi-circle corresponds to the capacitance and the charge-transfer resistance of the electrode/electrolyte interface. There is no significant change in the semi-circle until the MWCNTs oxidized in region B. From region C, the semi-circle gets larger with an increased amount of passed charges. It is probable that surface oxides start to cover the carbon surface. For the MWCNTs oxidized in region D, the impedance arc is obviously large and stable, indicative of the largest resistance. This is reasonably attributed to its poor electrical conductivity due to the formation of a passive oxide on the electrode. In addition, the spectra at high frequency – which is generally considered as ohmic resistance (R_Ω) – is shifted after the oxidation for 1.5 Coulomb shown in an expansion of EIS spectra (Figure 3.8(b)). The fact that the increase of R_Ω in region D provides that the existence of a passive oxide film on the carbon surface blocks electrolyte access.
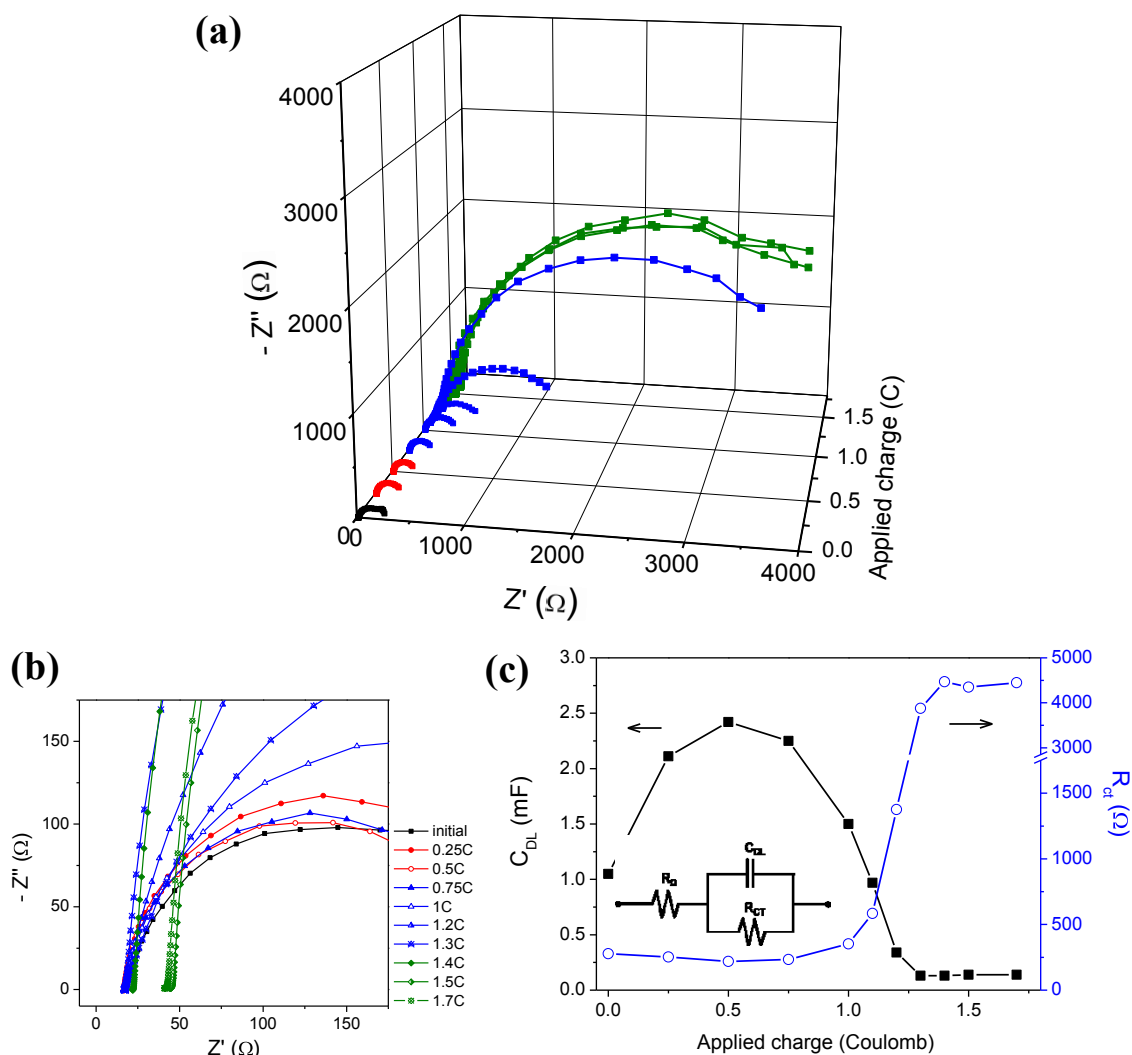
Figure 3.8. (a) Nyquist plots of the MWCNTs at 1.8 V during the electrochemical oxidation with a different amount of charge applied in 0.5 M H_2SO_4. (b) A magnified portion of the plot near the origin. MWCNTs oxidized in region B (red), region C (blue) and region D (green line). (c) Variation of the double layer capacitance (C_{DL}) and charge transfer resistance (R_{CT}) on MWCNTs during the electrochemical oxidation, fitted by the Randles circuit (inset Figure).

Fitting of the impedance spectra is performed using a basic Randles circuit, which consists of a cell resistance (R_Ω) and a double layer capacitance (C_{DL}) in parallel with a charge transfer resistance (R_{CT}), as shown in the inset of Figure 3.8(c). The values

45

obtained from the fitting are listed in Table S3.3 and the variation of C_{DL} and R_{CT} is plotted as a function of applied charge in Figure 3.8(c).

C_{DL} of the MWCNTs increases up to 0.5 Coulomb due to the surface modification during the electrochemical oxidation. It is likely to produce the electrode surface with a high dielectric constant, as it is known from oxide formation on semiconductors. The surface oxide formed on the MWCNTs by electrochemical oxidation may lower the dielectric properties and then decreases the overall capacitance. The observed decrease of the capacitance is related to the growth of a oxide film, since the capacitance is inversely proportional to the film thickness [96]. When the MWCNTs are reached in chronoamperometric region D, the capacitance value is almost constant, indicating a constant oxide thickness.

In contrast, the R_{CT} of MWCNTs shows the opposite behavior with C_{DL} during electrochemical oxidation. The R_{CT} until 0.75 Coulomb is slightly lower than its initial value, but increases substantially after 1 Coulomb. This trend is in accordance with the findings from the kinetics of electron transfer from $Fe(CN_6)^{3-/4-}$; the lower R_{CT} indicates faster ET kinetics. In Region D above 1.4 Coulomb, the R_{CT} is nearly 20 times larger than its initial value, and is stabilized. The observed increase of the R_{CT} supports the growth of a passive oxide film which means that surface oxides are fully covered in region D, indicated by the saturation in R_{CT}. Therefore, it is conclusive that carbon corrosion increases the electrode resistance owed to the oxide coverage on the carbon surface.

3.4 Discussion

The physicochemical and electrochemical characterizations of the MWCNTs during electrochemical oxidation contribute to better understanding of the electrochemical degradation of MWCNTs. When the MWCNTs are electrochemically oxidized at a high anodic potential, the structure and characteristics of the MWCNTs change with the transition of the oxidation current. Based on the above MWCNT analysis during the electrochemical oxidation, we demonstrate how MWCNTs electrochemically degrade at a high anodic potential, as shown in Figure 3.9. Surface functional groups such as carboxyl, hydroxyl, or other groups, formed by electrochemical oxidation processes on the MWCNTs are not shown in this scheme.

When high anodic potential is applied to the MWCNTs, water is reversibly adsorbed and surface oxides are formed on active sites that are defects and the edges of the carbon surface (region A and B). Some of these surface oxides promote the formation of gaseous products. A carbon with higher degree of disorder is susceptible to oxidization more rapidly than graphitized/ordered carbon [81]. Therefore, during this process, residual amorphous carbon on the MWCNT surface is removed and graphitic layers are exposed due to selective oxidation. Even though this study did not investigate it, the end of MWCNTs, which consist of amorphous carbon or discontinuous graphitic carbon, can be opened by electrochemical oxidation [97, 98]. Moreover, the oxygen-containing functional groups formed on the MWCNTs oxidized in region B are electrochemically active. It shows fast electron transfer and low charge transfer resistance [99, 100]. This step can be used for the electrochemical purification and activation of MWCNTs.

With the prolonged electrochemical oxidation of the MWCNTs, surface oxides cover and are saturated on the carbon. This induces the decrease of the oxidation current on the MWCNTs, indicative of the resistive properties of the oxygen coverage on the MWCNTs. In this state of carbon oxidation, the revealed graphitic layer on the sidewalls of the MWCNTs is further oxidized and collapses directly by introducing many surface defects, which is region C (Figure 3.9(c)). This destruction of graphitic carbon has been previously applied for the cutting or etching of MWCNTs [81, 101]. In region C, the

47

highest capacitance on MWCNTs was found due to surface functional groups and a high surface area by breaking the graphitic layers.

The coverage of surface oxides is fully dominant on the MWCNTs, it almost blocks the charge transfer and limits the oxidation current (Figure 3.9(d)). The surface oxide film on the MWCNTs prevents a further attack by electrochemical oxidation, acting as a passivation. It is evident that the graphitic layers beneath defective carbon layers are protected from further electrochemical degradation.
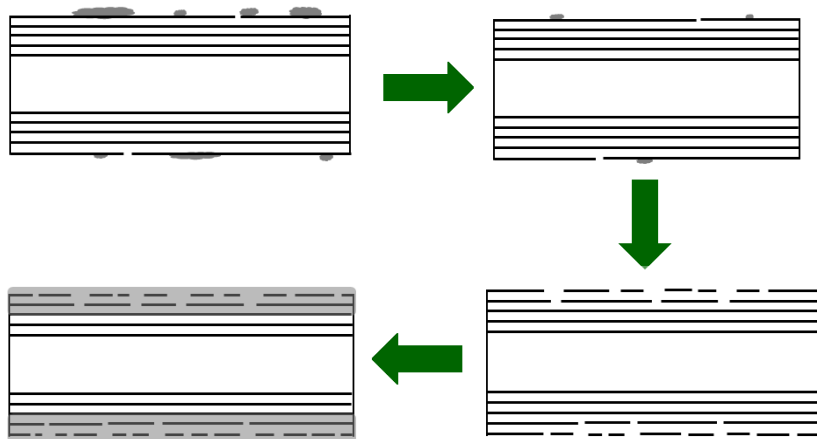
Figure 3.9. A schematic diagram of MWCNT electrochemical degradation.

The electrochemical properties of MWCNTs are affected by the electrochemical oxidation at a high anodic potential due to the change in structure and surface functional groups [102]. Initial oxidation of MWCNTs enhances electrochemical activity, increases capacitance and reduces resistance. With prolonged oxidation, the electrochemical activity of MWCNTs decreases with high resistance due to the formation of protective oxides on the electrode. It is proposed that the passive MWCNT electrode is electrochemically stable since it is protected from further oxidation.

3.5 Conclusion

We report here how MWCNTs degrade electrochemically at a high anodic potential accompanying both oxidations of carbon and water in acidic media. Through the characterization of morphology, structural order, functional groups and electrochemical properties, the change of the MWCNTs during the electrochemical oxidation is well understood. At the beginning of electrochemical oxidation, MWCNTs are not only purified but also activated by removing impurities and producing electrochemically active surface oxides. With prolonged oxidation, the MWCNT electrode is passivated by the oxides covering the carbon surface. This leads to the high electrical resistance and low electrochemical activity of MWCNTs. Due to the unique structure of MWCNTs, the graphitic layers beneath a passive oxide film can protect from further oxidation. This finding makes it possible to tune or control the suitable properties of MWCNT electrodes using the electrochemical oxidation for potential electrochemical applications. Moreover, it is helpful to understand the degradation of electrochemical systems when MWCNTs are used for the electrocatalyst support for a reaction involving oxygen, such as water electrolysis, fuel cells and metal-air batteries.

3.6 Supporting information

Figure S3.1. The electrochemical oxidation on MWCNTs with different applied ptentials in 0.5 M H_2SO_4. (a) the oxidation current as function of applied charge, (b) logarithm of the oxidation current and time
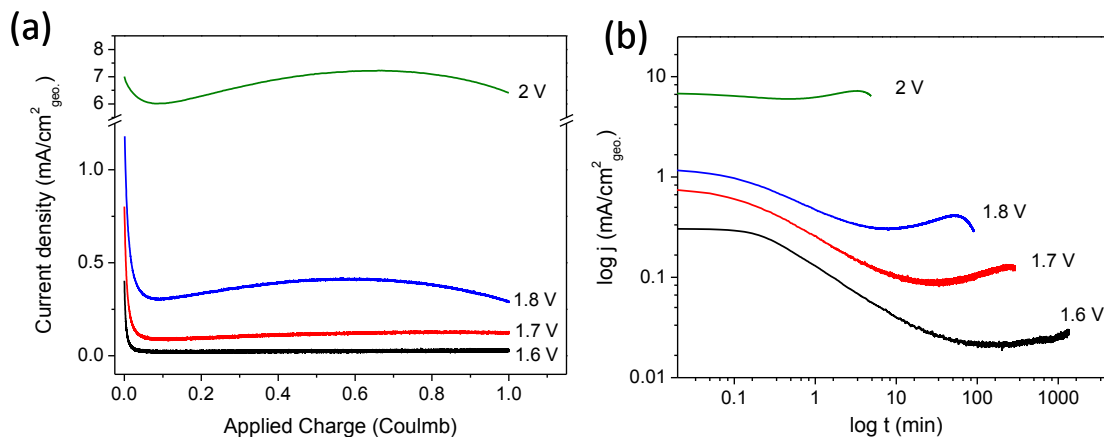
In logarithmic scale of the current-time on MWCNTs, the variation of oxidation current is nonlinear. Overall rate of oxidation reaction is not following approximated with a power law $i = kt^{-n}$. Probably, this is because the oxidation condition performed at high anodic potential is containing not only carbon but water oxidation on the MWCNTs electrode. It could be that oxygen from water oxidation affects the oxidation behavior of the MWCNTs. At the first stage of the oxidation, the oxidation current decrease exponentially with time. The slope of the current drop decreases with an increase in potential. The electrochemical oxidation of MWCNTs for extended time shows the change in the oxidation current. Furthermore, the time reached for the next stage in the electrochemical oxidation of MWCNTs is shorter as the higher potential is applied for the oxidation.

Figure S3.2. Distinct regions of oxidation current in overall chronoamperogram on MWCNTs at 1.8 V vs. RHE in 0.5 M H_2SO_4.
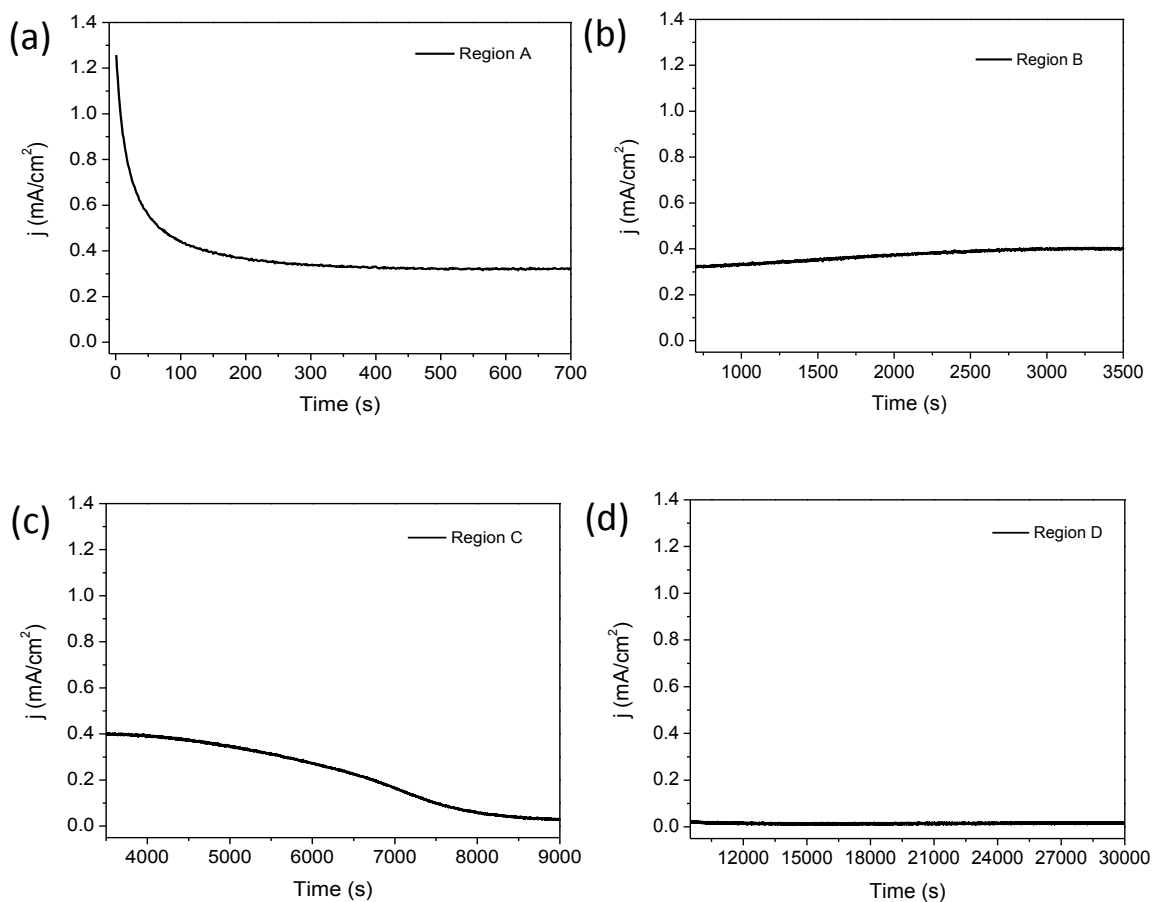

Figure S3.3. Fitting of chronoamperometric decay in region A.

$y = k \cdot x^n$
R2 = 0.9679
k = 1.56 ± 1.2e^{-3}
n = -2.65 ± 1.7e^{-2}

51
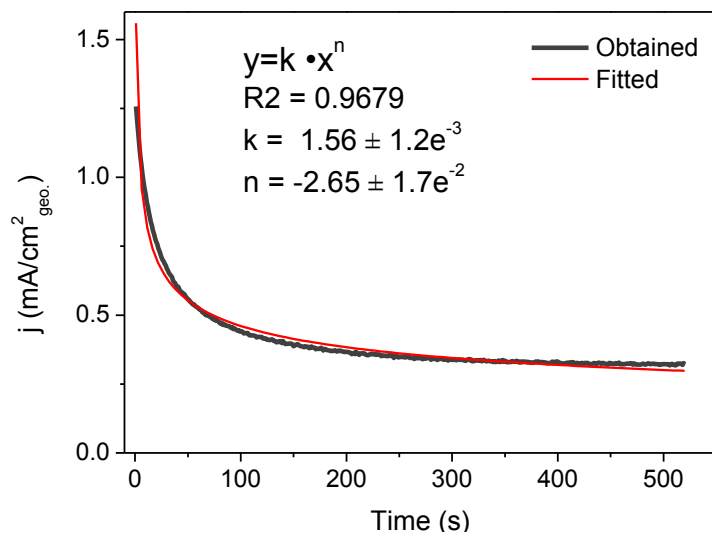
Figure S3.4. Chronoamperograms on as-received and purified MWCNTs at 1.8 V vs. RHE in 0.5 M H_2SO_4.
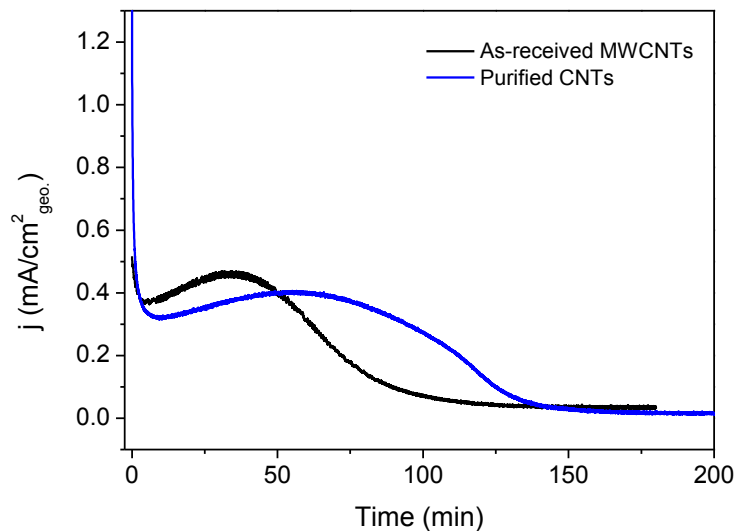
Figure S3.5. In region D of the electrochemical oxidation of MWCNTs, double step potential chronoamperogram on MWCNTs in 0.5 M H_2SO_4.
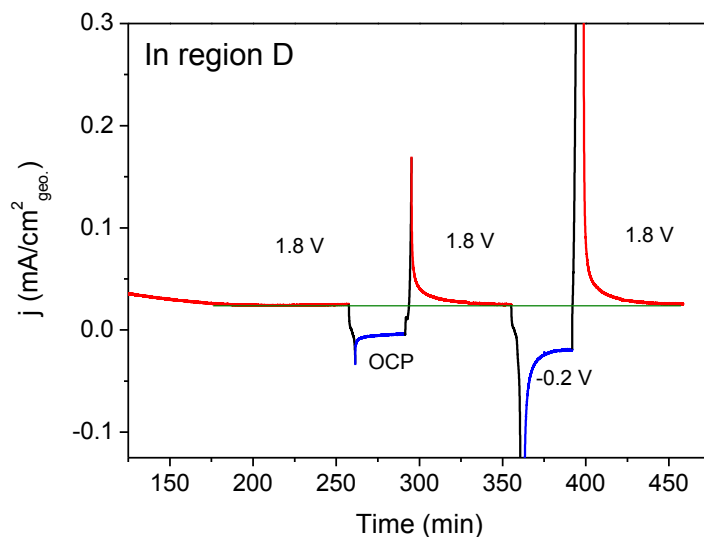
Returning the potential from open circuit potential (OCP) and reduction potential to 1.8 V shows that the oxidation current drops due to capacitive contribution and continuously decays towards a steady-state value. There is no obvious change of the steady-state value for the oxidation before and after the potential step. It could be inferred therefore that the surface oxide formed on MWCNT in region D is irreversible and quite stable.

Figure S3.6. Fitting procedure of the Raman spectra of the MWCNT electrode.
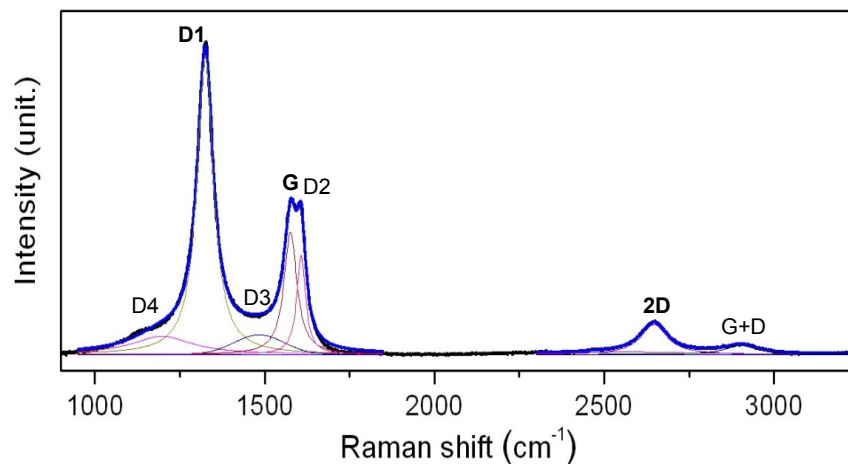
The Lorentzian peak at 1600 cm^{-1} (G) results from the graphitic structure of the sample, the Lorentzian peak at 1320 cm^{-1} (D) is attributed to the presence defects and edges. The Lorentzian peak at 1620 cm^{-1} (D2) and 1180 cm^{-1} (D4) are assigned to small graphite domains and polyene-like carbons respectively. The Gaussian peak at 1500 cm^{-1} (D3) is assigned to amorphous carbon. The Lorentian peak at 2700 cm^{-1} (2D) can be attributed to the first overtone of the D1 band and is sensitive in a crystal, thus a characteristic feature for highly ordered graphite lattices. The Lorentian peak at 2950 cm^{-1} has been assigned to a combination of the G and D modes characterstics for disturbed graphite structures [103].

Figure S3.7. TEM images of MWCNTs (a) – (c) pristine, electrochemically oxidized at 1.8 V vs. RHE for (d) – (f) 0.5 Coulomb (region B), (g) – (i) 1 Coulomb (region C) and (k) – (l) 1.5 Coulomb (region D).
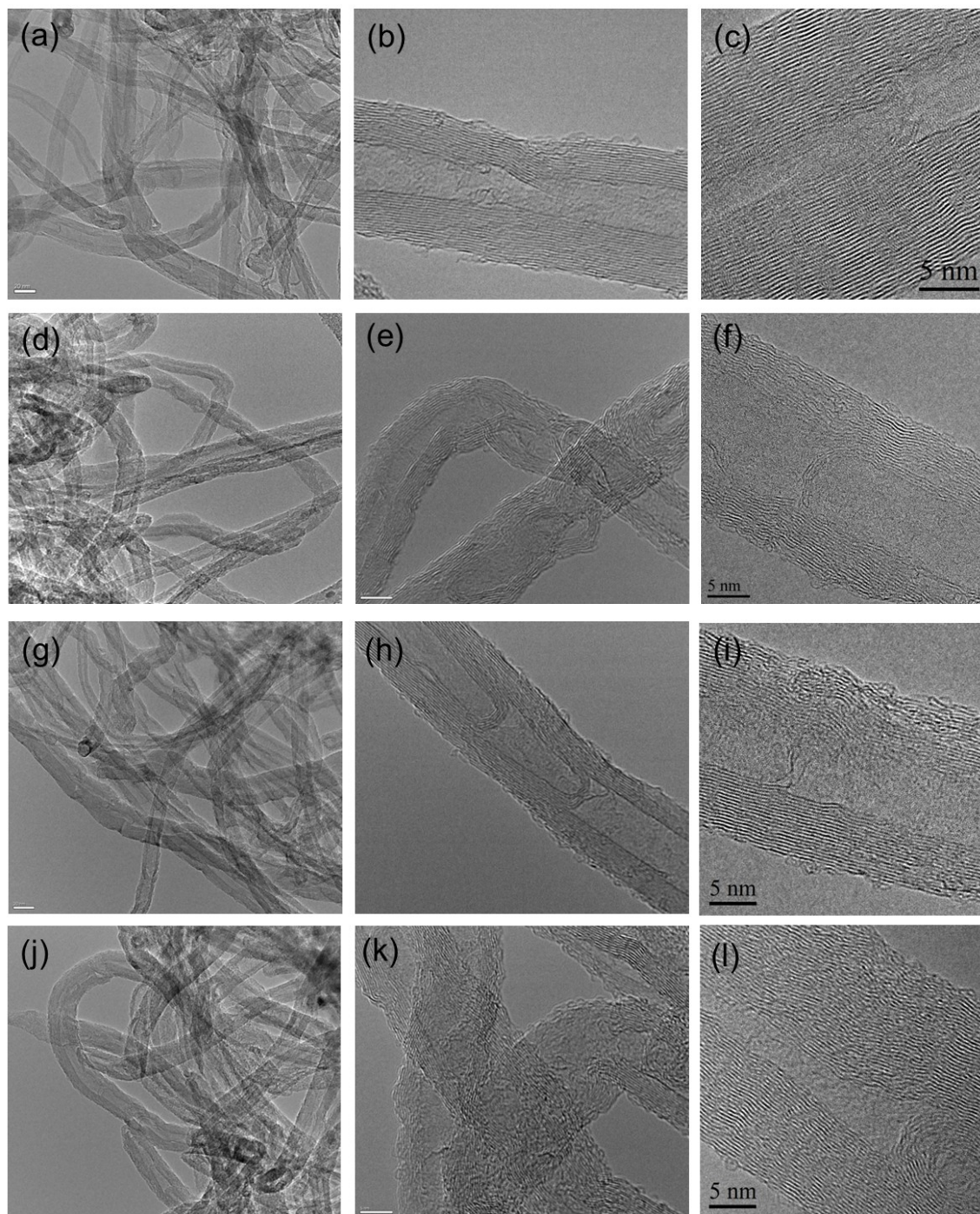
Figure S3.8. Mass loss of carbon during the electrochemical oxidation of MWCNTs as a function of oxidation time.
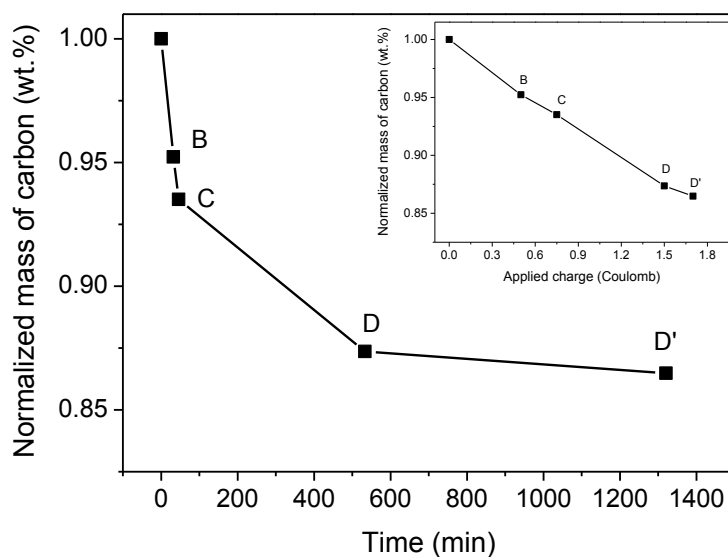
The mass of carbon is plotted as a function of oxidation time (representative figure) and applied charge (inset figure). It is linear with applied charge for the electrochemical oxidation of MWCNTs. It is evident that the applied charge is directly related to the oxidation from carbon to other products, i.e. CO_2, CO or surface oxides. With regard to the oxidation time, the mass of carbon rapidly decreases until region C. This is comparable with the variation of oxidation current from Figure 3.1. High oxidation current in region A, B and C induces a fast oxidation rate and considerable mass loss of carbon. The oxidation current reached steady-state in region D, there is a little mass loss of carbon.

Figure S3.9. Cyclic voltammogram in 5 mM K$_4$Fe(CN)$_6$ + 1 M KCl for the kinetics of electron transfer (ET) on the electrochemically oxidized MWCNTs, scan rate : 50 mV/s.
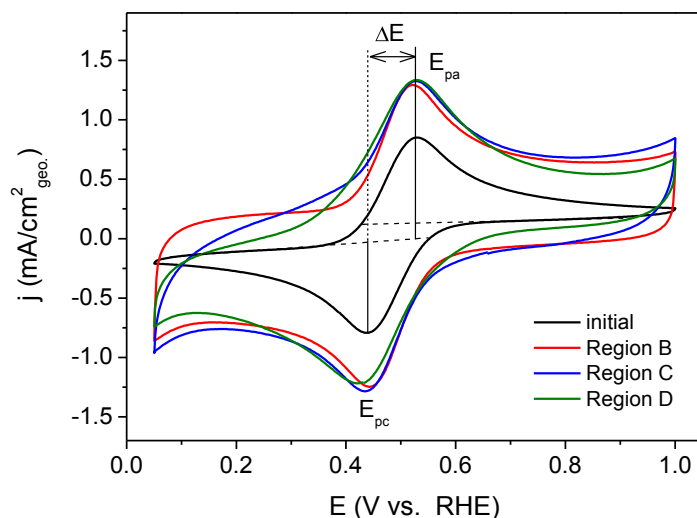
Figure S3.10. Tafel plots of MWCNTs during electrochemical oxidation in 0.5 M H$_2$SO$_4$, scan rate : 5 mV/s.
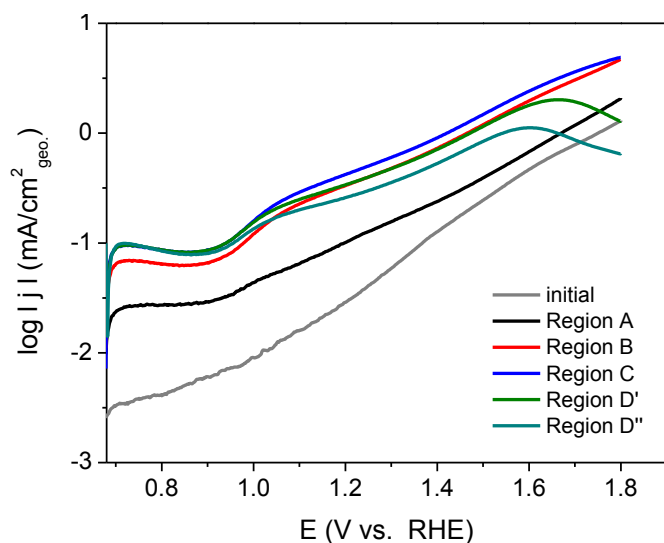
Table S3.2. The change of Tafel slope obtained from Figure S3.10.

Oxidation region	Low E (mV)	High E (mV)
initial	385	
A	529	
B	282	620
C	271	640
D	312	694
	339	839

Table S3.3. Parameters of equivalent circuits obtained by the fitting of Nyquist plot.

Oxidation region	Applied charge (C)	R_Ω (Ohm)	C_{DL} (mF)	R_{CT} (Ohm)
initial		16.9	1.05	277.8
B	0.25	16.7	2.11	252.7
	0.5	16.8	2.42	219.3
C	0.75	16.8	2.25	233.1
	1	17.0	1.50	352.2
	1.1	17.0	0.97	584.2
	1.2	16.8	0.34	1376
	1.3	17.7	0.13	3876
D	1.4	22.2	0.13	4471
	1.5	41.3	0.14	4348
	1.7	41.8	0.14	4447

4 Thermal-oxidative degradation of multiwall carbon nanotubes (MWCNTs); its effect for electrochemical activity and stability

Youngmi Yi, Xing Huang, Klaus Friedel Ortega, Marc Willinger, Julian Tornow, Robert Schlögl

Abstract

Multiwall carbon nanotubes (MWCNTs) degrade thermally under oxygen atmosphere. This degradation can limit the application of MWCNTs in heterogeneous catalysis and electrocatalysis. In this study, we investigated the morphological and structural changes of MWCNTs by a thermal oxidative treatment. The progress of the oxidative degradation was monitored by electron microscopy, elemental analysis, Raman and infrared spectroscopy. The thermal oxidation of MWCNTs leads to the formation of oxygen-containing functional groups and structural damage. Furthermore, its effect on the thermal and electrochemical behavior of MWCNTs was examined by temperature programmed desorption/oxidation (TPD/TPO) and electrochemical measurements. The prolonged thermal oxidation of MWCNTs induces a significant change in their thermal and electrochemical properties. Especially, the higher oxygen content in MWCNTs has a strong influence on thermal oxidation stability. Moreover, with respect to electrochemical measurements at an anodic potential, there are some noteworthy relations between the electrochemical activity/stability and the thermal oxidation of MWCNTs. Understanding the change of the thermal and electrochemical properties of MWCNTs during the thermal oxidative degradation makes it possible to effectively utilize MWCNTs in heterogeneous catalysis and electrochemical systems.
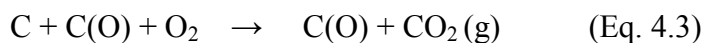
4.1 Introduction

The efficient utilization of sustainable energy is a key challenge for the future. Intermittent energy sources, such as solar and wind, need to be stored or converted into a storable energy carrier. Thus, energy conversion and storage have been extensively studied around the world. Carbon is one of the most economically competitive materials and has a variety of physicochemical properties for energy-related technologies [2, 3, 7]. Among many kinds of carbon materials, carbon nanotubes (CNTs) have been of great interest for decades. The unique structure of the CNTs imparts intrinsic physicochemical properties that make them suitable for many potential applications. Particularly, CNTs are extensively utilized in heterogeneous catalysis and electrocatalysis, either as a catalyst itself or as a catalyst support [104]. For example, CNTs have been used as direct catalysts in oxidative dehydrogenation (ODH) of hydrocarbons. Their performance is determined by the surface concentration of oxygen functionalities, the structural order, and the surface area of the CNTs. In the ODH of ethylbenzene and propane, more graphitized CNTs show higher and longer stability and a positive trend for the selectivity toward styrene and propene. The activity of CNTs for the ODH is proportional to the amount of active sites, that is, oxygen functional groups [105]. Compared to other carbon materials, CNTs are available in microporous forms as catalyst supports, and they offer tunable surface chemical properties by functionalization. Moreover, the functionalization of CNTs provides the specific metal-support interactions that can directly affect the catalytic activity and selectivity. Surface modification of CNTs could control their chemical and electronic properties by attaching specific molecules or incorporating heteroatoms into the carbon structure. The CNTs treated with NH_3 at different temperatures feature specific basic and acidic functional groups on the carbon surface [106]. N-containing species lead to a better metal dispersion and stabilize small nanoparticles. They provide a strong metal/support interaction with a beneficial effect on the activity and stability in the direct synthesis of hydrogen peroxide and the liquid phase oxidation of benzyl alcohol to benzaldehyde [107, 108].

In electrochemical applications, CNTs also exhibit unique properties for electrochemical reactions. For instance, nitrogen-containing CNTs enhance the interaction between metal

and carbon support and affect their electrocatalytic activity and stability for fuel cells [109, 110]. Furthermore, they are active for the oxygen reduction reaction (ORR) and the oxygen evolution reaction (OER), offering the possibility for metal-free electrocatalysts [42, 111, 112].

However, some applications of CNTs have been limited so far due to the inherent instability of carbon. Carbon is thermally oxidized to gaseous products at high temperature (above circa 400 - 600 °C) in oxidative atmosphere. There is general agreement about the mechanism of carbon oxidation [113];

$$2C(s) + O_2(g) \rightarrow 2C(O) \qquad \text{(Eq. 4.1)}$$
$$C(O) \quad \rightarrow \quad 2CO(g) \qquad \text{(Eq. 4.2)}$$
$$C + C(O) + O_2 \quad \rightarrow \quad C(O) + CO_2(g) \qquad \text{(Eq. 4.3)}$$
$$2C(O) \rightarrow C + CO_2(g) \qquad \text{(Eq. 4.4)}$$

where $C(O)$ represents adsorbed oxygen species on the carbon surface.

Thus, carbon oxidation in the high temperature regime inevitably results in a thermal degradation of CNTs. Gas phase oxidation of CNTs damages carbon structures and introduces oxygenated functional groups that represent the sites where the degradation is initiated upon utilization. On the other hand, it can be positively used for potential applications. Air oxidation of CNTs has been used to remove carbonaceous impurities and to open the ends of CNTs [114, 115]. The purification method is based on the selective oxidation of carbon, that is, the rate for the oxidation of amorphous carbon is faster than the one of graphitic carbon [116, 117]. Moreover, the addition of functional groups on the surface of CNTs via thermal oxidation can be considered for the immobilization of active species in catalysis. Oxygenated functional groups are also the active sites for metal-free catalyzed reactions. Therefore, it is important to understand how CNTs thermally degrade and the relationship between the thermal oxidation of CNTs and physicochemical properties.

Herein, we report on the thermal oxidative degradation of multiwall carbon nanotubes (MWCNTs). These allotropes were thermally oxidized at a temperature at which carbon starts to be oxidized and/or combusted. We monitored the thermal degradation process of

MWCNTs over a period of time and its effect on physicochemical properties. The morphological and structural changes of MWCNTs during thermal oxidative degradation were measured by electron microscopic investigation, elemental analysis, and Raman and infrared spectroscopy. Furthermore, to assist in the development of practical applications of CNTs, the thermal and electrochemical behavior of the thermally oxidized CNTs was investigated. With respect to electrochemical characterizations, we focused on the electrochemical oxidation activity and stability/degradation behavior at a high anodic potential. These findings are valuable for the research and application of MWCNTs in energy storage and conversion technology.

4.2 Experimental

4.2.1 Sample preparation

MWCNTs (Baytube, Bayer MaterialScience AG, Germany) were purified with mild wet-oxidation. Mild conditions were used to minimize structural damage of the MWCNTs during the cleaning procedure [73]. The MWCNTs were treated in 3 M HNO_3 with stirring under room temperature for 24 hours to remove metal(oxide) and carbon impurities from the MWCNTs. The oxidized sample was thoroughly washed and filtrated with deionized water until it achieved a neutral pH. To remove further amorphous carbon and oxidation debris, the sample dispersed in ethanol was sonicated with a Titanium tip sonicator (Bandolin sonopuls of 10% power, 5 cycles per second) for 3 hours. Afterwards, the MWCNTs suspension was treated with 1 M NH_4OH at 70 °C with stirring for 2 hours, subsequently filtered, and subjected to soxhlet extraction with deionized water twice in 24 hours and soxhlet extract with acetone for another 24 hours, followed by drying in an oven at 110 °C for 24 hours. For the thermal oxidation of the MWCNTs, the purified MWCNTs were treated with 5% O_2/Ar at 500 °C for 2 hours and 4 hours.

4.2.2 Physicochemical characterizations

The elemental compositions of MWCNT samples were examined by elemental analysis on CHN/O analyzer (Elementar Vario EL) through high temperature combustion.

For the investigation of the morphological change of the MWCNTs by thermal oxidation, scanning electron microscopy (SEM, Hitachi S4800 with cold field emission gun) was operated at 1.5 kV with secondary electrons. High resolution transmission electron microscopy (HR-TEM, Titan) was performed to examine the microstructure of the MWCNT samples. The specific surface area of the MWCNT samples was determined from N_2 adsorption-desorption at liquid nitrogen temperature using a Quantachrome Autosorb-6B-MP sorptometer. Prior to the measurement, the MWCNT samples were pretreated at 225 ∘C for 4 hours in He to remove moisture. The total surface area was calculated using the BET equation.

Raman spectroscopy (HORIBA Jobin Yvon spectrometer) was used to characterize the structural order of the MWCNTs on vibrational mode. The measurement was conducted using an excitation laser at 633 nm with 100× magnification.

Infrared spectroscopy at attenuated total reflection (ATR, company model) was carried out to identify the functional groups formed on the tube wall of the MWCNT samples. The spectra collected were equipped with a DTGS detector and a ZnSe crystal. A collected spectrum was on average scanned 1024 times with a resolution of 4 cm^{-1}.

4.2.3 Thermal characterizations

Temperature-programmed desorption (TPD) was performed in a home-built setup equipped with a gas chromatograph (Varian CP-4900 Micro-GC) and a mass spectrometer (Pfeiffer Omnistar) for on-line product analysis. The experiment was carried out at 100 °C in He at the flow rate of 25 ml per minute to evaporate water on the MWCNT samples, and then the temperate was increased until 1100 °C at the heating rate of 5 Kpm. The temperature was kept constant for 30 minutes before cooling down to ambient temperature.

Temperature-programmed oxidation (TPO) was carried out with Netzsch STA 449C Jupiter thermobalance for simultaneous thermal analysis, thermal gravimetric analysis-differential scanning calorimetry (TGA-DSC). The measurement was conducted using a 100 ml per minute flow of 5 % O_2 in Ar. The weighted amount of the MWCNTs was heated at 5 Kpm from room temperature to 1000 °C, and then held at that temperature for 10 minutes.

4.2.4 Electrochemical characterizations

All electrochemical measurements were conducted with a potentiostat/galvanostat (BioLogic VSP, France) at room temperature. A conventional three-electrode system was employed; a platinized Pt wire – as a counter electrode – and a standard calomel electrode (SCE, Hg/HgCl$_2$, 0.245 V versus SHE) as a reference electrode were used, respectively. The working electrode was prepared on a glassy carbon with a thin film coating method. A MWCNT ink with a concentration of 1.0 mg/ml was prepared by

ultrasonically dispersing 5 mg of powder in 5 ml of solvent, which contained isopropanol, water and 20 µl Nafion solution (5 wt.%, Aldrich). A 100 µl aliquot of the MWCNT ink was pipetted onto the polished glassy carbon (8 mm in diameter) and dried at 60 °C for 1 hour in air. The resulting carbon film loaded on the glassy carbon is 0.2 mg of MWCNTs per cm^2.

The electrochemical activity of the MWCNTs was determined from the electron transfer of simple redox system by measuring cyclic voltammetry in 5 mM $K_4Fe(CN)_6$ + 1 M KCl. To characterize further electrochemical performance of the MWCNTs samples, cyclic voltammetry and linear sweep voltammetry were carried out in N_2 saturated 0.5 M H_2SO_4. The electrochemical oxidation stability of the MWCNT samples was determined from the oxidation behavior at a high anodic potential in acidic media. For this experiment, the oxidation current on the MWCNT electrode was recorded for 3 hours at the fixed potential of 1.55 V versus SCE (1.8 V versus RHE). Electrochemical impedance spectroscopy was performed in the potentiostatic mode with the amplitude of 5 mV. The impedance before and after the electrochemical oxidation at an open circuit potential (OCP) was measured in the frequency range from 500 kHz to 100 mHz with 10 points per decade. It should be mentioned that the electrochemical experiments were reproduced several times and the data shown are thought to be representative of typical results.

4.3 Results and discussion

The onset of the weight loss and CO_2 produced on the purified MWCNTs (P-MWCNTs) are at around 500 °C in 5 % O_2/Ar from thermal gravimetric analysis (TGA) (Figure S4.1). Therefore, the thermal oxidation of P-MWCNTs was carried out at 500 °C for 2 h and 4 h. Samples are labeled as TO2h-MWCNTs and TO4h-MWCNTs. To monitor the progress of thermal oxidative degradation of the MWCNTs, we have chosen these oxidation conditions to avoid the fast combustion of the MWCNTs. Since the thermal oxidation runs under the relatively mild-oxidative conditions, there was no prominent mass loss of the MWCNTs after thermal oxidative treatment.

4.3.1 Physicochemical properties of the MWCNTs

Elemental analysis

The elemental compositions of the MWCNTs from elemental analysis are listed in Table 4.1. It shows that the total amount of carbon decreases with the time of thermal oxidation. TO2h-MWCNTs show a slight decrease in carbon contents from the starting materials of P-MWCNTs. However, the amount of carbon in TO4h-MWCNTs drops significantly. After the thermal oxidation of the MWCNTs, the amounts of hydrogen are reduced from 0.54 % to approximately 0.3 %, and nitrogen content appears. It is thought that there is the exchange of some C-H termination with C-O upon oxidation. Oxygen content was calculated as a residual percentage. The total amount of oxygen in the MWCNT samples increases with thermal oxidation. The change in the components of the MWCNTs by thermal oxidation may be due to surface oxidation or incorporation of nitrogen and oxygen within the carbon network of the MWCNTs. TO4h-MWCNTs contain considerably less carbon (94.8 %) and more oxygen (4.79 %) content compared to other MWCNT samples. It is generally accepted that significant oxidation happens at the MWCNTs with the prolonged thermal oxidation.

Table 4.1. CHN/O elemental analysis of thermally oxidized MWCNTs

Samples	Treatment of MWCNTs	Contents, wt.%			
		C	H	N	O
P-MWCNTs	purified by mild wet oxidation	98.49	0.54	0	0.97
TO2h-MWCNTs	500 °C in 5% O_2 for 2 hours	97.85	0.33	0.01	1.81
TO4h- MWCNTs	500 °C in 5% O_2 for 4 hours	94.80	0.35	0.06	4.79

Microscopic analysis

SEM images in Figure 4.1 (a)-(c) show the overall morphology of the MWCNTs during thermal oxidation. Bundles of MWCNTs are tangled and densely packed. P-MWCNTs and TO2h-MWCNTs have smooth tube walls. However, it is observed that the tube walls of TO4h-MWCNTs are broken, indicated by an arrow in Figure 4.1(c). Moreover, overall tube bundles are rough and form segmented tubes by damaging the carbon structure. Therefore, it is clear that the prolonged thermal oxidation induces large structural changes of the MWCNTs.
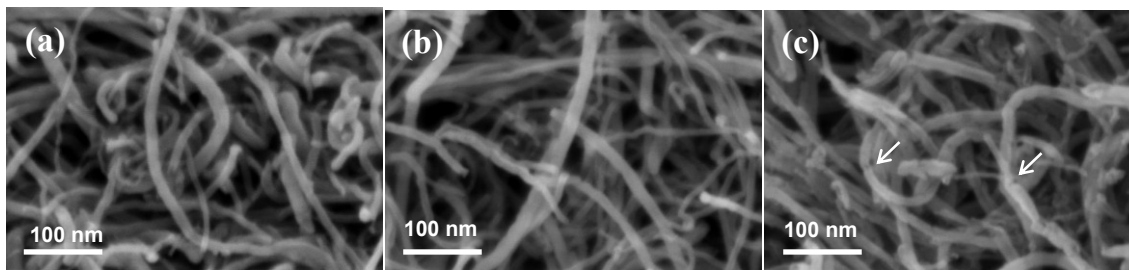
Figure 4.1. SEM images of (a) purified MWCNTs, thermally oxidized for 2 h (b) and 4 h (c) MWCNTs.

TEM investigation provides a closer look at the nanostructure of the MWCNTs. Lower magnification TEM images (Figure 4.2 (a), (c) and (e)) show that P-MWCNTs and TO2h-MWCNTs reveal smooth bundles of tubes, while TO4h-MWCNTs are rough and have defective segments on tubes. Higher magnification TEM images (Figure 4.2 (b), (d) and (f)) further confirm the morphological change of individual tubes by thermal

oxidation. Despite several purification procedures by mild wet oxidation of the MWCNTs, some pyrolytic/amorphous carbons are observed on the tube wall of P-MWCNTs. TO2h-MWCNTs have well-defined tube surface without local defects and relatively clean tube walls compared to P-MWCNTs. It could be inferred that the amorphous carbon and impurities remained on P-MWCNTs were eliminated by initial thermal oxidation [116].

In TO4h-MWCNTs, we found pit holes on the tube wall due to serious damage of graphitic layers. The prolonged oxidation leads to the damages of the tube walls, and initiates at some defects since it looks like holes in the walls. Interestingly, these defects are not only confined at the top of the graphitic layers, but also combust deeper layers. It is likely to cut the tube wall of the MWCNTs. Furthermore, we observed the presence of clumpy amorphous carbon inside the tube on TO4h-MWCNT in Figure 2(f). It seems that the opened MWCNTs may fill with the carbonaceous debris remaining after thermal oxidation [118-120]. Probably, additional oxidation debris are produced inside the wall of the MWCNTs via the pyrolysis of the gasified carbon species, and/or the amorphous carbon deposits are intermediates of the CNTs combustion [113].

Some previous studies observed a thinning of the MWCNTs from gas phase oxidation [115, 117, 121]. However, since as-received MWCNTs are inhomogeneous with various diameter distributions, we have not found the visible thinning of tube walls in the thermally oxidized MWCNTs.
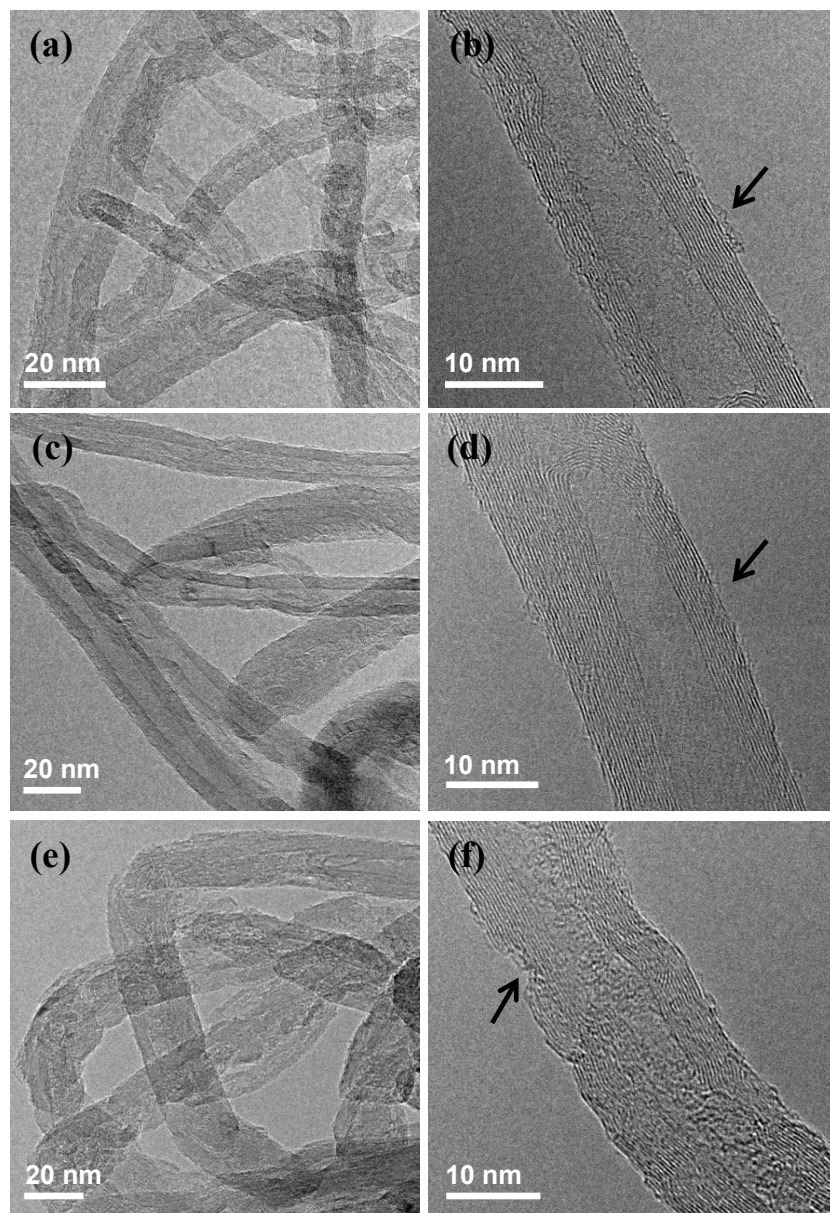
Figure 4.2. TEM images of purified MWCNTs (a, b), thermally oxidized for 2 h (c, d) and for 4 h (e, f).

Based on microscopic investigations, the structural change of the MWCNTs during thermal oxidative degradation is illustrated in Figure 4.3. Initial oxidation of the MWCNTs purifies the tube walls by removing residual amorphous carbon on the surface. Subsequently, further oxidation attacks to the graphitic layer and creates structural defects by destroying the outer wall of the tubular structure. The pit holes formed by

structural damage of the MWCNTs initiate successive gasification of graphitic walls and could lead to the cutting of the MWCNTs.

Figure 4.3. A schematic diagram for the thermal oxidative degradation of MWCNTs.

BET surface area

The surface area of the MWCNT samples, calculated using the BET method, is included in Table 4.2. The specific surface area of the MWCNT samples slightly increases after thermal oxidation for 2 h. Since there is no si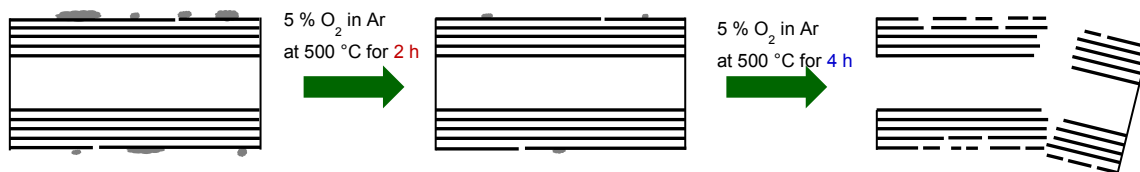gnificant morphological change of individual tubes in TO2h-MWCNTs, the slight increase of surface area could result from the loosening of MWCNT entanglement and the opening of tube ends [116, 122]. The surface area of TO4h-MWCNTs is over 3 times higher than one of the other MWCNT samples. This is evidence of an increased number of defects caused by broken tubes through prolonged thermal oxidation. It is therefore speculated that the structural damages on the sidewall of nanotubes in TO4h-MWCNTs increase the specific surface area of the MWCNTs.

Table 4.2. BET surface area and I_D/I_G intensity ratio from Raman spectra of the MWCNT samples.

	BET area (m^2/g)	**Raman** (I_D/I_G)
P-MWCNT	226	2.44
TO2h-MWCNT	268	2.35
TO4h- MWCNT	899	2.78

Raman spectroscopy

Raman spectroscopy captures structural changes in the MWCNTs by thermal oxidative degradation. As shown in Figure 4.4, the Raman spectra of the MWCNT samples show the two characteristic peaks: the D1 ("disorder," "defect") band centered at around 1320 cm^{-1} and the G ("graphite") band around 1580 cm^{-1}. All spectra were normalized with respect to the D1 band intensity for comparison purposes. Raman spectrum of TO2h-MWCNTs is similar to that of P-MWCNTs. In contrast, the G band intensity of TO4h-MWCNTs is much lower than for other MWCNT samples, suggesting less ordered carbon. The second peak in the spectrum of TO4h-MWCNTs was clearly distinguishable as a G band around 1580 cm^{-1} and D2 band around 1620 cm^{-1}. The D2 band comes from several graphene layers or small graphite domains on bulk graphite crystals, commonly found in defective graphite [105]. It can be inferred that the prolonged thermal oxidation of the MWCNTs induces the destruction of graphitic layer.
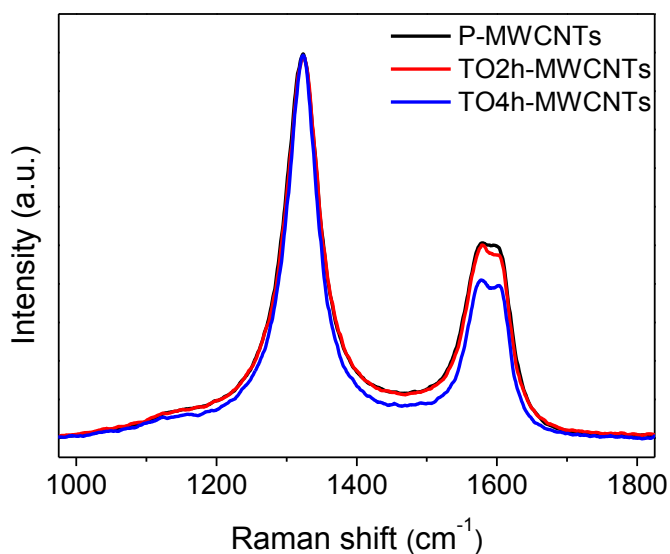
Figure 4.4. Raman spectra of the MWCNTs samples with thermal oxidative treatment. The spectra are normalized with respect to their intensity of D-band.

All Raman spectra of the MWCNTs samples was analyzed with four Lorentzian peaks at around 1180 cm^{-1}, 1320 cm^{-1}, 1580 cm^{-1}, and 1620 cm^{-1} and a Gaussian peak at around 1500 cm^{-1}, which was proposed by Sadezky et al. [103]. The fitting of Raman spectra in detail is presented in Figure S4.2(a). The ratio of relative intensities of the D1 and G

70

bands (I_{D1}/I_G) can be used to evaluate the defect density of carbon materials. These values, together with the BET surface area, are listed in Table 4.2. The I_{D1}/I_G ratio of TO2h-MWCNTs is slightly less than one of P-MWCNTs. It is believed that graphitic layers on a carbon surface are revealed by removing disordered amorphous carbon. This is in good agreement with the microscopic investigation that TO2h-MWCNTs have relatively clean tube walls without damaging the structure of tube wall. In contrast, TO4h-MWCNTs exhibit the highest value for I_{D1}/I_G of 2.73. It is evident that more defects and disordered carbons are produced from the prolonged thermal oxidation of the MWCNTs.

Figure S4.2 (b) compares all peak areas of the thermally oxidized MWCNTs against P-MWCNTs. Except for the D4 band, other disordered bands which are D1, D2 and D3 decrease after thermal oxidative treatment. The difference between P-MWCNTs and TO4h-MWCNTs are clearly higher than with TO2h-MWCNTs, indicating the significant change of carbon structure. The signal intensity at ~1500 cm^{-1} between two high peaks, which (designated D3) is attributed to amorphous carbon fraction. The peak area of the D3 band is remarkably reduced with the thermal oxidation of MWCNTs. It is evident that amorphous carbons are reduced on the MWCNTs by thermal oxidation. However, the peak area of D4 band at ~1200 cm^{-1} increases with a longer time period for thermal oxidation. The D4 band originates from mixed sp2-sp3 bonding, or C-C and C=C stretching vibration modes of a polyene-like structure [103, 123]. The increase of D4 band may explain the presence of functional groups on the MWCNTs produced by thermal oxidation.

Infrared spectroscopy

Infrared spectroscopy (IR) is a well-known qualitative technique for determining chemical structure on a carbon surface. Figure 4.5 shows the IR spectra of the MWCNT samples to identify which type of functional groups were formed on the MWCNTs by thermal oxidation. It was observed that all spectra have several peaks in the range of 2800-2960 cm^{-1} which has been assigned as C-H stretching. Since this band shows up in all spectra without any change, it could be from hydrocarbon contamination during the measurement [88].

In the spectrum of P-MWCNT, there are two interesting bands; a distinct peak at 1547 cm^{-1} and a broad peak around 3260 cm^{-1}. The band at 1547 cm^{-1} is from the graphitic structure of the MWCNTs and/or assigned to the localization of C=C bonds and coupling to C=O modes [124]. The band at 3260 cm^{-1} is identified with O-H stretching modes. Small peaks between 1100 and 1300 cm^{-1} are expected for C-O stretching vibration in ethers, ester, alcohol, and phenol functional group[86].

After thermal oxidation for 2 h, the IR band for C-O stretching is enhanced, indicating that initial thermal oxidation introduces some C-O groups to the end or the side of tube walls. Moreover, an additional broad peak appears at around 3500 cm^{-1}. This broad band is attributed to several different -OH containing groups. In the rage of 3100 ~ 3600 cm^{-1} which is sensitive to hydrogen bonding, the low frequency around 3250 cm^{-1} is identified with O-H stretching from coupled carboxylic acid groups and the higher frequency around 3500 cm^{-1} from alcoholic or phenolic groups [88]. Therefore, the peak at 1720 cm^{-1} of P-MWCNTs and TO2h-MWCNTs could be identified with carboxylic acid groups.
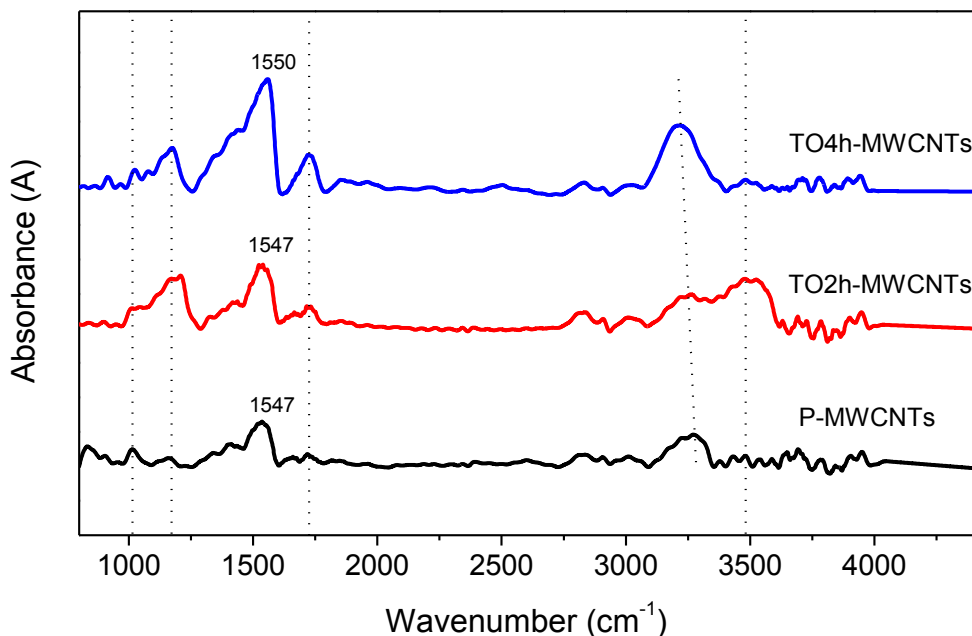

Figure 4.5. Infrared spectra of the MWCNTs samples with thermal oxidative treatment.

For the spectrum of TO4h-MWCNTs, we could observe the intense peak for carboxylic acid groups and the reduction of the band for C-O strength with the disappearance of the broad peak at 3500 cm^{-1}. It is assumed that alcoholic hydroxyl groups are oxidized and the functional groups for C=O strength and C=C bond are strongly produced with further thermal oxidation of the MWCNTs. We also found that the peak is shifted from 1547 cm^{-1} to 1550 cm^{-1} with a strong increase in intensity. This could account for additional defects on the carbon surface and the structural change of the MWCNTs [125]. Moreover, the broad band at a high frequency is downshifted, indicating a couple of hydroxyl groups, consistent with an increase in their population [88]. Therefore, the IR analysis proves that the prolonged thermal oxidation of MWCNTs creates defects via the destruction of graphitic layers and leads to the abundance of oxygen-containing surface groups formed on these defects.

4.3.2 Thermal behavior of the MWCNTs

Temperature programmed desorption

Temperature programmed desorption (TPD) of carbon materials provides information on the decomposition stability of the chemical nature on a carbon surface. Figure 4.6(a) shows the weight loss of the MWCNT samples under Ar. It can be seen that TO4h-MWCNTs have noticeably larger weight loss than other MWCNT samples. A temperature up to 150 °C corresponds to the evaporation of the adsorbed water. The temperature range between 150 °C and 500 °C is related to the removal of functional groups [126, 127]. It was observed that the weight loss of TO2h-MWCNTs is similar as P-MWCNTs in this temperature range. This means that there is no obvious change in the amount of surface functional groups during initial thermal oxidation of the MWCNTs for 2 h. The weight loss of TO4h-MWCNTs is approximately 2 % until 500 °C, indicative of the hydrophilic character. The temperature higher than about 500 °C is attributed to thermal decomposition of the disordered or amorphous carbon. The weight losses of the MWCNTs samples above 500 °C increase with time for thermal oxidative treatment. In

73

particular, the dramatic weight loss of TO4h-MWCNTs makes it clear that the significant amount of disordered carbon was created by the destruction of the graphitic structure.

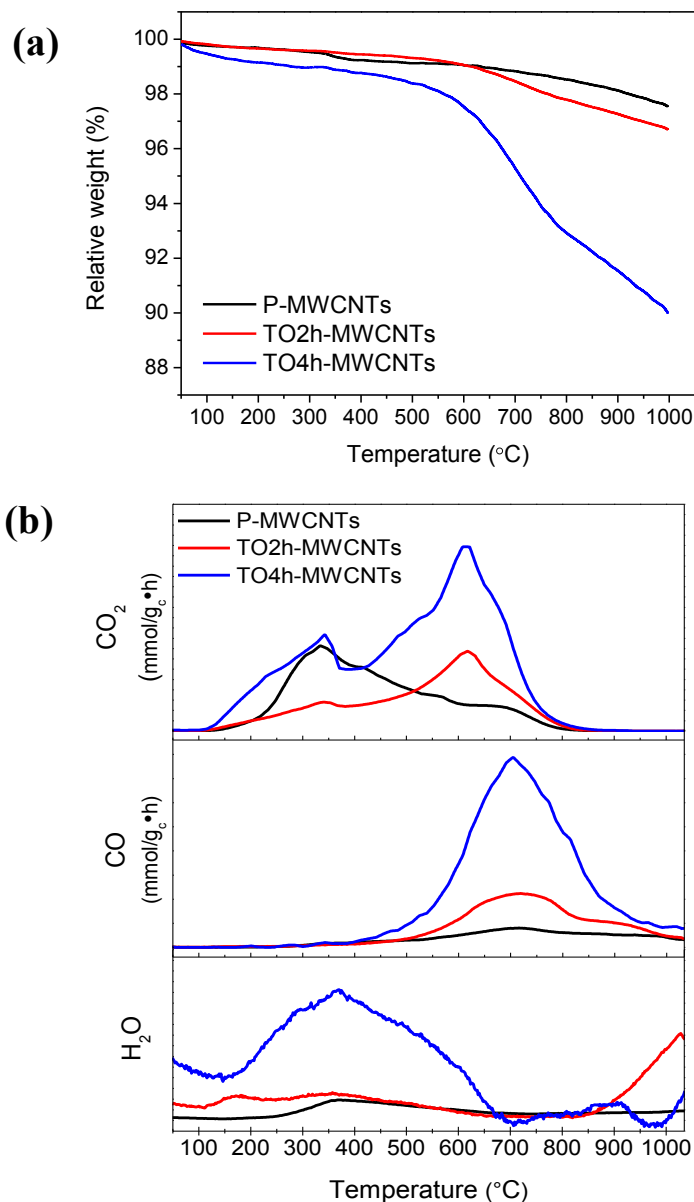Figure 4.6. Temperature programmed desorption (TPD) of the MWCNT samples in inert gas;(a) weight loss profiles and (b) CO_2, CO, and H_2O release profiles.

The volatile products decomposed from chemisorbed species at the carbon surface were simultaneously detected by online mass spectrometer. Figure 4.6(b) presents the mass profiles of CO_2, CO and H_2O as a function of temperature. The decomposition

temperature of these species depends on the surface functional groups on the carbon surface [12, 128, 129]. CO_2 peaks arise from the decomposition of carboxylic acid at a low temperature (~350 °C) and from anhydride, lactones or lactols at higher temperature (~600 °C). Since carboxylic groups are decomposed to anhydrides at a low temperature, carboxylic anhydrides produce the CO_2 peak an equal amount of CO. A CO peak at high temperature (~700 °C) is assigned to several types of surface oxygen groups, for example, ethers, phenols, carbonyls and quinones.

According to the CO_2 profiles in the TPD of the MWCNT samples, CO_2 generating groups on P-MWCNTs and TO2h-MWCNTs are quite different. The CO_2 complexes are decomposed rapidly on the P-MWCNTs at near 350 °C. After thermal oxidation for 2 h, the CO_2 peak is reduced at a low temperature and enhanced at a high temperature. This indicates that TO2h-MWCNTs have higher thermal stable oxygenated species than P-MWCNTs. Otake *et al* [130] reported that air oxidation of carbon leads to the dehydration of adjacent carboxyl groups to a carboxylic anhydride. The existence of water can be confirmed by the H_2O profiles that the H_2O evolved on TO2h-MWCNTs is more than on P-MWCNTs in the low temperature regime. In addition, hydroxyl group formed during this process could be supported by infrared analysis (Figure 4.5). Infrared spectrum of TO2h-MWCNTs exhibits the additional broad peak at a high frequency, which is identified with O-H stretching from alcoholic or phenolic groups.

TO4h-MWCNTs reveal much higher evolved CO_2 than other MWCNT samples. It is apparent that prolonged thermal oxidation produces a larger amount of the functional group. The CO_2 peak of TO4h-MWCNTs is relatively small at a low temperature and large at a high temperature. As we have seen previously, TO4h-MWCNTs have more defects than other MWCNTs samples due to the damage of graphitic layers on the sidewall of the MWCNTs. It is likely that nonadjacent acidic oxygen complexes such as carboxylic groups are formed on the edge carbon atoms on defects by further thermal oxidation of the MWCNTs.

The CO profiles clearly explain that oxygen-containing functional groups increase with time for thermal oxidative treatment of the MWCNTs. It can be seen that in TO4h-MWCNTs, the amount of CO evolving is noticeably larger than in other MWCNT samples. The broad CO peak indicates many kinds of surface functional groups. The

temperature in the range where CO and CO_2 curves overlap originates from carboxylic anhydride, which subsequently decomposes to equivalent amounts of CO and CO_2. Close examination of the CO profile of TO2h-MWCNTs reveals a main peak at around 700 °C with the shoulder around 900 °C. These two peaks are ascribed to phenols and ethers at a low temperature, and to carbonyl and quinones at a high temperature [128, 131]. TO4h-MWCNTs have a prominent peak at 700 °C, which means a large amount of phenolic groups were formed by prolonged thermal oxidation. Furthermore, the H_2O profiles support this examination. The evolution of H_2O from TPD experiment originates from H-bonded H_2O associated with acidic oxygen complexes and from condensation of neighboring phenolic species [132]. TO4h-MWCNTs have an appreciable amount of water during TPD, indicating hydrophilic properties.

The total amounts of CO and CO_2 evolved from the MWCNTs samples obtained by integration of the TPD spectra are presented in Table 4.3. The amount of CO in TO2h-MWCNTs is less than P-MWCNTs, probably due to the conversion or dehydration of some functional groups. However, since prolonged thermal oxidation induces the substantial increase of the surface oxides on carbon surfaces, TO4h-MWCNTs have over twice the amount of CO than the other MWCNTs samples. On the other hand, the amount of CO_2 increases linearly with time for thermal oxidative treatment. The ratio of oxygen can be obtained in the amount of CO to CO_2 evolution. After thermal oxidation, this CO/CO_2 ratio increases from initially 4 to about 9, suggesting less-acidic characteristics. This indicates that the amount of strong acidic groups is relatively lower than hydroxyl groups produced by thermal oxidative treatment. At the beginning of thermal oxidation for 2 h, CO evolving complexes are mainly formed on the carbon surface. However, further thermal oxidation produces an amount of CO_2 complexes together with CO evolving complexes, thus the ratio is not significantly different [130].

Table 4.3. Thermal properties of the MWCNT samples obtained from TPD and TPO measurements (Figures 4.6 and 4.7).

	TPD			TPO-TGA		TPO-DSC	
	CO, mmol/g	CO_2, mmol/g	CO/CO_2	T_{onset} (°C)	T_{oxi} (°C)	$T_{Max.}$ (°C)	Heat of oxidation, ΔH_C (kJ/mol)
P-MWCNTs	0.321	0.080	4.01	463	600	592	266
TO2h-MWCNTs	0.642	0.071	9.04	453	593	589	259
TO4h-MWCNTs	1.747	0.180	9.71	451	609	598	246

Temperature programmed oxidation

Thermogravimetric analysis in an oxidative atmosphere, that is temperature programmed oxidation (TPO), was used to investigate the oxidation stability of the MWCNT samples. Figure 4.7(a) shows the differences in the oxidation behavior through the weight loss of the MWCNT samples from TPO. According to overall curves, TO2h-MWCNTs resemble closely the P-MWCNTs with the slight deterioration of the oxidation stability, while the oxidation stability is enhanced in TO4h-MWCNTs. In general, the graphitized MWCNTs with less active sites show high oxidation stability [73]. However, TO2h-MWCNTs which have clean tubes due to selective thermal oxidation of amorphous/pyrolytic carbon show slightly lower oxidation stability than P-MWCNTs. In our case, starting MWCNTs were purified with several procedures. Subsequent thermal oxidation of the MWCNTs produces more surface oxides and opens the end of tubes from P-MWCNTs. Since these surface functional groups are thermally unstable and the edges on the end of tubes are more susceptible to thermal oxidative attack during TPO [117], it could result in low oxidation stability of TO2h-MWCNTs. Interestingly, even though TO4h-MWCNTs have many defects due to surface damage, as confirmed by previous morphological and structural investigations, its thermal-oxidative stability is improved compared to other MWCNTs samples. We looked closely at the initial weight loss of the MWCNTs (the inset of Figure 4.7(a)). The first 5% weight loss of TO4h-MWCNTs is faster than that of P-MWCNTs. This initial mass reduction results from the gasification of reactive surface

oxides on the MWCNTs. Since elemental analysis showed that TO4h-MWCNTs process a significant amount of oxygen, the gasification of an oxygen-rich carbon surface during TPO may slow down the rate for thermal oxidation of the MWCNTs. Therefore, it seems probable that the temperature increase on oxygen-rich TO4h-MWCNTs accumulates oxygen on the surface and forms an oxide barrier against further oxidation, which acts as a passivation. This behavior could be also supported by differential-scanning calorimetry (DSC), as shown in Figure 4.7(b). The DSC curve of TO4h-MWCNTs is broader than one of the other MWCNTs at the range for low temperature before the significant combustion of the MWCNTs. It may explain that the oxygen species is involved in initial oxidation of TO4h-MWCNTs and affects slow thermal oxidation later.

The residue remaining after TPO of TO4h-MWCNTs was observed. Through TEM-EDX analysis of this residue, it is confirmed that Co and Mn were metal catalysts used for growing carbon nanotubes. This is an unexplainable behavior of the thermally oxidized MWCNTs. The metal catalysts encaged in polyhedral graphitic particles might not be removed completely by previous purification of mild-wet oxidation. These particles were exposed and oxidized during thermal oxidative treatment and/or TPO measurement [124]. As the result, the mass was gained by the oxidation of remaining metal particles and was observed as residual in the weight loss curve.
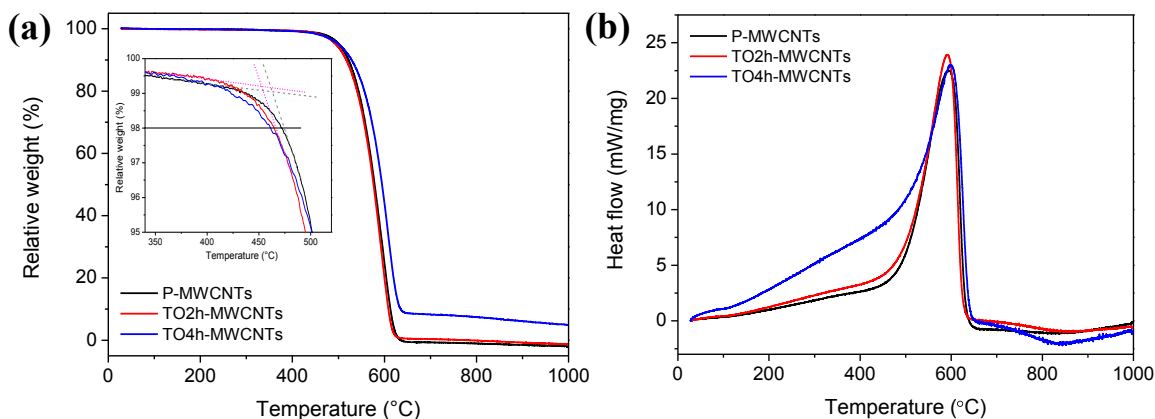

Figure 4.7. Temperature-programmed oxidation (TPO) of MWCNT samples in 5% O_2/Ar ; (a) weight loss profiles and (b) differential scanning calorimetry (DSC) signals.

Several comparative parameters were obtained from the weight loss curve to understand the oxidation stability of the thermally oxidized MWCNTs, summarized in Table 4.3. Onset temperature (T_{onset}) at which the weight loss begins is extrapolated in the range of 250 °C and 500 °C for initial oxidation of MWCNTs. The oxidation temperature (T_{oxi}), which is the peak of the derivative of the weight loss curve, indicates the point of greatest rate of change. These values demonstrate that initial oxidation increases with the treatment time for thermal oxidation on the MWCNTs, but overall oxidation exhibits a different trend. T_{oxi} of TO2h-MWCNT is lower whereas one of the TO4h-MWCNTs is higher than P-MWCNTs. Moreover, a DSC curve recorded during TPO gives the enthalpies associated with the thermal oxidation of the MWCNT samples. The position of the peak maximum in the DSC curves ($T_{Max.DSC}$), which is the maximum rate of heat evolution, exhibits a consistent trend with the oxidation temperature of the thermally oxidized MWCNTs samples. The integral heat of oxidation of the MWCNTs calculated from the DSC decreases slightly with time for thermal oxidative treatment. Therefore, since the prolonged thermal oxidation of MWCNTs produces an oxygen-rich surface, it ironically results in low heat of oxidation and high oxidation stability.

4.3.3 Electrochemical behavior of the MWCNTs

With respect to the thermal oxidative degradation of MWCNTs, its effects for electrochemical properties of the MWCNTs were investigated with several electrochemical measurements.

The effect of the electron transfer of Fe(CN)$_6^{3-}$/Fe(CN)$_6^{4-}$ redox couple

The influence of the thermal oxidation of the MWCNTs on their electron transfer properties was probed by simple redox reaction of Fe(CN)$_6^{3-}$/Fe(CN)$_6^{4-}$ redox couple. In Figure 4.8(a), cyclic voltammogram (CV) of the MWCNTs in K$_4$Fe(CN)$_6$ solution shows a reversible behavior of one electron transfer reaction. It can be seen that similar voltammograms were obtained for P-MWCNTs and TO2h-MWCNTs. However, TO4h-MWCNTs process higher background current, suggesting high capacitance. The

difference between anodic and cathodic peak potential (ΔE_p) is an indicative value for the electron transfer (ET) kinetics, listed in Table 4.4. ΔE_p increases with the thermal oxidation of the MWCNTs, meaning that slow kinetics of electron transfer on the MWCNT electrode. Actually, it was expected that the presence of functional groups and defects on the carbon surface would enhance ET kinetics [61, 100]. However, in the progress of thermal oxidative degradation of MWCNTs, the change of the carbon surface gives the MWCNTs electrode slow ET kinetics. It could be that surface oxides formed by the thermal oxidation do not contribute to electron transfer, and deteriorate the ET kinetics on the MWCNT electrode.
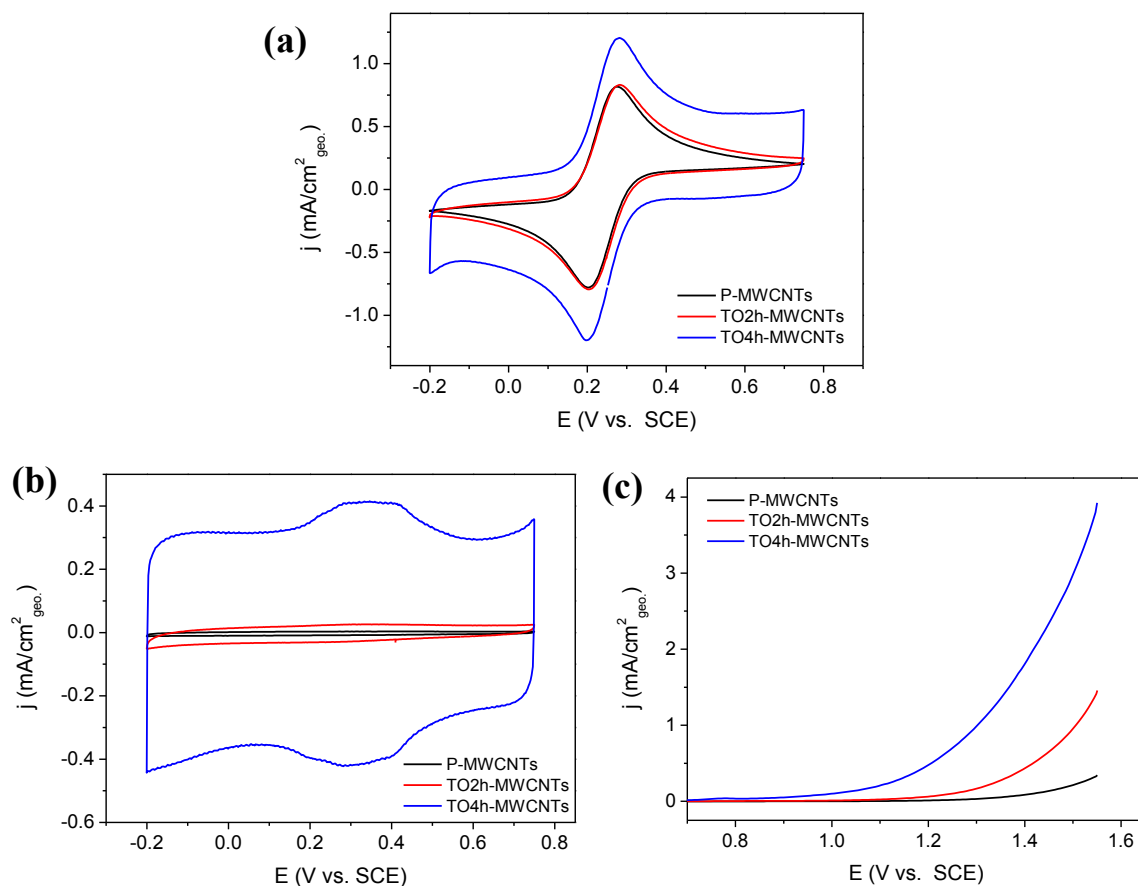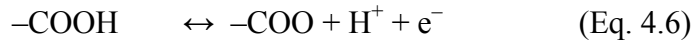

Figure 4.8. Electrochemical measurement of MWCNTs samples; cyclic voltammetry in (a) 5 mM $K_4Fe(CN)_6$ + 1 M KCl, (b) 0.5 M H_2SO_4, scan rate : 50 mV/s, and (c) linear sweep voltammetry in 0.5 M H_2SO_4, scan rate : 5 mV/s.

Table 4.4. Electrochemical properties of the MWCNTs samples obtained from Figure 4.8.

	ET kinetics ΔE_p (mV)	specific capacitance		Tafel plot	
		mF/cm^2	uF/cm$^2_{BET}$	Tafel slope b (mV/dec)	exchange current density -log j$_0$(mA/cm^2)
P-MWCNTs	71	0.1	0.23	234	7.1
TO2h-MWCNTs	76	0.5	0.85	245	6.1
TO4h-MWCNTs	83	6.8	3.80	308	3.9

Cyclic voltammetry in acidic media

Figure 4.8(b) shows the cyclic voltammetry (CV) of the MWCNT samples in 0.5 M H$_2$SO$_4$. P-MWCNTs and TO2h-MWCNTs feature a rectangular-shaped curve, which indicates a typical shape for electrochemical double layer capacitance. After the prolonged thermal oxidation of the MWCNTs, a pair of broad peaks appears around 0.6 V, and the specific capacitance increases significantly. It is widely accepted that the oxidative treatment of a carbon material increases the electrochemical capacitance due to an increase in the surface area and the generation of functional groups on the carbon surface. The following reactions of surface functional groups could be considered a contribution to electrochemical capacitance [6].

$$>C–OH \quad \leftrightarrow \; >C=O + H^+ + e^- \qquad (Eq.\ 4.5)$$
$$–COOH \quad \leftrightarrow \; –COO + H^+ + e^- \qquad (Eq.\ 4.6)$$
$$>C=O + e^- \; \leftrightarrow \; >C–O^- \qquad (Eq.\ 4.7)$$

In particular, the intensified redox peak originates from a surface redox reaction of the oxygen-containing functional groups that are electrochemically active. Redox processes of surface oxides on carbon are responsible for a pseudocapacitance. With consideration for the carbon structures in TO4h-MWCNTs, the oxygen functional groups formed at the exposed edges of the broken and rough tube wall may contribute to the redox reaction of surface oxides. Thus, it is demonstrated that initial thermal oxidation of MWCNTs

enhances only double layer capacitance, and the prolonged thermal oxidation induces the significant increase in double layer capacitance with the contribution of pseudocapacitance. A value for the specific capacitance of the MWCNTs was calculated from CV by dividing the voltammetric current with the potential scan rate. These values are presented against geometric area and BET surface area, respectively, in Table 4.4. The specific capacitance of TO4h-MWCNTs is about 70 times and 16 times regarding the geometric area and the surface area respectively higher than one of P-MWCNTs.

Linear sweep voltammetry in acidic media

Linear sweep voltammetry (LSV) was measured on the MWCNT samples at anodic potentials, as shown in Figure 4.8. As the applied potential increases, electrochemical oxidation of both carbon and water occur at the MWCNTs electrode. The electrochemical oxidation activity of MWCNTs, which is monitored by the oxidation current, increases with thermal oxidative treatment. It is clearly seen that the concentration of the functional groups formed on the carbon surface is directly related to the electrochemical oxidation activity. For a more quantitative assessment, Tafel slope ($\frac{2.3RT}{n\alpha F}$) and exchange current density (a) were obtained from Tafel plot which is the linear relationship between the potential and logarithm of the current. Tafel equation is following;

$$E = a + \frac{2.3RT}{n\alpha F}\log i \qquad \text{(Eq. 4.8)}$$

where R is the ideal gas constant, F is the Faraday constant, and T is absolute temperature. These values are the kinetic parameters of an electrochemical reaction, listed in Table 4.4. Tafel slope of all MWCNTs samples are getting higher as the time for thermal oxidative treatment increases. The parameters determining the Tafel slope are transfer coefficient α and electron number n. High Tafel slope has been attributed either to a potential drop in the space charge region or to the accumulation of oxygen species on the electrode [93]. It is demonstrated that the reaction kinetics on the MWCNTs, which means low transfer coefficient in Tafel slope, is slower by thermal oxidation, as confirmed in redox response of $Fe(CN)_6^{3-}/Fe(CN)_6^{2-}$. Moreover, it is reasonable to suppose that the presence of

oxygen-containing surface functional groups acts as a barrier to the oxidation reaction on the MWCNT electrode. Furthermore, the higher exchange current density indicates higher oxidation activity. The value for the exchange current density on P-MWCNTs is 10^{-7} mA/cm^2, whereas on TO4h-CNT leads about 10^{-4} mA/cm^2, 3 orders of magnitude for the rate for the reaction.

Electrochemical impedance spectroscopy of MWCNTs in acidic media

To determine all components of complex resistance, such as charge transfer resistance and capacitance of the MWCNT electrode, electrochemical impedance spectroscopy (EIS) was measured at open circuit potential (OCP) in which no current flows. Figure 4.9 displays impedance spectra in the form of a Nyquist plot.

A detailed interpretation of EIS requires the fitting of spectra with an appropriate electrical equivalent circuit. Considering the electrode preparation and chemical processes on the MWCNTs, we used the equivalent electrical circuit proposed by Obradovic *et al.* [133], as shown in the inset of Figure 4.9. The equivalent electrical circuit consists of three parts: first, cell resistance (R_{cell}) of the electrolyte and carbon surface film; second, in series with a parallel combination of a contact resistance and capacitance (R_c, CPE_c) which represent the resistances between the carbon film and glassy carbon electrode; and third, in series with the resistance from electrochemical process at the electrolyte/carbon interface. The third part is our interesting point because it contains double layer capacitance (CPE_{dl}) in parallel to pseudocapacitance (C_p) with charge transfer resistance (R_{ct}). Instead of capacitance, the constant phase element (CPE), which is a non-ideal capacitance with a roughness factor (α), was used for EIS fitting because of a porous carbon film.

The results obtained from the fitting are summarized in Table 4.5. The factor for contact resistance (R_c, CPE_c) is not presented. The cell resistance decreases in TO2h-MWCNTs, since initial surface oxides formed by the thermal oxidation are likely to allow a better accessibility. The value of R_{cell} decreases slightly in TO2h-MWCNTs and then increases again in TO4h-MWCNTs, compared to P-MWCNTs. The thermal oxidative treatment initially makes the surface of the MWCNTs hydrophilic, but further oxidation induces surface oxides that prevent the flow of the electrolyte to the electrode. The value of CPE_{dl}

increases linearly by thermal oxidative treatment of the MWCNTs. The roughness factor maintains around 0.8 without significant difference. The value for C_p is tremendously improved in TO4h-MWCNTs. In accordance with the findings of cyclic voltammogram on TO4h-MWCNTs, it is evident that the surface oxides formed on a broken tube wall by prolonged thermal oxidation contribute to the redox response of oxygen-containing functional groups. The value of R_{ct} is the lowest in TO2h-MWCNTs, and increases in TO4h-MWCNTs about 5 times against TO2h-MWCNTs. This supports the fact that the prolonged thermal oxidation of MWCNTs interferes with the charge transfer on MWCNT electrodes.
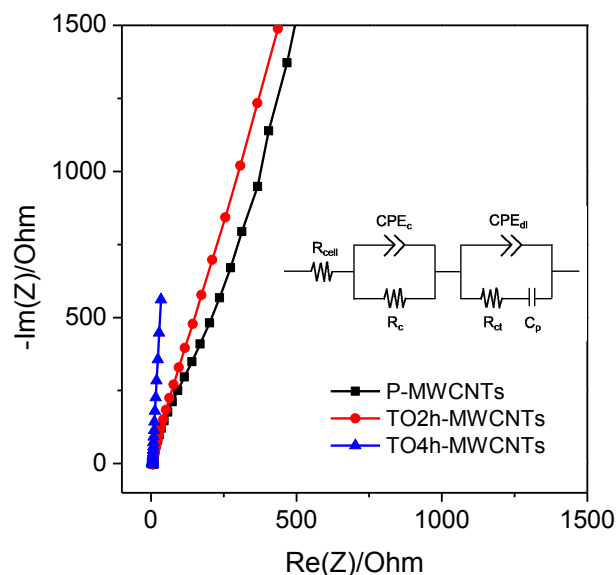
Figure 4.9. Electrochemical impedance spectroscopy (EIS); Nyquist plots of the MWCNT samples at open circuit potential (OCP) in 0.5 M H_2SO_4. Inset figure is an equivalent electrical circuit used for the fitting.

Table 4.5. EIS fitting values obtained from Figure 4.9.

	R_{cell} (Ω)	CPE_{dl} (uF s$^{(\alpha-1)}$)	CPE_{dl}-α	C_p (μF)	R_{ct} (mΩ)
P-MWCNTs	5.6	35	0.81	10.88	48.05
TO2h-MWCNTs	4.8	171	0.77	32.78	16.81
TO4h-MWCNTs	5.4	477	0.81	2341	103.4

The stability of the electrochemical oxidation on MWCNTs

The electrochemical oxidation stability of MWCNTs was measured by chronoamperommetry at a high anodic potential where the oxidation of carbon and water can take place simultaneously, 1.8 V versus RHE in 0.5 M H_2SO_4. Our previous study reported on the electrochemical degradation of MWCNTs via the change of oxidation current under the constant potential [134]. Initial oxidation current rapidly drops to a steady state, and then increases slightly. Beyond this change of initial oxidation current, the current decays again, and finally reaches a constant current that is close to zero. Therefore, at the end of the electrochemical oxidation, the MWCNTs are stabilized due to the formation of a passive oxide film. In this study, we investigated the effect of thermal oxidative treatment on the MWCNTs for the electrochemical stability at high anodic potential.

Figure 4.10 shows a current-time transient on the MWCNTs at a fixed potential of 1.8 V versus RHE for 3 hours. The oxidation current transition on P-MWCNTs is the same as the one found in previous investigations. Compared with P-MWCNTs, chronoamperograms of TO2h-MWCNTs and TO4h-MWCNTs have no region for the oxidation current increase and reach the last region of constant current after the current decay. This indicates fast degradation of the thermally oxidized MWCNTs. Since the thermally oxidized MWCNTs have relatively less amorphous carbon and more surface oxides than the starting P-MWNCTs, these characteristics of the MWCNTs have an effect on their electrochemical oxidization. The degradation region/stage of the oxidation current increase provides that initial surface oxides formed on carbon promote further oxidation of gaseous products. The current decay of TO4h-MWCNTs is faster than TO2h-MWCNTs. It is clear that more defective MWCNTs by prolonged thermal oxidation have more reactive sites and induce fast degradation. On the other hand, this result could be associated with the oxygen concentration on the MWCNTs by thermal oxidative treatment. In general, surface oxides are also formed on the carbon by the electrochemical oxidation of MWCNTs. In the region of the oxidation current decay, surface oxides start to cover the carbon surface, and block the electron transfer on the MWCNT electrode. It seems that the pre-existence of oxygen on the carbon electrode

85

accelerates the formation of the protective oxide layers on the MWCNT electrode and interrupts further the electrochemical oxidation reaction. Therefore, it is conclusive that the oxygen coverage on the carbon surface determines the stage of the electrochemical degradation of MWCNTs.
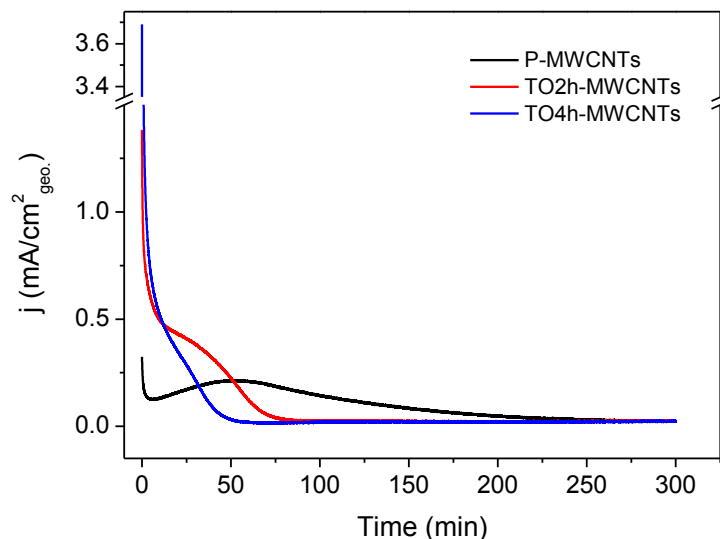

Figure 4.10. Chronoamperogram of the MWCNTs samples at 1.8 V versus RHE for 3 hours in 0.5 M H_2SO_4.

The electrochemical behavior of the MWCNT electrodes before and/or after the electrochemical oxidation performed by chronoamperommetry at 1.8 V versus RHE for 3 h was compared to supporting information, Figure S4.3 – S4.5. As we can see in Figure 4.10, the oxidation current of all MWCNT electrodes reached the last stage of the electrochemical degradation, which is constant with a low value of the oxidation current. In Figure S4.3, cyclic voltammetry of the $Fe(CN)_6^{3-}/Fe(CN)_6^{2-}$ redox couple shows a significant increase of the capacitive current after the electrochemical oxidation of the MWCNTs. The values of peak separation (ΔE_p) in all MWCNTs later are larger than initial MWCNTs, indicating slow ET kinetics. The relationship between peak current (i_p) values and the square root of scan rate is linear in the initial MWCNT electrodes. However, after the electrochemical oxidation, its relationship is nonlinear. This indicates that the electrode process on the MWCNTs after electrochemical oxidation is not only limited by diffusion, but might be due to surface adsorption of reactants to the electrode

[61]. Furthermore, The evidence suggests that the oxide barriers are formed on the carbon surface by the electrochemical oxidation of the MWCNTs. Cyclic voltammetry in 0.5 M H_2SO_4 on MWCNTs shows a considerable increase in the capacitance with the intensified redox peak after electrochemical oxidation (Figure S4.4). Interestingly, cyclic voltammograms of all MWCNT samples after the electrochemical oxidation have the same features, despite different initial electrochemical properties of each MWCNT sample. It is likely that there is no surface change by further electrochemical oxidation, once the oxidation current reached a constant current. For better confirmation, the impedance behavior of the MWCNTs samples before/after electrochemical oxidation was analyzed with a Bode plot, shown in Figure S4.5. The impedance magnitude and phase decrease at high- and intermediate-frequencies and are nearly vertical to the real axis at low frequencies after the electrochemical oxidation of the MWCNTs. Moreover, it shows that the plateau at low frequencies may result from a new process occurring on the interface of electrode and electrolyte. It probably supports that surface oxides fully cover the electrode and form an oxide barrier against further surface reaction. The impedance spectra of all MWCNT samples show almost the same curves after the electrochemical oxidation. As the results of cyclic voltammetry in acidic media, impedance spectra support the view that the electrochemical state of the MWCNT electrode is the same after the electrochemical oxidation in which the oxidation current is close to zero in the last stage of chronoamperommetry. According to the results shown in the supporting information, it is conclusive that regardless of the initial state of MWCNTs, the electrochemical behavior of the fully degraded MWCNT electrodes shows the same high capacitance and losses in the electrochemical activity due to the effect of inactive surface oxide barriers on MWCNTs.

4.4 Conclusion

We reported in this study how MWCNTs thermally degrade in oxidative environment. MWCNTs were treated under an oxygen atmosphere at the temperature in which the combustion of carbon takes place. Through the microscopic investigations of the thermally oxidized MWCNTs with time, we could elucidate the progress of thermal oxidative degradation of the MWCNTs. Initial thermal oxidation of the MWCNTs induces a purification that reveals graphitic walls by removing pyrolytic/amorphous carbon due to selective oxidation. The prolonged thermal oxidation damages the graphitic layer and creates many structural defects. Especially, the MWCNTs in the prolonged thermal oxidation show a significant change of their physicochemical properties; high BET surface area, many defective sites, and large amounts of oxygen-containing functional groups.

The thermal and electrochemical behavior of MWCNTs is strongly influenced by the thermal oxidative degradation of MWCNTs. By means of thermal analysis in inert gas, volatile compounds such as CO and CO_2 clearly confirmed the presence of surface functional groups formed on MWCNTs during thermal oxidative treatment. In thermal analysis in oxygen gas, compared to P-MWCNTs, the overall stability for thermal oxidation is lower in TO2h-MWCNTs due to more reactive sites by opened ends of the tubes, whereas is higher in TO4h-MWCNTs. It may be tentatively explained that the oxide barriers were formed on the oxygen-rich carbon surfaces.

Based on electrochemical characterizations of the MWCNT samples, we could observe the effect of thermal oxidative degradation in the electrochemical activity and stability of the MWCNTs. Surface oxides formed by thermal oxidation do not contribute to electron transfer on the electrode surface. Furthermore, the MWCNTs treated in the prolonged thermal oxidation starkly show the largest capacitance, high electrochemical oxidation activity and low stability. As the time for thermal oxidative treatment of the MWCNTs increases, overall electrochemical oxidation activity at high anodic potential is enhanced, but degrades faster – which means that the oxidation current drops and becomes constant at a low value. This behavior is related to the oxygen concentration on the carbon surface and many defects. It is therefore conclusive that the thermal oxidation of the MWCNTs

determines the stage for the electrochemical oxidation. However, regardless of the thermally oxidized MWCNTs, the complete electrochemical oxidation of the MWCNTs which have passive oxide films on the electrode surface shows a limited increase in electrochemical capacitance and high resistance.

These findings have profound implications for various applications of MWCNTs. In particular, significant surface modification for essential nanotube materials is of great interest for many electrochemical applications. For example, clean MWCNTs with the opened end obtained using thermal oxidative treatment for a short time is a hydrophilic surface; this could be preferable for a catalyst support to deposit metal(oxide) with better dispersion. The MWCNTs with high surface area obtained from the prolonged thermal oxidation have considerably high electrochemical capacitance, making them favorable for supercapacitors and batteries. Tuning of the electrochemical or thermal properties of MWCNTs by thermal oxidative treatment enlarges the feasibility of MWCNTs in a wide range of potential applications in heterogeneous catalysis and electrochemical systems.

4.5 Supporting information

Figure S4.1. Thermogravimetric analysis (TGA) of MWCNTs in 5% O_2/Ar, 5 Kpm; weight loss and mass of CO_2 produced of the purified MWCNTs (P-MWCNTs).
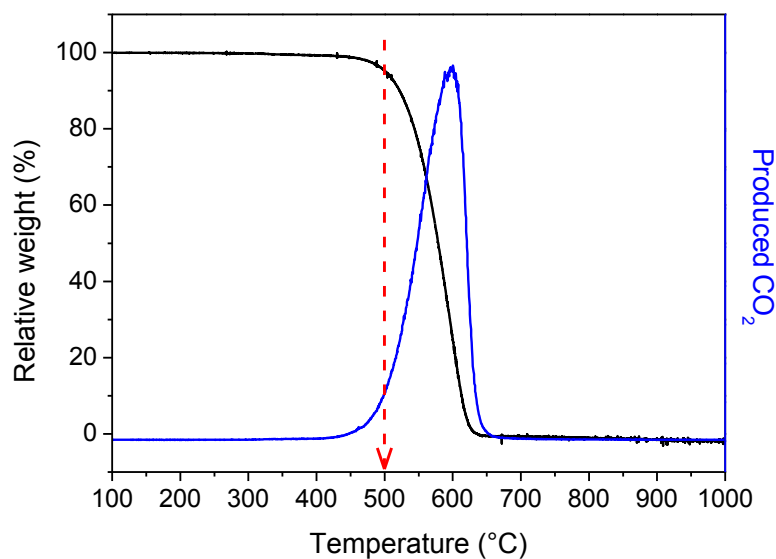

Figure S4.2. (a) The fitting of Raman spectra (b) Fitting values of thermally oxidized MWCNTs compared to purified MWCNTs.

Figure S4.3. Cyclic voltammetry (CV) of the MWCNTs before (dotted) and after (solid line) electrochemical oxidation (at 1.8 V versus RHE for 3 h in H_2SO_4). CVs were measured in 5 mM $K_4Fe(CN)_6$ + 1 M KCl. at the scan rate of 50 mV/s. (a) P-MWCNTs, (b) TO2h-MWCNTs and (c) TO4h-MWCNTs. (d) Anodic peak current of cyclic voltammetry obtained with the MWCNTs samples versus the square root of scan rate.
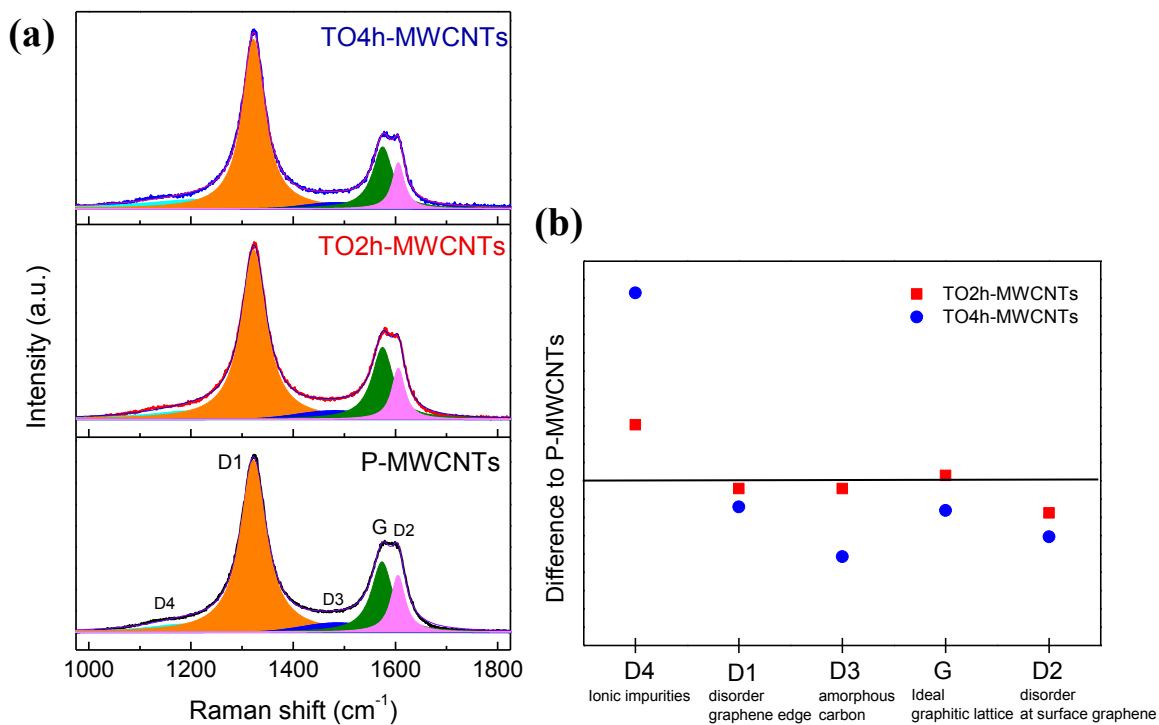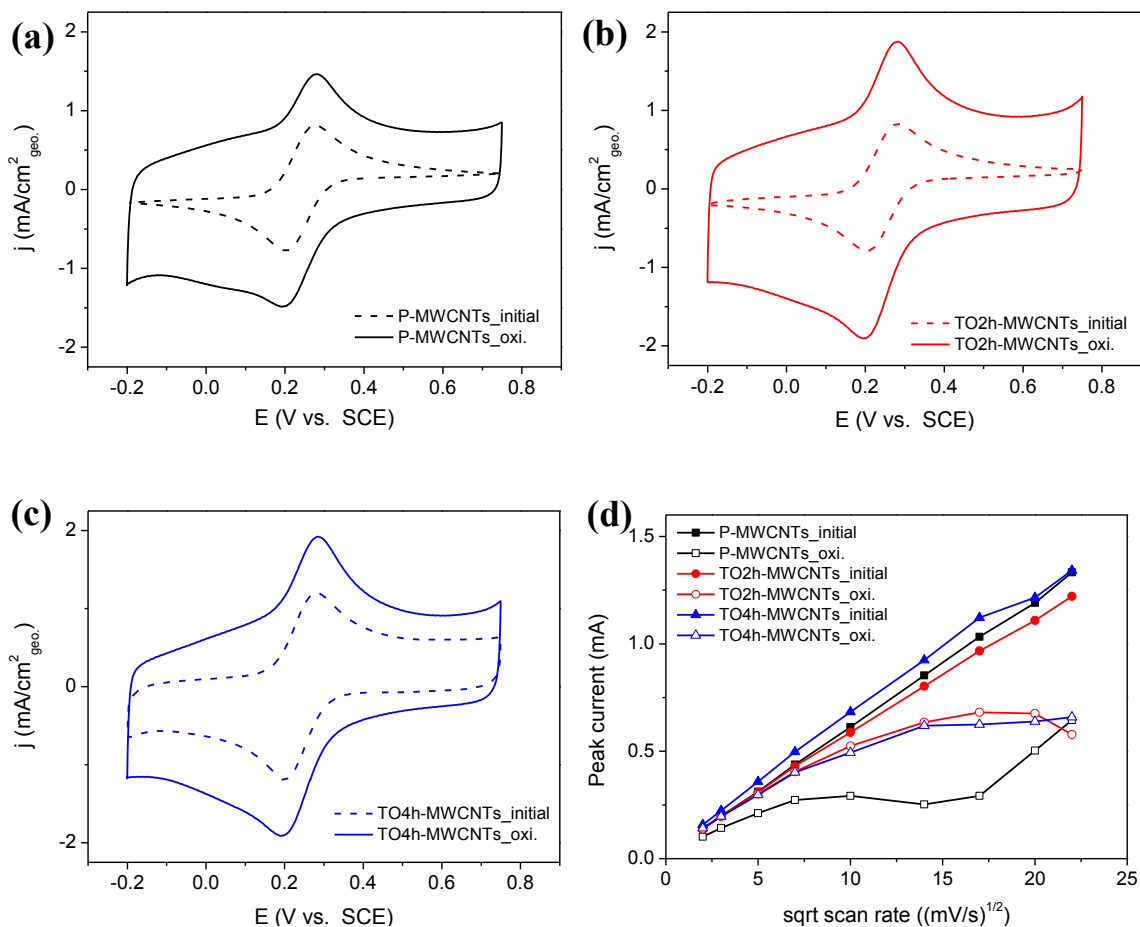
Figure S4.4. Cyclic voltammetry of the MWCNTs before (dotted) and after (solid line) electrochemical oxidation (at 1.8 V versus RHE for 3 hrs in 0.5 M H_2SO_4). CV was measured in 0.5 M H_2SO_4 at the scan rate of 50 mV/s.
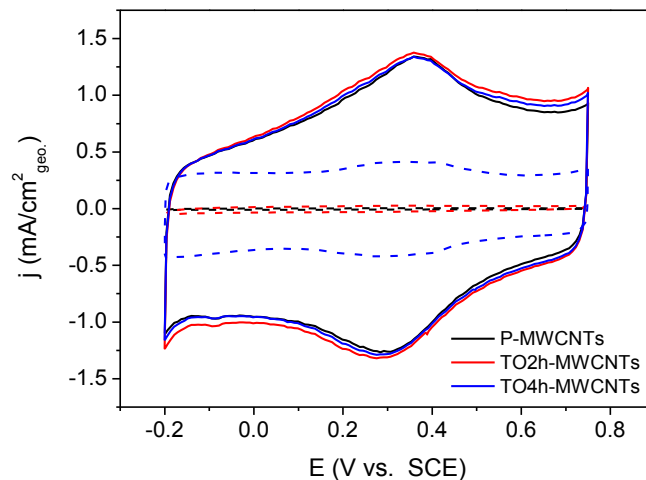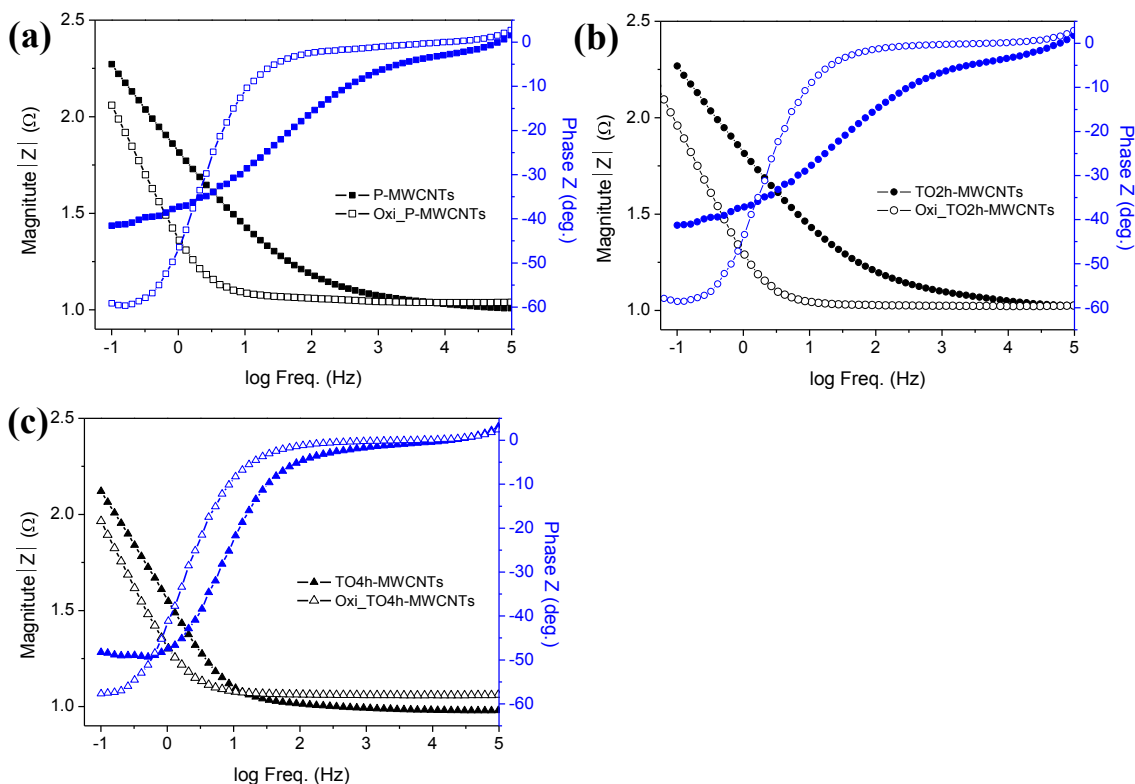

Figure S4.5. Bode plots of the MWCNTs samples before (closed) and after (open) electrochemical oxidation at 1.8 V versus RHE for 3 hrs. Electrochemical impedance of the MWCNTs electrodes was measured at open circuit potential (OCP) in 0.5 M H_2SO_4 (a) P-MWCNTs, (b) TO2h-MWCNTs and (c) TO4h-MWCNTs.

5 Conclusion and outlook

5.1 Conclusion

Carbon materials have widespread applications for efficient energy conversion and storage. However, some applications in heterogeneous catalysis and electrocatalysis are limited due to the degradation of carbon via its instability in oxidizing environments. This thesis deals with the electrochemical and thermal oxidative degradation of multiwall carbon nanotubes (MWCNTs). Each oxidation progress is associated with liquid-phase and gas-phase reactants, respectively. The change of physicochemical and electrochemical properties was investigated during these two types of degradations. In this conclusion part, I compare the electrochemical and thermal oxidative degradation of the MWCNTs and their effects on electrochemical behavior.

A similarity was found to exist in the morphological change induced electrochemical and thermal oxidative degradation respectively. Initial oxidation of the MWCNTs purifies the carbon surface by removing residual amorphous carbon due to selective oxidation. Whereas prolonged oxidation attacks the exposed graphitic walls on the MWCNTs and introduces many defects. The structural defects cause a significant change in physicochemical properties of the MWCNTs. With respect to the prolonged oxidation of MWCNTs, in the case of electrochemical degradation, passive oxides are formed on the outer wall of the MWCNTs, so the inner graphitic layer beneath the defective layer is protected from further oxidation. In contrast, thermal oxidative degradation breaks the graphitic wall and forms pits on the tube wall. Furthermore inside the wall, carbonaceous species formed by pyrolysis of the gasified carbon species were observed.

According to the structural order obtained from Raman spectroscopy, the MWCNTs are less graphitic after electrochemical degradation, but there is only minor change in the degree of disorder. However, the thermally oxidized MWCNTs show considerable change in the structural order in accordance with the morphological change. The degree of disorder in the MWCNTs is slightly lower with initial thermal oxidation due to the purification of the MWCNTs, but the disorder is much higher with prolonged thermal oxidation.

93

Both degradations produce oxides on the carbon surface. The identification of surface functional groups from infrared spectroscopy, the similarities and differences between electrochemical- and thermal-degradation were clearly observed. The formation of carbonyl (C=O) stretching in ketones, aldehydes, or carboxylic acid groups are conspicuous in both oxidations. Moreover, we could confirm additional defects on the carbon surface and the structural change of the MWCNTs through prolonged thermal or electrochemical oxidations. The difference in the change in surface functional groups between electrochemical and thermal oxidative degradation could come from a different oxidant. In electrochemical degradation, the oxidant is water, whereas molecular oxygen is responsible for oxidation in thermal oxidative degradation. In the case of electrochemical oxidation, carboxylic groups are dominant with initial oxidation, and then alcoholic and/or phenolic hydroxyl groups appear prominently with prolonged oxidation. In contrast to this, thermal oxidation initially produces both carbonyl groups and alcoholic hydroxyl groups. But carbonyl groups are dominant on the carbon surface of the thermally oxidized MWCNTs in the prolonged oxidation. Hydroxyl groups are likely oxidized and the formation of carbonyl groups increases with further thermal oxidation of the MWCNTs. The analysis of surface functional groups by temperature programmed desorption (TPD) provides more information on the change in chemical species during the thermal oxidation of the MWCNTs. The electrochemically oxidized MWCNTs were not able to be analyzed with TPD, since the amount of the sample obtained from the MWCNTs electrode is not sufficient for this measurement. Adjacent carboxyl groups on the MWCNTs dehydrate to carboxylic anhydride in initial thermal oxidation. It is clear that the amount of surface oxides on the MWCNTs significantly increases during the prolonged thermal oxidation. Moreover, the thermally oxidized MWCNTs show less acidic character than the purified one due to the effect of hydroxyl groups involved in the thermal oxidation.

The effect of electrochemical and thermal oxidative degradation on electrochemical behavior was discussed. Both degradations of the MWCNTs induce the increase in specific capacitance of the MWCNTs and the growth of reversible surface oxides which contribute to pseudocapacitance. The specific capacitance of the electrochemically oxidized MWCNTs increases linearly with oxidation time until the oxygen covers the

carbon surface completely. The full coverage of surface oxides on the MWCNTs limits the increase of the specific capacitance. However in thermal oxidative degradation, the specific capacitance is associated with the surface area of the MWCNTs. The loosening of MWCNTs entanglement in initial thermal oxidation leads to small increases in the surface area and the specific capacitance of MWCNTs. The MWCNTs with a prolonged thermal oxidation possess a higher surface area due to many structural defects caused by broken tubes. Thus, a significant increase of the specific capacitance with the contribution of reversible surface oxides is observed.

The electrochemical activity for the oxidation on the MWCNTs was measured by linear sweep voltammetry recorded at high anodic potentials where the oxidation of water and carbon occur simultaneously. During the electrochemical degradation of the MWCNTs, the electrochemical activity of the MWCNTs increases in the initial oxidation, but it decreases in the prolonged oxidation. The fact that the MWCNTs in the initial oxidation have a higher oxidation activity than pristine MWCNTs suggests that initial electrochemical oxidation produces the surface functional groups that are electrochemically active. In contrast, lower oxidation activity in the prolonged electrochemical oxidation supports the formation of passive surface oxides which inhibits further oxidation. The change in electron transfer (ET) kinetics for $Fe(CN)_6^{3-}/Fe(CN)_6^{2-}$ redox during the electrochemical degradation of the MWCNTs follows the same trend of the electrochemical oxidation activity. However, the thermally oxidized MWCNTs proportionally increase the electrochemical oxidation activity of MWCNTs during the thermal oxidative degradation. However, the change of the carbon surface by the thermal oxidation of MWCNTs permits slow ET kinetics.

Carbon oxidation is usually concerned with two pathways [1];

Carbon → gaseous products CO_2

Carbon → surface oxide → gaseous product CO_2

The progress of carbon degradation can be elucidated with these pathways based on the above results of the change in physicochemical and electrochemical properties. The progress of electrochemical oxidative degradation of the MWCNTs is associated with the oxidation current transition. The MWCNTs are first activated by facilitating both

pathways, and then passivated through full coverage of oxides on the carbon surface. The progress of thermal oxidative degradation of the MWCNTs is provided by the weight loss during temperature programmed oxidation (TPO). Initially, thermal oxidation is activated by creating more reactive sites, indicated by lower thermal oxidative stability. With prolonged oxidation, the thermal oxidative stability of the MWCNTs is higher than pristine MWCNTs, likely caused by oxide barriers that may be formed on the oxygen-rich carbon surfaces. Therefore, it is inferred that surface oxides produced by both oxidations affect the degradation of MWCNTs. The functional groups formed in the initial oxidation promote the subsequent oxidation of carbon. However, the covered surface oxides on the carbon in the prolonged oxidation inhibit further oxidation.

The effect of the thermally oxidized MWCNTs on the electrochemical oxidation stability was examined using chronoamperommetry at a high anodic potential. The thermally oxidized MWCNTs exclude the region for an initial current increase during the electrochemical degradation, meaning that active sites could already be occupied by oxygen. As the time period for thermal oxidative treatment of the MWCNTs increases, the overall electrochemical oxidation activity at a high anodic potential also gets higher, but it degrades faster – which means that the oxidation current decays and reaches the steady-state at a low value. This behavior is related to the coverage of oxygen on the carbon surface. Since the thermally oxidized MWCNTs in the prolonged oxidation process a large amount of oxygen, the oxidation current reaches a limiting value much faster than other MWCNT samples. Therefore, it is conclusive that the oxygen coverage is one of the determining factors for the electrochemical degradation of carbon. Furthermore, regardless of the initial state of the MWCNTs, once the electrochemical oxidation of the MWCNTs is completed through the formation of a passive oxide film on the electrode surface, the MWCNTs show similar electrochemical behavior. There is no further increase of specific capacitance and resistance. Moreover, the MWCNTs electrode is deprived of the electrochemical activity. Therefore, we could speculate that the surface oxides fully covered on the carbon are inactive for further reactions.

The results presented in this thesis unveil the degradation of carbon materials under electrochemically and thermally oxidative conditions. The change in physicochemical properties during carbon oxidation makes it possible to control its properties for suitable applications. Therefore, tuning the electrochemical or thermal properties of MWCNTs by oxidative treatment enhances the feasibility of MWCNTs in a wide range of electrochemical applications. Furthermore, this research shows the possibility of using carbon-based materials for applications involving oxygen. This work presents a foundational understanding of degradation in electrochemical systems, which is relevant to applications, such as water electrolysis, fuel cells and metal-air batteries.

5.2 Outlook

This research has the potential to provide the foundation for interesting future projects. Suggested follow-up investigations are listed below.

1. Gaseous products analysis during the electrochemical oxidation of carbon materials at high anodic potential will provide further understanding of carbon degradation. The oxidation of carbon at a high anodic potential involves both an O_2 and a CO_2 evolution reaction. The dominant reaction during the carbon degradation can be determined by monitoring gaseous products using online electrochemical mass spectroscopy. This approach can distinguish water and carbon oxidation on the carbon electrode, and further test the applicability of carbon-based materials for oxygen evolution reaction in water electrolysis.

2. The treatment of carbon materials affects the electrochemical properties of carbon, as the effect of the thermal oxidation for electrochemical activity and stability was demonstrated in chapter 4. More information is presented in Appendix 1. We could consider the electrochemical behavior of the carbon materials which are modified by various treatments, such as chemical and thermal treatments. It is possible to study the relationship between the physicochemical and electrochemical properties of carbon. Furthermore, this approach to electrochemical stability could clarify the determining factors for the electrochemical degradation of carbon.

3. During the oxidative degradation of carbon, many kinds of surface oxides are introduced onto the carbon surface. These surface oxides could provide anchoring sites to deposit metal and/or metal oxide on carbon. Subsequently, we could synthesize a carbon-supported catalyst using the multiwall carbon nanotubes (MWCNTs) modified by the electrochemical and/or thermal oxidative treatment. It would be an interesting to compare the impact of active- and passive-surface oxides for carbon supported catalysts. The instinct properties of the MWCNTs as

a catalyst support could affect the activity and stability of carbon supported catalysts for electrocatalytic applications.

4. Based on an informed understanding of the electrochemical degradation of carbon, we could speculate on the performance of a carbon-based catalyst at a high anodic potential, as this is the condition for oxygen evolution reaction (OER) in water electrolysis. Further study should also include the electrochemical performance of metal/metal oxide supported on carbon for OER. Ir in acidic media and transition metals, such as Ni and Co in alkaline media, are attractive elements for this approach.

6 Bibliography

[1] K. Kinoshita, Carbon:Electrochemical and Physicochemical properties, Wiley-Interscience, (1988).

[2] L. Dai, D.W. Chang, J.B. Baek, W. Lu, Carbon nanomaterials for advanced energy conversion and storage, Small, 8 (2012) 1130-1166.

[3] S.L. Candelaria, Y.Y. Shao, W. Zhou, X.L. Li, J. Xiao, J.G. Zhang, Y. Wang, J. Liu, J.H. Li, G.Z. Cao, Nanostructured carbon for energy storage and conversion, Nano Energy, 1 (2012) 195-220.

[4] E.F. Francois Beguin, Carbons for Electrochemical Energy Storage and Conversion Systems, CRC Press, (2009).

[5] D.K. Singh, P.K. Iyer, P.K. Giri, Diameter dependence of oxidative stability in multiwalled carbon nanotubes: Role of defects and effect of vacuum annealing, Journal of Applied Physics, 108 (2010) 084313.

[6] E. Frackowiak, F. Beguin, Carbon materials for the electrochemical storage of energy in capacitors, Carbon, 39 (2001) 937-950.

[7] D.S. Su, R. Schlögl, Nanostructured Carbon and Carbon Nanocomposites for Electrochemical Energy Storage Applications, ChemSusChem, 3 (2010) 136-168.

[8] R. Borup, J. Meyers, B. Pivovar, Y.S. Kim, R. Mukundan, N. Garland, D. Myers, M. Wilson, F. Garzon, D. Wood, P. Zelenay, K. More, K. Stroh, T. Zawodzinski, J. Boncella, J.E. McGrath, M. Inaba, K. Miyatake, M. Hori, K. Ota, Z. Ogumi, S. Miyata, A. Nishikata, Z. Siroma, Y. Uchimoto, K. Yasuda, K.I. Kimijima, N. Iwashita, Scientific aspects of polymer electrolyte fuel cell durability and degradation, Chemical Reviews, 107 (2007) 3904-3951.

[9] S. Maass, F. Finsterwalder, G. Frank, R. Hartmann, C. Merten, Carbon support oxidation in PEM fuel cell cathodes, Journal of Power Sources, 176 (2008) 444-451.

[10] B. Avasarala, R. Moore, P. Haldar, Surface oxidation of carbon supports due to potential cycling under PEM fuel cell conditions, Electrochimica Acta, 55 (2010) 4765-4771.

[11] K.G. Gallagher, T.F. Fuller, Kinetic model of the electrochemical oxidation of graphitic carbon in acidic environments, Physical Chemistry Chemical Physics, 11 (2009) 11557-11567.

[12] K.H. Kangasniemi, D.A. Condit, T.D. Jarvi, Characterization of Vulcan Electrochemically Oxidized under Simulated PEM Fuel Cell Conditions, Journal of The Electrochemical Society, 151 (2004) E125.

[13] L.C. Colmenares, A. Wurth, Z. Jusys, R.J. Behm, Model study on the stability of carbon support materials under polymer electrolyte fuel cell cathode operation conditions, Journal of Power Sources, 190 (2009) 14-24.

[14] A. Laisa, Handbook of Fuel Cells- Fundamentals, technology and Applications; Volume 2: Electrocatalysis, John Wieley & Sons, (2003).

[15] H. Dau, C. Limberg, T. Reier, M. Risch, S. Roggan, P. Strasser, The Mechanism of Water Oxidation: From Electrolysis via Homogeneous to Biological Catalysis, ChemCatChem, 2 (2010) 724-761.

[16] S. Trasatti, Electrocatalysis by Oxides - Attempt at a Unifying Approach, Journal of Electroanalytical Chemistry, 111 (1980) 125-131.

[17] K. Kinoshita, Electrochemical Oxygen Technology, Wiley, (1992).

[18] M.G. Walter, E.L. Warren, J.R. McKone, S.W. Boettcher, Q.X. Mi, E.A. Santori, N.S. Lewis, Solar Water Splitting Cells, Chemical Reviews, 110 (2010) 6446-6473.

[19] A.S. M. R. TARASEVICH, and ERNEST YEAGER, Oxygen elctrochemistry, B. E. Conway et al. (eds.), Comprehensive Treatise of Electrochemistry © Plenum Press, New York (1983).

[20] D. Pletcher and D. J. Schiffrin, The Electrochemistry of Oxygen, Chapter 4 in Electrochemistry, Specialist Periodical Reports, Vol. 8, The Royal Society of Chemistry, London, (1983).

[21] B.H. Bernard, Improvements in or relating to electrodes for electrolysis, British Patent 1147442-A, (1969).

[22] A. Di Blasi, C. D'Urso, V. Baglio, V. Antonucci, A.S. Arico, R. Ornelas, F. Matteucci, G. Orozco, D. Beltran, Y. Meas, L.G. Arriaga, Preparation and evaluation of RuO2-IrO2, IrO2-Pt and IrO2-Ta2O5 catalysts for the oxygen evolution reaction in an SPE electrolyzer, Journal of Applied Electrochemistry, 39 (2009) 191-196.

[23] A. Marshall, B. Borresen, G. Hagen, M. Tsypkin, R. Tunold, Electrochemical characterisation of IrxSn1-xO2 powders as oxygen evolution electrocatalysts, Electrochimica Acta, 51 (2006) 3161-3167.

[24] E. Rios, J.L. Gautier, G. Poillerat, P. Chartier, Mixed valency spinel oxides of transition metals and electrocatalysis: case of the MnxCo3-xO4 system, Electrochimica Acta, 44 (1998) 1491-1497.

[25] R.L. Doyle, I.J. Godwin, M.P. Brandon, M.E.G. Lyons, Redox and electrochemical water splitting catalytic properties of hydrated metal oxide modified electrodes, Physical Chemistry Chemical Physics, 15 (2013) 13737-13783.

[26] L. Trotochaud, S.W. Boettcher, Precise oxygen evolution catalysts: Status and opportunities, Scripta Mater, 74 (2014) 25-32.

[27] J. Jirkovsky, H. Hoffmannova, M. Klementova, P. Krtil, Particle size dependence of the electrocatalytic activity of nanocrystalline RuO_2 electrodes, Journal of the Electrochemical Society, 153 (2006) E111-E118.

[28] J. Jirkovsky, M. Makarova, P. Krtil, Particle size dependence of oxygen evolution reaction on nanocrystalline RuO_2 and $Ru_{0.8}CO_{0.2}O_{2-x}$, Electrochemistry Communications, 8 (2006) 1417-1422.

[29] K. Macounova, J. Jirkovsky, M.V. Makarova, J. Franc, P. Krtil, Oxygen evolution on $Ru_{1-x}Ni_xO_{2-y}$ nanocrystalline electrodes, Journal of Solid State Electrochemistry, 13 (2009) 959-965.

[30] Y. Lee, J. Suntivich, K.J. May, E.E. Perry, Y. Shao-Horn, Synthesis and Activities of Rutile IrO_2 and RuO_2 Nanoparticles for Oxygen Evolution in Acid and Alkaline Solutions, The Journal of Physical Chemistry Letters, (2012) 399-404.

[31] A.J. Esswein, M.J. McMurdo, P.N. Ross, A.T. Bell, T.D. Tilley, Size-Dependent Activity of Co_3O_4 Nanoparticle Anodes for Alkaline Water Electrolysis, The Journal of Physical Chemistry C, 113 (2009) 15068-15072.

[32] M.W. Kanan, D.G. Nocera, In situ formation of an oxygen-evolving catalyst in neutral water containing phosphate and Co^{2+}, Science, 321 (2008) 1072-1075.

[33] Y. Surendranath, M.W. Kanan, D.G. Nocera, Mechanistic Studies of the Oxygen Evolution Reaction by a Cobalt-Phosphate Catalyst at Neutral pH, Journal of the American Chemical Society, 132 (2010) 16501-16509.

[34] M. Dinca, Y. Surendranath, D.G. Nocera, Nickel-borate oxygen-evolving catalyst that functions under benign conditions, Proceedings of the National Academy of Sciences, 107 (2010) 10337-10341.

[35] L.R. Ma, S. Sui, Y.C. Zhai, Preparation and characterization of Ir/TiC catalyst for oxygen evolution, Journal of Power Sources, 177 (2008) 470-477.

[36] R.E. Fuentes, J. Farell, J.W. Weidner, Multimetallic Electrocatalysts of Pt, Ru, and Ir Supported on Anatase and Rutile TiO_2 for Oxygen Evolution in an Acid Environment, Electrochemical and Solid-State Letters, 14 (2011) E5-E7.

[37] S. Siracusano, V. Baglio, C. D'Urso, V. Antonucci, A.S. Arico, Preparation and characterization of titanium suboxides as conductive supports of IrO_2 electrocatalysts for application in SPE electrolysers, Electrochimica Acta, 54 (2009) 6292-6299.

[38] A.T. Marshall, R.G. Haverkamp, Electrocatalytic activity of IrO_2-RuO_2 supported on Sb-doped SnO_2 nanoparticles, Electrochimica Acta, 55 (2010) 1978-1984.

[39] X. Wu, K. Scott, RuO_2 supported on Sb-doped SnO_2 nanoparticles for polymer electrolyte membrane water electrolysers, International Journal of Hydrogen Energy, 36 (2011) 5806-5810.

[40] S. Ferro, A. De Battisti, Electrocatalysis and chlorine evolution reaction at ruthenium dioxide deposited on conductive diamond, The Journal of Physical Chemistry B, 106 (2002) 2249-2254.

[41] P.N. Ross, H. Sokol, The Corrosion of Carbon-Black Anodes in Alkaline Electrolyte; 1. Acetylene Black and the Effect of Cobalt Catalyzation, Journal of the Electrochemical Society, 131 (1984) 1742-1750.

[42] Y. Zhao, R. Nakamura, K. Kamiya, S. Nakanishi, K. Hashimoto, Nitrogen-doped carbon nanomaterials as non-metal electrocatalysts for water oxidation, Nature Communications, 4 (2013).

[43] T. Reier, M. Oezaslan, P. Strasser, Electrocatalytic Oxygen Evolution Reaction (OER) on Ru, Ir, and Pt Catalysts: A Comparative Study of Nanoparticles and Bulk Materials, ACS Catalysis, 2 (2012) 1765-1772.

[44] F.M. Toma, A. Sartorel, M. Iurlo, M. Carraro, P. Parisse, C. Maccato, S. Rapino, B.R. Gonzalez, H. Amenitsch, T. Da Ros, L. Casalis, A. Goldoni, M. Marcaccio, G. Scorrano, G. Scoles, F. Paolucci, M. Prato, M. Bonchio, Efficient water oxidation at carbon nanotube-polyoxometalate electrocatalytic interfaces, Nature Chemistry, 2 (2010) 826-831.

[45] F.M. Toma, A. Sartorel, M. Iurlo, M. Carraro, S. Rapino, L. Hoober-Burkhardt, T. Da Ros, M. Marcaccio, G. Scorrano, F. Paolucci, M. Bonchio, M. Prato, Tailored Functionalization of Carbon Nanotubes for Electrocatalytic Water Splitting and Sustainable Energy Applications, ChemSusChem, 4 (2011) 1447-1451.

[46] K. Mette, A. Bergmann, J.P. Tessonnier, M. Havecker, L.D. Yao, T. Ressler, R. Schlögl, P. Strasser, M. Behrens, Nanostructured Manganese Oxide Supported on Carbon Nanotubes for Electrocatalytic Water Splitting, ChemCatChem, 4 (2012) 851-862.

[47] A. Bergmann, I. Zaharieva, H. Dau, P. Strasser, Electrochemical water splitting by layered and 3D cross-linked manganese oxides: correlating structural motifs and catalytic activity, Energy & Environmental Science, 6 (2013) 2745-2755.

[48] Y.Y. Liang, Y.G. Li, H.L. Wang, J.G. Zhou, J. Wang, T. Regier, H.J. Dai, Co_3O_4 nanocrystals on graphene as a synergistic catalyst for oxygen reduction reaction, Nat Mater, 10 (2011) 780-786.

[49] M. Gong, Y.G. Li, H.L. Wang, Y.Y. Liang, J.Z. Wu, J.G. Zhou, J. Wang, T. Regier, F. Wei, H.J. Dai, An Advanced Ni-Fe Layered Double Hydroxide Electrocatalyst for Water Oxidation, Journal of the American Chemical Society, 135 (2013) 8452-8455.

[50] C.F. Stefania Specchia, and Paolo Spinelli, Electrochemical Technologies for Energy Storage and Conversion; Volume 2, Chapter 13 Polymer electrolyte membrane fuel cells, Wiley-VCH (2012).

[51] M.Z. Sharon Thomas, Fuel Cells - Green Power, Los Alamos National Laboratory, (1999).

[52] K.O.a.Y. Koizumi, Handbook of Fuel cells - Fundamentals, Technology and Applications; Volume 5, Chapter 15 Platinum dissolution models and voltage cycling effects: platinum dissolution in polymer electrolyte fuel cell and low temperature fuel cells, John Wiley & Sons, (2009).

[53] Y.Y. Shao, G.P. Yin, Y.Z. Gao, Understanding and approaches for the durability issues of Pt-based catalysts for PEM fuel cell, Journal of Power Sources, 171 (2007) 558-566.

[54] C.A. Reiser, L. Bregoli, T.W. Patterson, J.S. Yi, J.D.L. Yang, M.L. Perry, T.D. Jarvi, A reverse-current decay mechanism for fuel cells, Electrochemical and Solid-State Letters, 8 (2005) A273-A276.

[55] S.-E. Jang, H. Kim, Effect of Water Electrolysis Catalysts on Carbon Corrosion in Polymer Electrolyte Membrane Fuel Cells, Journal of the American Chemical Society, 132 (2010) 14700-14701.

[56] H.S. Oh, J.G. Oh, S. Haam, K. Arunabha, B. Roh, I. Hwang, H. Kim, On-line mass spectrometry study of carbon corrosion in polymer electrolyte membrane fuel cells, Electrochemistry Communications, 10 (2008) 1048-1051.

[57] S. Vinod Selvaganesh, G. Selvarani, P. Sridhar, S. Pitchumani, A.K. Shukla, Graphitic Carbon as Durable Cathode-Catalyst Support for PEFCs, Fuel Cells, 11 (2011) 372-384.

[58] E. Bakker, Electrochemical sensors, Analytical Chemistry, 76 (2004) 3285-3298.

[59] Y.Y. Shao, J. Wang, H. Wu, J. Liu, I.A. Aksay, Y.H. Lin, Graphene Based Electrochemical Sensors and Biosensors: A Review, Electroanalysis, 22 (2010) 1027-1036.

[60] R.O. Kadara, N. Jenkinson, C.E. Banks, Characterisation of commercially available electrochemical sensing platforms, Sensors and Actuators B: Chemical, 138 (2009) 556-562.

[61] P. Papakonstantinou, R. Kern, L. Robinson, H. Murphy, J. Irvine, E. McAdams, J. McLaughlin, T. McNally, Fundamental electrochemical properties of carbon nanotube electrodes, Fullerenes Nanotubes and Carbon Nanostructures, 13 (2005) 91-108.

[62] M. Elrouby, Electrochemical applications of carbon nanotube, Journal of Nanotechnology & Advanced Materials, 1 (2013) 23-38.

[63] M. Moumene, D. Rochefort, M. Mohamedi, Electrochemical Functionalization as a Promising Avenue for Glucose Oxidase Immobilization at Carbon Nanotubes: Enhanced Direct Electron Transfer Process, International Journal of Electrochemical Science, 8 (2013) 2009-2022.

[64] R. Schlögl, The Role of Chemistry in the Energy Challenge, ChemSusChem, 3 (2010) 209-222.

[65] L.M. Roen, C.H. Paik, T.D. Jarvi, Electrocatalytic Corrosion of Carbon Support in PEMFC Cathodes, Electrochemical and Solid-State Letters, 7 (2004) A19.

[66] I. Dumitrescu, P.R. Unwin, J.V. Macpherson, Electrochemistry at carbon nanotubes: perspective and issues, Chemical Communications, (2009) 6886-6901.

[67] Y.Y. Shao, G.P. Yin, Z.B. Wang, Y.Z. Gao, Proton exchange membrane fuel cell from low temperature to high temperature: Material challenges, Journal of Power Sources, 167 (2007) 235-242.

[68] E. Antolini, Carbon supports for low-temperature fuel cell catalysts, Applied Catalysis B: Environmental, 88 (2009) 1-24.

[69] S. Zhang, Y.Y. Shao, X.H. Li, Z.M. Nie, Y. Wang, J. Liu, G.P. Yin, Y.H. Lin, Low-cost and durable catalyst support for fuel cells: Graphite submicronparticles, Journal of Power Sources, 195 (2010) 457-460.

[70] F. Hasche, M. Oezaslan, P. Strasser, Activity, stability and degradation of multi walled carbon nanotube (MWCNT) supported Pt fuel cell electrocatalysts, Physical Chemistry Chemical Physics , 12 (2010) 15251-15258.

[71] N. Jha, P. Ramesh, E. Bekyarova, X.J. Tian, F.H. Wang, M.E. Itkis, R.C. Haddon, Functionalized Single-Walled Carbon Nanotube-Based Fuel Cell Benchmarked Against US DOE 2017 Technical Targets, Scientific reports, 3 (2013).

[72] R. Verdejo, S. Lamoriniere, B. Cottam, A. Bismarck, M. Shaffer, Removal of oxidation debris from multi-walled carbon nanotubes, Chemical Communications, (2007) 513-515.

[73] A. Rinaldi, B. Frank, D.S. Su, S.B.A. Hamid, R. Schlögl, Facile Removal of Amorphous Carbon from Carbon Nanotubes by Sonication, Chemistry of Materials, 23 (2011) 926-928.

[74] J.B. K.Kinoshita, Electrochemical oxidation of carbon black in concentrated phosphoric acid at 135 °C, Carbon, 11 (1973) 237-247.

[75] P. STONEHART, CARBON SUBSTRATES FOR PHOSPHORIC ACID FUEL CELL CATHODES, Carbon, 22 (1984) 423-431.

[76] J.N. Barisci, G.G. Wallace, R.H. Baughman, Electrochemical studies of single-wall carbon nanotubes in aqueous solutions, Journal of Electroanalytical Chemistry, 488 (2000) 92-98.

[77] L. Li, Y.C. Xing, Electrochemical durability of carbon nanotubes in noncatalyzed and catalyzed oxidations, Journal of the Electrochemical Society, 153 (2006) A1823-A1828.

[78] H.J. Wang, G.P. Yin, Y.Y. Shao, Z.B. Wang, Y.Z. Gao, Electrochemical durability investigation of single-walled and multi-walled carbon nanotubes under potentiostatic conditions, Journal of Power Sources, 176 (2008) 128-131.

[79] Y.Y. Shao, G.P. Yin, J. Zhang, Y.Z. Gao, Comparative investigation of the resistance to electrochemical oxidation of carbon black and carbon nanotubes in aqueous sulfuric acid solution, Electrochimica Acta, 51 (2006) 5853-5857.

[80] S.E. group, Instrumental methods in electrochemistry, John Wiley & Sons, (1985).

[81] D.C. Wei, Y.Q. Liu, L.C. Cao, H.L. Zhang, L.P. Huang, G. Yu, H. Kajiura, Y.M. Li, Selective Electrochemical Etching of Single-Walled Carbon Nanotubes, Advanced Functional Materials, 19 (2009) 3618-3624.

[82] H. Binder, A. Köhling, K. Richter, G. Sandstede, Über die anodische oxydation von aktivkohlen in wässrigen elektrolyten, Electrochimica Acta, 9 (1964) 255-274.

[83] J.O. Muller, D.S. Su, U. Wild, R. Schlögl, Bulk and surface structural investigations of diesel engine soot and carbon black, Physical Chemistry Chemical Physics, 9 (2007) 4018-4025.

[84] M.S. Dresselhaus, G. Dresselhaus, R. Saito, A. Jorio, Raman spectroscopy of carbon nanotubes, Physics Reports, 409 (2005) 47-99.

[85] M.A. Pimenta, G. Dresselhaus, M.S. Dresselhaus, L.G. Cancado, A. Jorio, R. Saito, Studying disorder in graphite-based systems by Raman spectroscopy, Physical Chemistry Chemical Physics, 9 (2007) 1276-1290.

[86] P.E. Fanning, M.A. Vannice, A Drifts Study of the Formation of Surface Groups on Carbon by Oxidation, Carbon, 31 (1993) 721-730.

[87] M. Laporta, M. Pegoraro, L. Zanderighi, Perfluorosulfonated membrane (Nafion): FT-IR study of the state of water with increasing humidity, Physical Chemistry Chemical Physics, 1 (1999) 4619-4628.

[88] U.J. Kim, C.A. Furtado, X.M. Liu, G.G. Chen, P.C. Eklund, Raman and IR spectroscopy of chemically processed single-walled carbon nanotubes, Journal of the American Chemical Society, 127 (2005) 15437-15445.

[89] R. Bowling, R.T. Packard, R.L. Mccreery, Mechanism of Electrochemical Activation of Carbon Electrodes - Role of Graphite Lattice-Defects, Langmuir, 5 (1989) 683-688.

[90] M. Pumera, Imaging of Oxygen-Containing Groups on Walls of Carbon Nanotubes, Chemistry – An Asian Journal, 4 (2009) 250-253.

[91] O.V. Cherstiouk, V.L. Kuznetsov, A.N. Simonov, I.N. Mazov, K.V. Elumeeva, N.S. Moseva, Electrocorrosion properties of multiwall carbon nanotubes, Physica Status Solidi (B), 247 (2010) 2738-2742.

[92] Z. Ahmad, Principles of corrosion engineering and corrosion control, Elsevier Science & Technology Books, (1999).

[93] A. Kapałka, G. Fóti, C. Comninellis, Determination of the Tafel slope for oxygen evolution on boron-doped diamond electrodes, Electrochemistry Communications, 10 (2008) 607-610.

[94] L.R.F. Allen J. Bard, ELECTROCHEMICAL METHODS: Fundamentals and Applications, JOHN WILEY & SONS, (2001).

[95] S.J. Guo, X.H. Qu, S.J. Dong, Nanoelectrode ensembles based on semi-interpenetrating network of carbon nanotubes, Electrochimica Acta, 52 (2007) 6186-6191.

[96] M.A.A. Rahim, Variation of the Dielectric-Constant of Anodic Oxide-Films on Titanium with Oxygen Evolution, Journal of Applied Electrochemistry, 25 (1995) 881-885.

[97] H.T. Fang, C.G. Liu, L. Chang, L. Feng, L. Min, H.M. Cheng, Purification of single-wall carbon nanotubes by electrochemical oxidation, Chemistry of Materials, 16 (2004) 5744-5750.

[98] J.M. Skowronski, P. Scharff, N. Pfander, S. Cui, Room temperature electrochemical opening of carbon nanotubes followed by hydrogen storage, Advanced Materials, 15 (2003) 55.

[99] M. Musameh, N.S. Lawrence, J. Wang, Electrochemical activation of carbon nanotubes, Electrochemistry Communications, 7 (2005) 14-18.

[100] M. Pumera, T. Sasaki, H. Iwai, Relationship between Carbon Nanotube Structure and Electrochemical Behavior: Heterogeneous Electron Transfer at Electrochemically Activated Carbon Nanotubes, Chemistry – An Asian Journal, 3 (2008) 2046-2055.

[101] T. Ito, L. Sun, R.M. Crooks, Electrochemical etching of individual multiwall carbon nanotubes, Electrochemical and Solid-State Letters, 6 (2003) C4-C7.

[102] C.M. Liu, H.B. Cao, Y.P. Li, H.B. Xu, Y. Zhang, The effect of electrolytic oxidation on the electrochemical properties of multi-walled carbon nanotubes, Carbon, 44 (2006) 2919-2924.

[103] A. Sadezky, H. Muckenhuber, H. Grothe, R. Niessner, U. Poschl, Raman micro spectroscopy of soot and related carbonaceous materials: Spectral analysis and structural information, Carbon, 43 (2005) 1731-1742.

[104] P. Serp, M. Corrias, P. Kalck, Carbon nanotubes and nanofibers in catalysis, Applied Catalysis A: General, 253 (2003) 337-358.

[105] A. Rinaldi, J. Zhang, B. Frank, D.S. Su, S.B. Abd Hamid, R. Schlögl, Oxidative purification of carbon nanotubes and its impact on catalytic performance in oxidative dehydrogenation reactions, ChemSusChem, 3 (2010) 254-260.

[106] R. Arrigo, M. Havecker, S. Wrabetz, R. Blume, M. Lerch, J. McGregor, E.P.J. Parrott, J.A. Zeitler, L.F. Gladden, A. Knop-Gericke, R. Schlögl, D.S. Su, Tuning the Acid/Base Properties of Nanocarbons by Functionalization via Amination, Journal of the American Chemical Society, 132 (2010) 9616-9630.

[107] R. Arrigo, M.E. Schuster, S. Abate, S. Wrabetz, K. Amakawa, D. Teschner, M. Freni, G. Centi, S. Perathoner, M. Havecker, R. Schlögl, Dynamics of Palladium on Nanocarbon in the Direct Synthesis of H_2O_2, ChemSusChem, (2013).

[108] R. Arrigo, S. Wrabetz, M.E. Schuster, D. Wang, A. Villa, D. Rosenthal, F. Girsgdies, G. Weinberg, L. Prati, R. Schlögl, D.S. Su, Tailoring the morphology of Pd nanoparticles on CNTs by nitrogen and oxygen functionalization, Physical Chemistry Chemical Physics, 14 (2012) 10523-10532.

[109] Z. Chen, D. Higgins, H.S. Tao, R.S. Hsu, Z.W. Chen, Highly Active Nitrogen-Doped Carbon Nanotubes for Oxygen Reduction Reaction in Fuel Cell Applications, The Journal of Physical Chemistry C, 113 (2009) 21008-21013.

[110] Y.K. Zhou, K. Neyerlin, T.S. Olson, S. Pylypenko, J. Bult, H.N. Dinh, T. Gennett, Z.P. Shao, R. O'Hayre, Enhancement of Pt and Pt-alloy fuel cell catalyst activity and durability via nitrogen-modified carbon supports, Energy & Environmental Science, 3 (2010) 1437-1446.

[111] K.P. Gong, F. Du, Z.H. Xia, M. Durstock, L.M. Dai, Nitrogen-Doped Carbon Nanotube Arrays with High Electrocatalytic Activity for Oxygen Reduction, Science, 323 (2009) 760-764.

[112] A.Q. Zhao, J. Masa, W. Schuhmann, W. Xia, Activation and Stabilization of Nitrogen-Doped Carbon Nanotubes as Electrocatalysts in the Oxygen Reduction Reaction at Strongly Alkaline Conditions, The Journal of Physical Chemistry C, 117 (2013) 24283-24291.

[113] B. Frank, A. Rinaldi, R. Blume, R. Schlögl, D.S. Su, Oxidation Stability of Multiwalled Carbon Nanotubes for Catalytic Applications, Chemistry of Materials, 22 (2010) 4462-4470.

[114] J.L. Zimmerman, R.K. Bradley, C.B. Huffman, R.H. Hauge, J.L. Margrave, Gas-phase purification of single-wall carbon nanotubes, Chemistry of Materials, 12 (2000) 1361-1366.

[115] P.X. Hou, C. Liu, H.M. Cheng, Purification of carbon nanotubes, Carbon, 46 (2008) 2003-2025.

[116] C. Li, D. Wang, T. Liang, X. Wang, J. Wu, X. Hu, J. Liang, Oxidation of multiwalled carbon nanotubes by air: benefits for electric double layer capacitors, Powder Technology, 142 (2004) 175-179.

[117] M.Q. Tran, C. Tridech, A. Alfrey, A. Bismarck, M.S.P. Shaffer, Thermal oxidative cutting of multi-walled carbon nanotubes, Carbon, 45 (2007) 2341-2350.

[118] P.M. Ajayan, T.W. Ebbesen, T. Ichihashi, S. Iijima, K. Tanigaki, H. Hiura, Opening carbon nanotubes with oxygen and implications for filling, Nature, 362 (1993) 522-525.

[119] N. Yao, V. Lordi, S.X.C. Ma, E. Dujardin, A. Krishnan, M.M.J. Treacy, T.W. Ebbesen, Structure and oxidation patterns of carbon nanotubes, Journal of Materials Research, 13 (1998) 2432-2437.

[120] J.H. Lehman, M. Terrones, E. Mansfield, K.E. Hurst, V. Meunier, Evaluating the characteristics of multiwall carbon nanotubes, Carbon, 49 (2011) 2581-2602.

[121] T. Shimada, H. Yanase, K. Morishita, J.-i. Hayashi, T. Chiba, Points of onset of gasification in a multi-walled carbon nanotube having an imperfect structure, Carbon, 42 (2004) 1635-1639.

[122] S.A. Carabineiro, M.F. Pereira, J.N. Pereira, C. Caparros, V. Sencadas, S. Lanceros-Mendez, Effect of the carbon nanotube surface characteristics on the conductivity and dielectric constant of carbon nanotube/poly(vinylidene fluoride) composites, Nanoscale research letters, 6 (2011) 302.

[123] B. Dippel, H. Jander, J. Heintzenberg, NIR FT Raman spectroscopic study of flame soot, Physical Chemistry Chemical Physics, 1 (1999) 4707-4712.

[124] S. Osswald, M. Havel, Y. Gogotsi, Monitoring oxidation of multiwalled carbon nanotubes by Raman spectroscopy, Journal of Raman Spectroscopy, 38 (2007) 728-736.

[125] M. Liu, Y. Yang, T. Zhu, Z. Liu, Chemical modification of single-walled carbon nanotubes with peroxytrifluoroacetic acid, Carbon, 43 (2005) 1470-1478.

[126] V. Datsyuk, M. Kalyva, K. Papagelis, J. Parthenios, D. Tasis, A. Siokou, I. Kallitsis, C. Galiotis, Chemical oxidation of multiwalled carbon nanotubes, Carbon, 46 (2008) 833-840.

[127] G. Moraitis, Z. Spitalsky, F. Ravani, A. Siokou, C. Galiotis, Electrochemical oxidation of multi-wall carbon nanotubes, Carbon, 49 (2011) 2702-2708.

[128] H.F. Gorgulho, J.P. Mesquita, F. Gonçalves, M.F.R. Pereira, J.L. Figueiredo, Characterization of the surface chemistry of carbon materials by potentiometric titrations and temperature-programmed desorption, Carbon, 46 (2008) 1544-1555.

[129] G.S. Szymański, Z. Karpiński, S. Biniak, A. Świątkowski, The effect of the gradual thermal decomposition of surface oxygen species on the chemical and catalytic properties of oxidized activated carbon, Carbon, 40 (2002) 2627-2639.

[130] Y. Otake, R.G. Jenkins, Characterization of oxygen-containing surface complexes created on a microporous carbon by air and nitric acid treatment, Carbon, 31 (1993) 109-121.

[131] J.L. Figueiredo, M.F.R. Pereira, M.M.A. Freitas, J.J.M. Órfão, Modification of the surface chemistry of activated carbons, Carbon, 37 (1999) 1379-1389.

[132] S. Haydar, C. Moreno-Castilla, M.A. Ferro-García, F. Carrasco-Marín, J. Rivera-Utrilla, A. Perrard, J.P. Joly, Regularities in the temperature-programmed desorption spectra of CO2 and CO from activated carbons, Carbon, 38 (2000) 1297-1308.

[133] M.D. Obradovic, G.D. Vukovic, S.I. Stevanovic, V.V. Panic, P.S. Uskokovic, A. Kowal, S.L. Gojkovic, A comparative study of the electrochemical properties of carbon nanotubes and carbon black, Journal of Electroanalytical Chemistry, 634 (2009) 22-30.

[134] Y.i Yi, E. Willinger, M. Willinger, J. Tonow, R. Schlögl, Electrochemical degradation of multiwall carbon nanotubes (MWCNTs) at high anodic potential in acidic media, (2014) to be submitted.

Appendix 1 Influence of the purification of carbon nanotubes on their electrochemical stability at high anodic potential

As-received carbon nanotubes (CNTs) require a purification procedure in order to remove carbonaceous impurities and residual metal catalyst. Several purification methods of CNTs have been reported. However, the treatment of CNTs influences the chemical and physical properties of the purified CNTs. It may damage carbon structure with creating defects and/or functionalize oxygen-containing groups. In this study, the purification of CNTs and its effect for the electrochemical behavior at high anodic potentials were investigated.

A1.1 Air oxidation and annealing

Air oxidation removes carbonaceous impurities by means of the different oxidation rate of amorphous and graphitic carbon. Annealing of CNTs reduces the surface oxide and rearranges carbon structure. Table A1.1 listed the treatment procedure of CNTs for air oxidation and annealing.

Table A1.1. Sample notation and details of corresponding treatment procedures.

Sample	Treatment/Purification
Pristine CNTs	Pristine CNTs_As received
AO-CNTs	oxidation at 400 °C for 12 hrs under Air
AO-HT-CNTs	oxidation at 400 °C for 12 hrs under Air + heat treated at 1700 °C for 1.5 hrs under N_2

Figure A1.1 shows cyclic voltammetry (CV) of the MWCNTs samples. P-CNTs show a typical curve for double layer capacitance of carbon. After air oxidation, the capacitance of AO-CNTs increases significantly and a redox peak of surface oxide appears. Further treatment of the annealing process under an inert atmosphere, such as nitrogen, removes

the surface functionalities and rearranges graphitic carbon structures. Therefore, CV of AO-HT-CNTs exhibits the decrease of electrochemical capacitance.
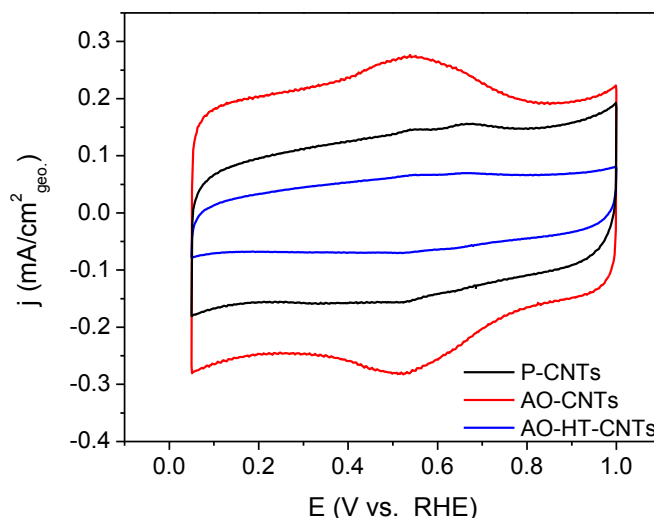

Figure A1.1. Cyclic voltammetry of the CNTs samples in 0.5 M H_2SO_4, Scan rate: 50 mV/s.

The stability of electrochemical oxidation on the CNTs samples was carried out by potential cycling up to 1.8 V versus RHE. As the number of potential cycling increase, the oxidation current of the CNTs decreases, indicating the degradation of the CNTs. Figure A1.2 (a) shows the change of CV on the CNTs before and after 30 scans of potential cycling. Even though the capacitance of P-CNTs is lower than AO-CNTs, the oxidation current at high anodic potential is higher. Probably, residual metal catalyst on P-CNTs catalyzes the oxidation. The oxidation current above 1.2 V of P-CNTs and AO-CNTs is lower than the initial current after potential cycling. However the oxidation current below 1.2 V increases. It is evident that surface functional groups formed during potential cycling contribute to an increase of capacitance. On the other hand, the CV curves of AO-HT-CNTs show no obvious change. The oxidation current of AO-HT-CNTs slightly increases with potential cycling at high anodic potential. AO-HT-CNTs that are the graphitized CNTs have fewer defects than other samples, thus the initial oxidation activity is lower, whereas the stability is higher than the other CNTs samples. During the potential cycling on AO-HT-CNTs, the carbon surface may be activated by

producing surface oxides and defects, and thus induces the increase of the oxidation current after the electrochemical oxidation of CNTs. Therefore, it is conclusive that the annealing of CNTs improves the stability of electrochemical oxidation.
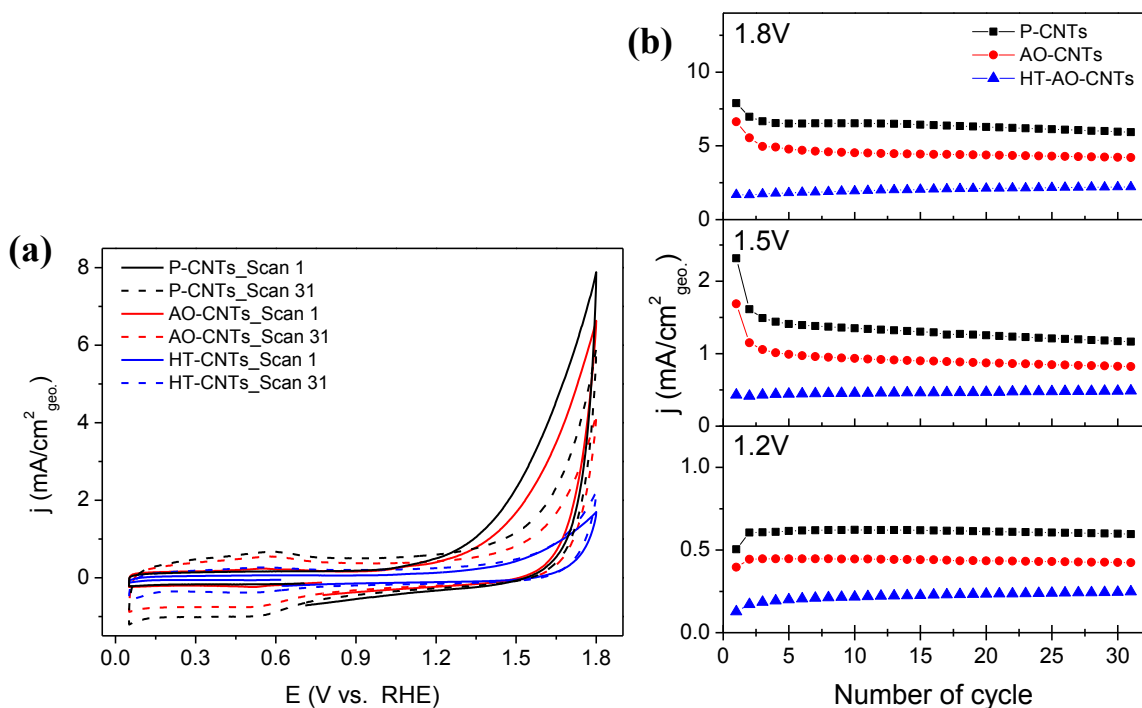

Figure A1.2. (a) Potential cycling for the oxidation stability of the MWCNTs samples in 0.5 M H_2SO_4. Scan rate: 50 mV/s. A solid line is initial scan and a dotted line is 31 scan. (b) The variation of the current at 1.2 V, 1.5 V and 1.8 V obtained from the potential cycling.

A1.2 Chemical oxidation and purification

CNT treatment with nitric acid is a common method to remove metal(oxide) and carbon impurities, and subsequently functionalizes the carbon surface. The formation of functional groups on the CNTs is dependent on the concentration of nitric acid and temperature. In this part, the different concentration of nitric acid and temperature were considered to treat the CNTs. Furthermore, additional purification methods were applied after nitric acid treatment. Base washing and sonication steps dissolve further oxidation debris and decompose into organic frames. Labeling assignments and treatment procedures are listed in Table A1.2.

Table A1.2. Sample notation and details of corresponding treatment procedures.

Sample	Treatment/Purification
CNA110-CNTs	treated in 65% Nitric acid at 110 °C for 16 hrs
CNA110-P-CNTs	treated in 65% Nitric acid at 110 °C for 16 hrs + purification (NH$_4$OH& Sonication)
CNART-CNTs	treated in 65% Nitric acid at room temperature for 16 hrs
CNART-P-CNTs	treated in 65% Nitric acid at room temperature for 16 hrs + purification (NH$_4$OH & Sonication)
1MNART-CNTs	treated in 1M Nitric acid at room temperature for 16 hrs
1MNART-P-CNTs	treated in 1M Nitric acid at room temperature for 16 hrs + purification (NH$_4$OH & Sonication)

As shown in Figure A1.3, the CV of CNA110-CNTs indicates the largest capacitance of the CNTs samples. The CNTs treated in concentrated nitric acid at high temperature produce more functional groups on the surface. The CNTs treated at room temperature do not increase total capacitance, but high concentration of nitric acid arouses a redox peak that result from electrochemically active surface oxides. Thus, it could be inferred that the concentration of nitric acid affects the formation of surface oxides that contribute to

pseudocapacitance. The effect of a further purification step was clearly observed in CV of the CNT samples. The CNTs treated in nitric acid have a redox current peak around 0.6 V. However, after a further purification step of the CNTs, the peak is reduced which means the removal of functional groups on the carbon surface. It is interesting that the CV contributed by double layer capacitance has no change, only pseudocapacitance is affected. The CNT treated in low temperature and concentration (1MNART-CNTs) has no carbon redox current peak. Mild conditions of cleaning procedures minimize structural damage of the CNTs.
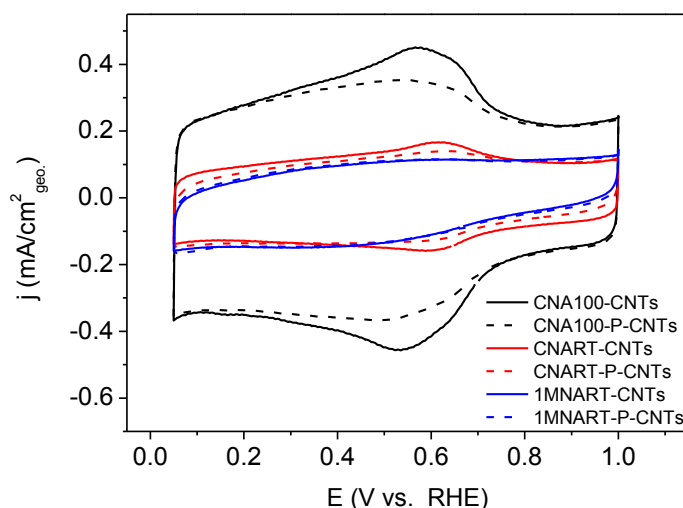

Figure A1.3. Cyclic voltammetry of the MWCNTs samples in 0.5 M H_2SO_4.
Scan rate: 50 mV/s

Figure A1.4 shows the variation of the oxidation current on the CNTs samples during potential cycling. The oxidation activity of 1MNART-CNTs is higher than one of the other CNTs samples. The CNTs treated in high concentration of nitric acid (CNA100-CNTs and CNART-CNTs) degrade faster at high anodic potential. Moreover, even though there are some different features on CV with and without the further purification step, the oxidation behavior at high anodic potential is the same. There is no effect of more redox surface oxide species on the surface at high anodic potential. On the contrary, 1MNART-CNTs have no difference in CV with and without further purification step but show higher oxidation current than 1MNART-P-CNTs. Through these results, high

116

concentration of nitric acid induces structural defects on the CNTs. The functional groups formed on these defects contribute to redox surface oxides, but leads to less oxidation stability and activity at high anodic potential. The CNTs treated in mild conditions (1MNART-P-CNTs) are more conductive at high anodic potential, and show good oxidation stability due to fewer defects on the surface.
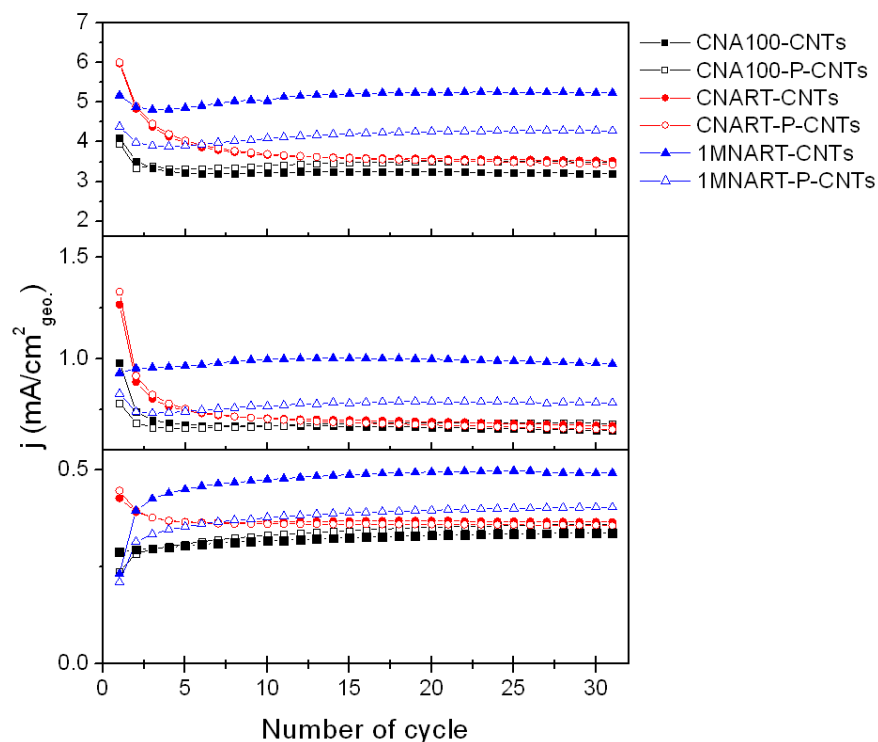

Figure A1.4. The variation of current at 1.2 V, 1.5 V and 1.8 V obtained from potential cycling scan for the oxidation stability of the MWCNTs samples in 0.5 M H_2SO_4. Scan rate: 50 mV/s.

A1.3 The effect of boron modified CNTs

Besides the purification of CNTs, this part deals with heteroatoms with CNTs. The modification with heteroatoms, such as nitrogen, boron and phosphorous, can affect their properties such as pH, catalytic activity, conductivity and their crystallinity. 5 wt.% boron modified CNTs were prepared by nitric acid treatment and further modified with H_3BO_3 solution.

Table A1.3. Sample notation and details of corresponding treatment procedures.

Sample	Treatment/Purification
P-CNTs	Pristine CNTs_As received
B-CNTs	Nitric acid treatment + impregnation of $B(OH)_3$ + heat treatment at 1500 °C for 4 h under Ar

There is no change of the capacitance with and without boron modification of the CNTs, as shown in Figure A1.5.
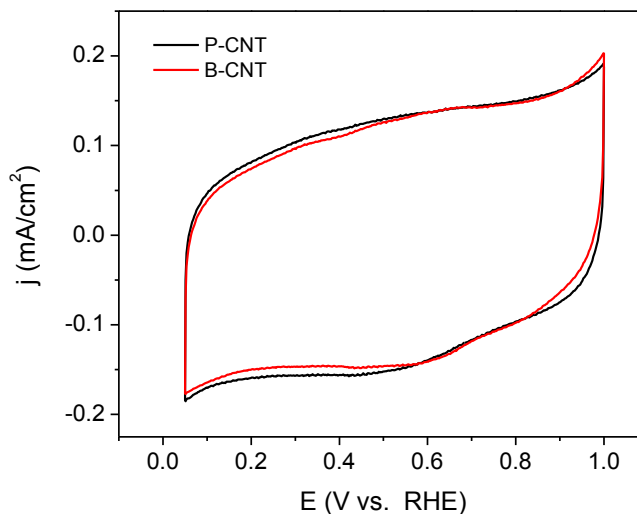

Figure A1.5. Cyclic voltammetry of the MWCNTs samples in 0.5 M H_2SO_4. Scan rate: 50 mV/s

Interestingly, the oxidation current of B-CNTs is much lower than P-CNTs, despite no difference in the potential range for the capacitance. It could be that boron containing functional groups inhibit the oxidation of carbon and water at high anodic potential.

Furthermore, B-CNTs reach constant CV curves after 1 scan of potential cycling. The change of the capacitance on B-CNTs during the carbon oxidation is much less compared to P-CNTs. Therefore, boron oxide is likely to act as an inhibitor for the electrochemical oxidation of carbon.
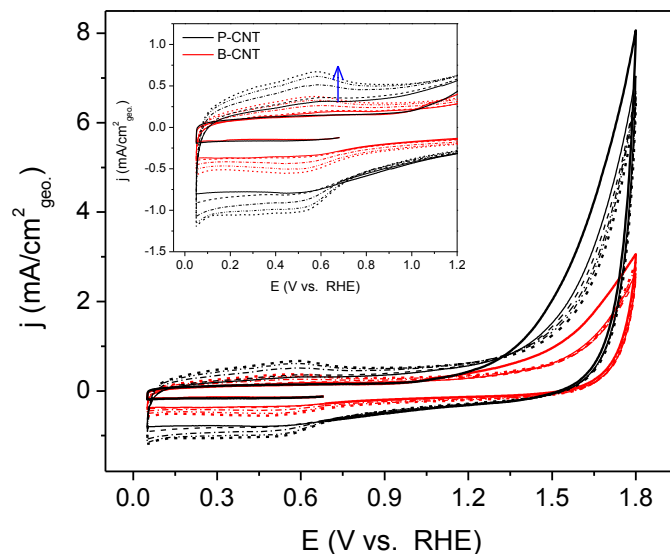

Figure A1.6. Potential cycling for the oxidation stability of the MWCNTs samples in 0.5 M H_2SO_4. Scan rate: 50 mV/s. Solid line is initial scan curve and dotted line is during the scan. Inset figure is the magnification of the overall curves.

Appendix 2 The effect of pH media for electrochemical degradation of carbon materials

Herein, the electrochemical behavior of multiwall carbon nanotubes (MWCNTs) and carbon black (CB) with different pH media were compared. For different pH media, 0.5 M H2SO4 for acidic media (pH 1, 23 mS/cm), 0.1 M phosphate buffer for neutral media (pH 7, 2 mS/cm) and 0.1 M KOH for neutral media (pH 13, 24 mS/cm) were used.

The MWCNTs have high electrochemical capacitance compared to CB because of high surface area. The difference of the electrochemical behavior between CB and MWCNTs is higher in neutral media. Figure A2.1 shows the typical CV curves for the capacitance with different pH media. In the CV of MWCNTs in neutral media, the cathodic current peak is undefined, probably comes from the effect of phosphate ion. The relative value of capacitance from CVs increase as the pH of the electrolyte is higher.
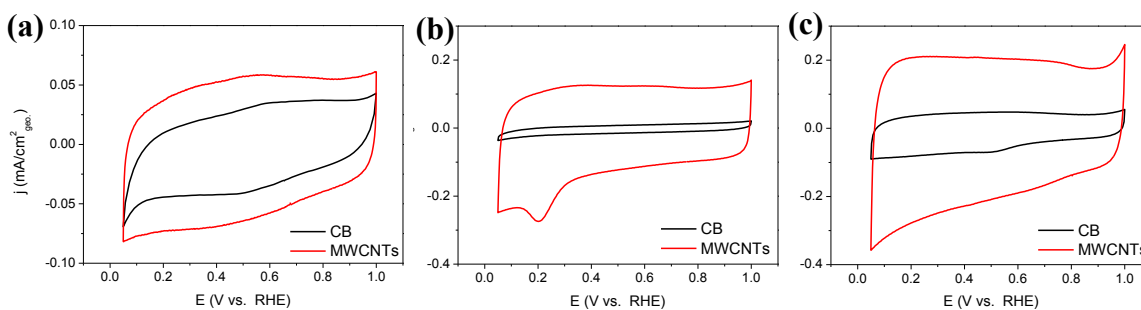

Figure A2.1. Cyclic voltammetry of carbon black (CB) and multiwall carbon nanotubes (MWCNTs) in (a) 0.5 M H_2SO_4 (pH 1), (b) 0.1 M phosphate buffer (pH 7) and (c) 0.1 M KOH (pH 13), Scan rate: 50 mV/s.

Linear sweep voltammetry (LSV) at high anodic potential represents the activity of electrochemical oxidation of carbon materials. In contrast with the trend of CVs, the electrochemical activity of carbon is the highest in acidic media, and lowest in neutral media. Low activity in neutral media could result from low solution conductivity compared to other electrolytes. The MWCNTs show higher activity than CB due to high surface area and more active sites.
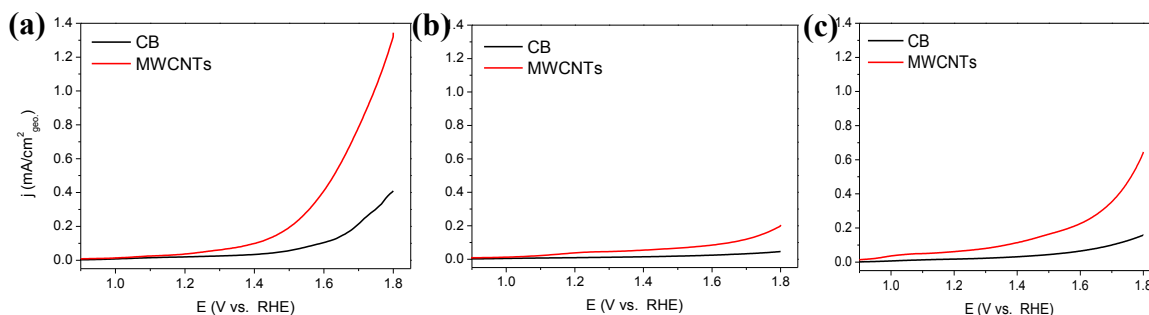
Figure A2.2. Linear sweep voltammetry of carbon black (CB) and multiwall carbon nanotubes (MWCNTs) in (a) 0.5 M H_2SO_4 (pH 1), (b) 0.1 M phosphate buffer (pH 7) and (c) 0.1 M KOH (pH 13), Scan rate: 10 mV/s.

Complex resistance of the MWCNTs with different pH media was measured by electrochemical impedance spectroscopy. Figure A2.3 (a-c) show the Nyquist plots of the MWCNTs with different applied potential. Total resistance of the MWCNTs decreases as the applied potential increases. Semicircle appears when the gas evolution occurs on the electrode with mass transfer. The impedance spectra at open circuit potential was fitted with the equivalent electrical circuit in Figure A2.3(d). The equivalent electrical circuit consist cell resistance (R_{cell}) of the electrolyte and carbon surface film, contact resistance and capacitance (R_c, CPE_c) between the carbon film and glassy carbon electrode, and the resistances from electrochemical process at the electrolyte/carbon interface containing double layer capacitance (CPE_{dl}) pseudocapacitance (C_p) and charge transfer resistance (R_{ct}). The factor for contact resistance is not presented. The results obtained from the fitting are summarized in Table A2.1. The highest value of R_{cell} and Rct in neutral media comes from low solution conductivity. CPE_{dl} and Cp increase with pH media. This is in a good agreement with the trend of CV. Roughness factor (α) indicates a porous electrode.
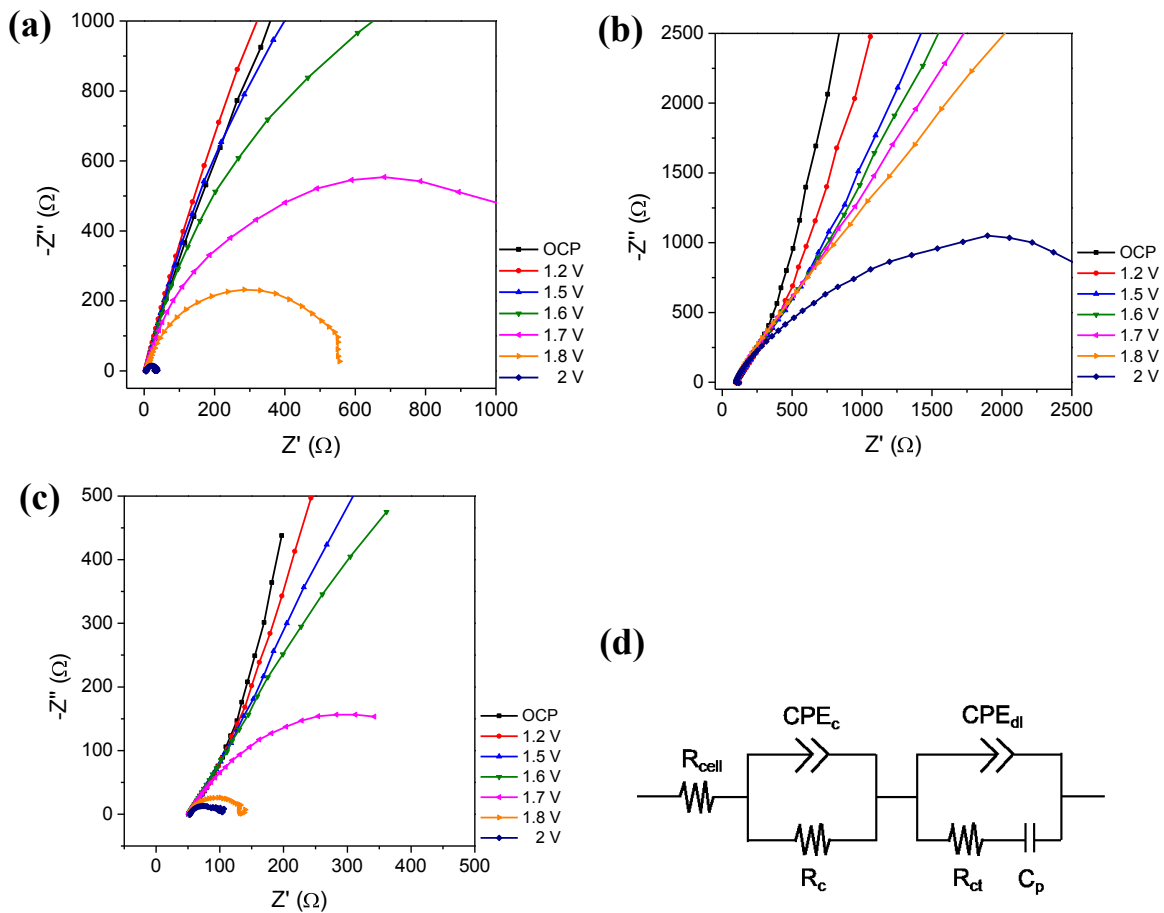
Figure A2.3. Nyquist plots of MWCNTs with different applied potentials in (a) 0.5 M H$_2$SO$_4$ (pH 1), (b) 0.1 M phosphate buffer (pH 7) and (c) 0.1 M KOH (pH 13). (d) equivalent electrical circuit for EIS fitting.

Table A2.1. Impedance spectra fitting values obtained from Figure A2.3.

At OCP	acidic	neutral	alkaline
R$_s$ (Ω)	5.17	99.15	51.46
CPE$_{dl}$-A 10^{-6} F .s^(α-1)	83.3	107.6	831
CPE$_{dl}$-α	0.74	0.88	0.87
C$_p$ (μF)	9.46	11.76	14.22
R$_{ct}$ (Ω)	76.95	705.8	300

Figure A2.4. show that the electrochemical oxidation behavior of CB and MWCNTs at high anodic potential with different pH media.
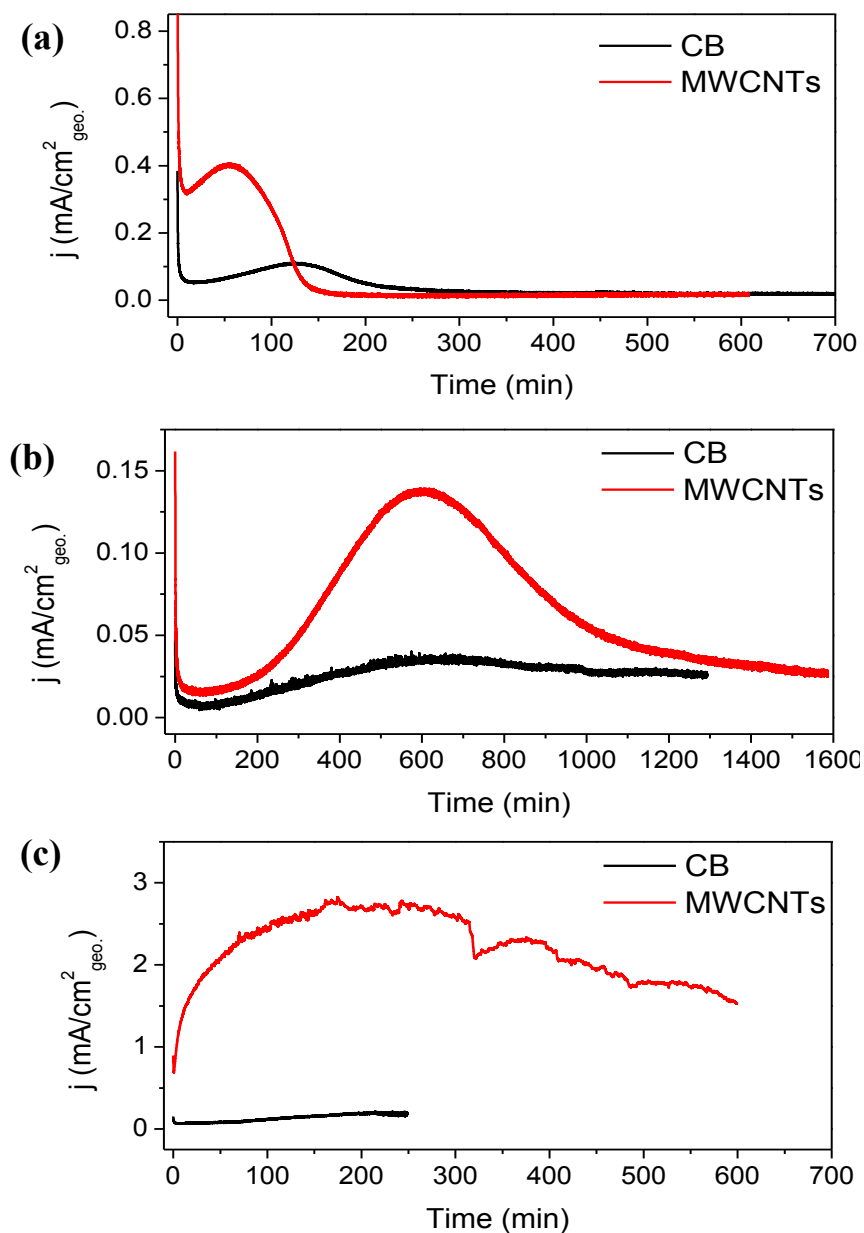

Figure A2.4. Chronoamperommetry of CB and MWCNTat 1.8 V versus RHE in (a) 0.5 M H₂SO₄ (pH 1), (b) 0.1 M phosphate buffer (pH 7) and (c) 0.1 M KOH (pH 13).

Curriculum vitae

Youngmi Yi

이 영 미 (李英美)

Department of inorganic chemistry, Fritz-Haber-Institute der Max-Planck Gesellschaft,
Faradayweg 4-6, 14195 Berlin, Germany
Email: youngmi@fhi-berlin.mpg.de and youngmi05@gmail.com

Nationality	South Korea
Place of Birth	Busan, South Korea
Date of Birth	20 May 1985

Research topics: Carbon electrochemistry, Nanostructure synthesis, Electrodeposition, Electrocatalyst for water electrolysis and fuel cell, Hydrogen production from chemical hydrides

Education

Nov. 2010 –
Present

Fritz-Haber-Institute der Max-Planck Gesellschaft, Berlin, Germany
<u>Doctoral candidate</u> in department of inorganic chemistry
Prof. Dr. Robert Schlögl
- Carbon supported catalyst for oxygen evolution in water electrolysis Cathode stability of carbon supported on Pt for PEM fuel cells
- Thesis: Study on the degradation of carbon materials for electrocatalytic applications

Sep. 2007 –
Aug. 2009

Gwangju Institute of Science and Technology (GIST), Gwangju, South Korea
<u>Master of Science</u> (School of Environmental Science and Engineering)
Electrochemical Reaction and Technology Laboratory (ERTL)
Prof. Dr. Jaeyoung Lee
- Nanostructured Ni and Ni-Pd alloys for hydrogen evolution in water electrolysis and ethanol oxidation, Electrochemical deposition
- Thesis: The template-based simple synthesis of various nano-structures for an efficient electrocatalyst

Mar. 2004 –
Aug. 2007

Changwon National University, Changwon, South Korea
<u>Bachelor of Science</u> (Department of Environmental Engineering)
- Environmental chemistry, physical/organic chemistry, Electrochemistry, Biological/chemical/physical water treatment, etc.

Mar. 2001 –
Feb. 2004

Keumjeong Girls' High School, Busan, South Korea

Work Experience

Sep. 2009 – Oct. 2010	Gwangju Institute of Science and Technology (GIST), Gwangju, South Korea Ertl center for Electrochemistry & Catalysis *Researcher / Secretary* Prof. Dr. Jaeyoung Lee
Jul 2006	Gwangju Institute of Science and technology (GIST), Gwangju, South Korea Laboratory for Environmental0oriented Electrochemical Engineering *Intern student* Prof. Seung-Hyeon Moon
Jun. 2005 – Dec. 2005	Changwon National University, Changwon, South Korea Water treatment laboratory *Undergraduate Researcher* Prof. Gyutae Seo

Other Experience

Jan. 2007 – Feb. 2007	**Language training** RMIT English work wide in RMIT university, Melbourne, Australia -. Complete the intermediate of ELICOS course -. Supported in Changwon national university
Mar. 2006 – Dec. 2006	**Service experience** Cultural house for teenagers, Changwon, South Korea -. Assistant teacher of teenager digital camera program
Mar. 2004 – Dec. 2006	**Club activity experience** Academic Photo Club (APC) in Changwon national university

Certificates of Qualifications

Jun. 2007	Water quality environment certificate Grade 1
Aug. 2006	Office automatic (OA) certificate Grade 2
Feb. 2006	Auto-CAD certificate Grade 2

Awards and Scholarships

Doctoral scholarship in Max Planck Society (2010-present)

Full Korean Government Scholarship (2007-2009)

Undergraduate Scholarship, Changwon national university (2004-2007)

New University for Regional Innovation (NURI) Scholarship (2004-2007)

List of Publications

[1] <u>Youngmi Yi</u>, Chinmoy Ranjan, Elena Willinger, Marc Willinger, Julian Tornow, Robert Schlögl, Electrochemical degradation of multiwall carbon nanotubes (MWCNTs) at high anodic potential in acidic media, (2014) to be submitted.

[2] Jin Won Kim, Jae Kwang Lee, Doungkamon Phihusut, <u>Youngmi Yi</u>, Hye Jin Lee, Jaeyoung Lee*, Self-organized One-dimensional Cobalt Compound Nanostructures from CoC_2O_4 for Superior Oxygen Evolution Reaction, Journal of Physical Chemistry C 117 (2013) 23712-23715.

[3] Trinh Ngoc Tuan, <u>Youngmi Yi</u>, Jae Kwang Lee, Jaeyoung Lee*, Fe-B catalyst fabricated by hybrid capacitive adsorption-chemical reduction method and its application for hydrogen production from $NaBH_4$ solution, Catalysis Today 216 (2013) 240-245.

More publications : 2 papers as first author, 6 papers as co-author

List of Presentations

[1] <u>Youngmi Yi</u>, Elena Willinger, Robert Schlögl, Julian Tornow, Electrochemical degradation of multiwall carbon nanotubes (MWCNTs) in acidic media, *47. Jahrestreffen Deutscher Katalytiker*, Weimar, Germany (2014).

[2] <u>Youngmi Yi</u>, Chinmoy Ranjan, Elena Kudrenko, Marc Willinger, Robert Schlögl, Julian Tornow, Electrochemical corrosion of carbon nanotube in an environment for electrochemical water splitting, *6th International Conference on Polymer Batteries and Fuel Cells (PBFC‑6)*, Ulm, Germany (2013).

[3] <u>Youngmi Yi</u>, Chinmoy Ranjan, Xing Huang, Elena Kudrenko, Marc Willinger, Robert Schlögl, Julian Tornow, Electrochemical corrosion of carbon nanotubes for water splitting, *46. Jahrestreffen Deutscher Katalytiker*, Weimar, Germany (2013).

More 12 presentations

Acknowledgement

Many people have encouraged and helped me during my Ph.D. Without their help, I can't imagine that I manage to get my doctoral degree in Germany.

First, I would like to express my sincere gratitude and appreciation to Prof. Dr. Robert Schlögl for the opportunity to study in the department of Inorganic Chemistry at the Fritz Haber Institute. His academic advice and guidance let me think deeply and differently about my research. It could produce this excellent topic and broaden my horizon.

I would like to thank my committee members, Prof. Dr. Peter Strasser and Prof. Dr. Jaeyoung Lee for their invaluable input and patience.

I especially appreciate Prof. Dr. Jaeyoung Lee who recommended me to study abroad. As a great mentor for my development, he infinitely encourages and trusts me for my scientific life.

I would like to thank Dr. Julian Tornow who supervised me over two years. His help and support made me carefully consider my results for reliable and valuable research. I am also grateful to other supervisors, Dr. Chinmoy Ranjan, Prof. Dr. Dang Sheng Su and Prof. Dr. Malte Behrens for setting up a research project at the beginning of my Ph.D. I thank Dr. Sébastien Cap, who is new group leader in Electrochemistry group, for the correction and comment for the thesis.

I would like to thank technical support from Elena Willinger, Marc Willinger Xing Huang, Nobert Pfänder (TEM), Gisela Weinberg (SEM), Maike Hashagen (BET), Jasmin Allen (TGA) and Olaf Timpe (Chemical lab). In addition, Dr. Sylvia Reiche arranged to measure elemental analysis (EA) in Max Planck institute for chemical energy conversion in Mühlheim. I also thank Klaus Friedel to discuss and share his experience about the characterization of carbon. Thanks extend to lab and office mates; Bambar Davaasuren, Martin Pradel, David Klein, Adriana Bernal, Sabine Wasle, Sebastian lüneberg and Verena Pfeifer.

Special thanks to Dr. Rosa Arrigo for not only scientific but personal advices. Even though she was pregnant, she helped me the review and correction for my thesis. I congratulate on the birth of her baby.

I was very happy to share working experience, knowledge and friendship with people in Fritz-Haber institute. In particular, I am very grateful to Katharina Mette, Pia Nielson, Julia Schumann and other Ph.D students helped me to adapt to German culture. I have never forgotten a good impression and a precious memory with them.

To my dear friends from graduate school, undergraduate school, high school, and middle school in Korea, thank you for the encouragement through texting and calling. I could relieve my homesickness from them, and do always treasure our friendship.

Whenever I called my grandmother in Korea, she asked me when I complete my Ph.D. I can say now I am a doctor in Chemistry. I hope that my grandmother is recovering her health soon. I would not have been able to achieve my goals without the love and support of my family. I heartily appreciate to my parents for their unconditional love and infinite trust. I also thank my younger sister and brother, Youngkyung and Gidae who have given care and support to my parents while I am far away from home for a long time.

Thank you for all of them again. I wish them good health, great happiness, and success in their work.

I am excited that I have a new start with the knowledge that I learned from Ph.D.

독을 차고

내 가슴에 독을 찬 지 오래로다
아직 아무도 해한 일 없는 새로 뽑은 독
벗은 그 무서운 독 그만 흩어 버리라 한다
나는 그 독이 선뜻 벗도 해할지 모른다 위협하고

독 안 차고 살아도 머지않아 너 나 마저 가 버리면
누억천만 (屢億千萬) 세대가 그 뒤로 잠자코 흘러가고
나중에 땅덩이 모지라져 모래알이 될 것임을
"허무한데!" 독은 차서 무엇 하느냐고?

아! 내 세상에 태어났음을 원망 않고 보낸
어느 하루가 있었던가 "허무한데!" 허나
앞뒤로 덤비는 이리 승냥이 바야흐로 내 마음을 노리매
내 산 채 짐승의 밥이 되어 찢기우고 할퀴우라 내맡긴 신세임을

나는 독을 품고 선선히 가리라
마감 날 내 외로운 혼 건지기 위하여

Carrying Poison

My breast has long been full of poison,
newly drawn poison that so far has harmed nobody.
A friend tells me I should pour away that dreadful poison.
I threaten: that poison might suddenly harm even my friend.

Even if our lives are not full of poison, very soon you and I will have gone for good,
then a trillion generations will flow away in silence,
ultimately the earth will wear away to a grain of sand.
Such things are all vanity! Why be full of poison?
Ah! Was there one single day that I spent without resenting
having been born in this world? All vanity, I say.

Before and behind me, wolves, coyotes rush for my heart.
My destiny is to be eaten alive by beasts, to be torn apart,
clawed.

Full of poison still, I will readily go,
to save my soul on the last day of my life.

**Kim Yeong-Nang
(1903–1950)**